



Title	High-power semiconductor die-attachment : Application of Zn with minor metal additions
Author(s)	Park, Sungwon
Citation	大阪大学, 2013, 博士論文
Version Type	VoR
URL	https://hdl.handle.net/11094/27585
rights	
Note	

The University of Osaka Institutional Knowledge Archive : OUKA

<https://ir.library.osaka-u.ac.jp/>

The University of Osaka

Ph.D. Dissertation

**High-power semiconductor die-attachment:
Application of Zn with minor metal additions**

Sungwon Park

January 2013

Department of Adaptive Machine Systems

Graduate School of Engineering

Osaka University

Ph.D. Dissertation

**High-power semiconductor die-attachment:
Application of Zn with minor metal additions**

Sungwon Park

Department of Adaptive Machine Systems
Graduate School of Engineering
Osaka University

January 2013

Approved by

Professor Katsuaki Suganuma

Professor Hideyuki Yasuda

Professor Masato Yoshiya

High-power semiconductor die-attachment: Application of Zn with minor metal additions

Abstract

Wide-gap semiconductor devices have been developed for next generation power electronics applications due to their excellent physical and electrical properties. In particular, SiC devices are expected to realize higher operating temperature than that of Si devices available today, and reduce the size of cooling system, or even eliminate it. The elevated operating temperature also requires further improvement of die-bonding materials in their physical properties, e.g. melting temperature, thermal stress relaxation, heat transfer, to assure the reliability and durability of the application devices. One of the prospective candidate materials is pure Zn, showing excellent joining properties, as well as the low cost of the material. However, some concerns of the brittleness and oxidation of the material has not yet clarified especially used in elevated temperature. This thesis investigates the joining characteristics and thermo-mechanical properties of metal Zn for SiC die-attach, particularly in the effect of minor addition of other metal elements (Ca, Mn, Cr, and Ti) in pure Zn. As well, a discrete application of pure Zn to non-metallization Si wafer bonding process is presented to show further potential of the bonding material.

It is found that the minor element additions effectively enhances the ductility of Zn; Ca, Mn, Cr achieves eight times higher ductility than that of pure Zn without degrading the strength under thermal-mechanical stress. Slightly less ductility is obtained by Ti addition than others due to fine precipitates formation on grain boundaries. These minor metal additions, particularly Cr, bring considerable oxidation resistance in Zn. This is because the active metal element like Cr forms a compact and stable barrier layer at the surface or subsurface of Zn, preventing further oxidation.

The interface of the Zn alloys with Cu substrate is investigated in detail, focusing on the growth of inter-metallic compounds (IMCs). The brittle nature of thicker IMCs degrades the joining reliability. Two reaction layers of γ -Cu₅Zn₈ and ϵ -CuZn₅ phases are observed at the interface, and the growth rate of the IMCs is reduced by the minor element addition, particularly Cr addition. The shear strength degradation by thermal aging at 150 °C is accordingly moderated. Zn with 0.1 wt% Cr has recorded a remarkable suppression of IMCs growth during the aging test at 250 °C.

Based on the improved bonding characteristics as described above, Zn-0.1Cr alloy has been tested for SiC chip attachment to Si₃N₄ direct bonded copper (DBC) substrate, followed by thermal cycle reliability tests carried out in comparison with pure Zn, and with conventional high-temperature solder Pb-5Sn. The Zn-0.1Cr solder shows a sound bonding interface between SiC die with a metallization of TiN/Au and the DBC substrate. Moreover, the bonding structure of SiC and DBC provides excellent heat-cycle resistance between -50 °C and 300 °C without cracking, while Pb-5Sn solder encounters severe cracks.

The minor element addition in Zn explored in the present study confirms the great potential of Zn alloys as a die-attachment material for high-temperature power devices.

Table of contents

Abstract	i
Table of contents	ii
Chapter 1 Introduction	1
Abstract	2
1. 1 Die-attach technologies for power semiconductor devices	3
1.1.1 Power semiconductor device packaging.....	3
1.1.2 Next generation power semiconductor devices: Silicon Carbide (SiC)	6
1.1.3 Die-attach technologies	9
1.1.4 Conventional die-attach material: High-lead solder	11
1.1.5 Requirement for lead-free die-attach materials	13
1. 2 Candidate of lead-free solders for Silicon Carbide die-attachment	14
1.2.1 Au-based die-attach materials	15
1.2.2 Bi-Ag based die-attach materials	20
1.2.3 Sn-Sb based die-attach materials	23
1.2.4 Zn-Al based die-attach materials	25
1.2.5 Zn-Sn based die-attach materials	28
1. 3 Motivation and objective of the thesis	31
1.3.1 Pure Zn die-attachment	31
1.3.2 Objective of this thesis	32
References	34

Chapter 2 Enhanced ductility and oxidation resistance of Zn by the addition of minor elements for use in SiC die-attachment	39
Abstract	40
2.1 Introduction	41
2.2 Experimental procedures	43
2.3 Results and discussion	45
2.3.1 Enhancement of ductility	45
2.3.2 Microstructure change	50
2.3.3 Improvement of oxidation resistance	53
2.4 Conclusions	55
Appendix	56
References	58
Chapter 3 Effects of minor elements on the reaction between Zn and Cu substrate during thermal aging	61
Abstract	62
3.1 Introduction	63
3.2 Experimental procedures	64
3.3 Results and discussion	66
3.3.1 Bonding interface as soldered	66
3.3.2 IMC growth during thermal aging	72
3.4 Conclusions	80
Appendix	82
References	83
Chapter 4 Joining properties and thermal shock reliability of SiC die-attached joints	85
Abstract	86
4.1 Introduction	87
4.2 Experimental procedures	88

4.3	Results and discussion	91
4.3.1	Interfacial reaction of the SiC die-attached joints	91
4.3.2	Thermal cycle reliability	93
4.4	Conclusions	95
	Appendix	96
	References	97
Chapter 5 Non-metallization Si wafer bonding by self-regulated eutectic reaction with pure Zn		99
	Abstract	100
5.1	Introduction	101
5.2	Experimental procedures	103
5.3	Results and discussion	104
5.3.1	Bonding strength	104
5.3.2	Microstructure of wafer bonding interface	105
5.3.3	Self-regulated eutectic reaction	109
5.4	Conclusions	111
	References	112
Chapter 6 Conclusions		115
List of Publication		119
Acknowledgements		121

Chapter 1

Introduction

Abstract

In this chapter, the technology background about next-generation wide-gap semiconductor devices and their packaging technologies such as die-attach materials is reviewed. Wide-gap semiconductors, such as SiC, GaN, and InP have been receiving considerable attention as an alternative technology to replace Si power semiconductor devices. These compound semiconductors possess excellent physical and electrical properties, such as a higher breakdown voltage, lower power loss and higher thermal conductivity, which are suitable for power devices. Among the wide-gap semiconductors, this thesis focuses on the die-attach of SiC wide-gap semiconductors due to the superior physical and electronic properties of SiC. The SiC wide-gap semiconductor devices are prospected to realize higher operating temperature, and reduce the size of cooling system, or even eliminate it from the product devices. The high operation temperature requires improved die-bonding materials with higher melting point and higher thermal conductivity. Particularly for automobiles, ceasing the use of radiators is critical to reduce both the total weight and number of fragile parts. In the following sections of chapter 1, the current die-attachment technologies would be discussed, and shows no existing lead-free materials can be applied to SiC power devices operated at high temperatures around 300 °C. The major objectives of this thesis are hence to study the characteristics of Zn as one of the prospective candidates for SiC die-attachment materials, and to enhance the physical properties with minor additions of other elements together with detailed investigations of the joining properties.

1.1 Die-attach technologies for power semiconductor devices

1.1.1 Power semiconductor device packaging

Semiconductor switching devices are key components in the power electronics technology. Various types of power semiconductor devices have been applied for on/off switching, current/power conversion, and energy storage [1]. In other words, power semiconductor enables to control the various forms of electric energy (e.g. AC or DC and the magnitude of currents and voltages). These semiconductor switching devices for electrical power conversions are simply called as “power device”, which performs the functions like rectifying (AC to DC), inverting (DC to AC), boosting (DC to DC), and frequency conversion (AC to AC) [1–3] of electricity. Since electricity and electronics are the fundamental technologies of the modern human society, power devices can be found in diverse application fields in our daily life as shown in Fig. 1.1 [4].

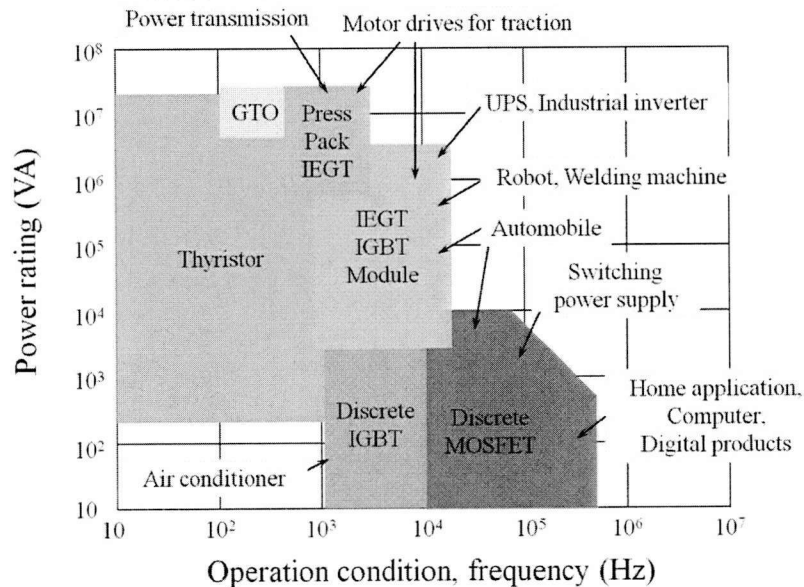


Fig. 1.1 Various device application fields [4].

The application of power devices have widely been used for controlling and converting electronics. With the continuous progress in technologies, the power devices have faced increased demands for cost-effective, high power, high density, and high operating temperature, particularly in high power electronics systems, like electrical automotives, since the main target of the power devices is to transfer power from an electrical source to an electrical load. To meet the requirements, the packaging technology of these devices have important roles such as mechanical support, device protection, cooling and electrical connection and isolation. Controlling and reducing power loss from packaging materials is thus becoming more and more important [1, 3].

Until recently, power devices had been studied and developed almost exclusively on Si-based semiconductor technologies. As mentioned above, however, the development of power devices is necessary to operate at high current densities, high internal electric fields and, consequently, high temperatures environment for energy and cost efficiency. To achieve the required energy and cost effectiveness, the research of power devices places emphasis on more powerful, efficient, durable, downsizing, and lighter in weight. All of these bring us new motivation to present Si based power electronics technology. The requirements of advanced performance cause high operating temperatures due to integration and downsizing of devices. For applications at high temperatures, it is very challenging to use conventional Si base semiconductor electronics because they are generally limited to operating temperatures below 150 °C due to the limitations of the physical/electrical properties and the absence of advanced packaging technology [1, 3].

The detailed limitations of Si power devices are described in the following paragraph [1, 3, 5]:

A. Small band gap energy

Band-gap energy is a fundamental characteristic of semiconductor materials. The small band-gap of only 1.12 eV for Si semiconductor causes to lose the designed p-n junction characteristics around at 200 – 350 °C according to their doping conditions. Increasing leakage current with increasing

temperature is also a challenge, and this may require to use silicon-on-insulator (SOI) process for an operating temperatures approaching 200 °C. Therefore, the small band-gap fails to satisfy the requirement for power devices in future.

B. Low breakdown voltage

The small band-gap energy of Si as described above causes the low breakdown voltage of devices, because the voltage blocking capacity of discrete Si devices is less than 12 kV. One way to achieve higher breakdown voltage is serial stacking package, but such workaround inevitably results in higher on-state resistance, larger energy-loss, less current density, and lower switching frequency, and higher cost of devices as well. There is hence a strong motivation to develop power semiconductor devices that intrinsically have greater breakdown voltage.

C. Low thermal conductivity

The operation temperature of Si power devices is also limited by the low thermal conductivity of Si to effectively spread and transfer the generated heat. The critical thermal dissipation of power applications thus needs cooling system like heat-sink, which typically occupies one-third of the total volume of power converters. Developing a power electronics that can withstand higher temperature is one way of decreasing the cooling requirements to reduce the size and cost of the converter. Wide band-gap semiconductor materials with higher thermal conductivity have been proven to be good candidates to replace Si.

The constraints of the present power devices thus come from the intrinsic materials' properties of Si. Post-Si power devices will be introduced in the following sections, to solve the facing requirements of future power devices.

1.1.2 Next generation power semiconductor devices: Silicon Carbide (SiC)

As mentioned in the previous section, Si is the most commonly used semiconductor material in manufacturing power devices mainly due to its high availability and low production cost. For the application, however, under high frequency, high temperature and high voltage condition, wide band-gap compound materials (e.g. SiC, GaN, or InP) are demanded as replacements of Si [6–10]. Among these wide band-gap semiconductors, SiC receive attention because of the relatively high quality crystal substrates available by the progressing epitaxial growth technology. SiC exhibits a wide variety of poly-types, but only 4H-SiC and 6H-SiC are commercially available to date. It has been found that SiC offers a higher thermal conductivity, higher breakdown electric field, larger band-gap, and higher saturation velocity than Si. These principal physical properties are listed in Table 1.1 [7, 11, 12].

Table 1.1 Physical properties of wide band-gap semiconductor materials. [12]

	Si	3C-SiC	4H-SiC	6H-SiC	GaN
Band Gap (eV)	1.12	2.23	3.26	2.93	3.39
Break down Voltage (MV/cm)	0.3	1.2	2.5	2.8	3.3
Thermal conductivity (W/cmK)	1.5	4.9	4.9	4.9	2.0
Saturated velocity (cm/s)	1.7×10^7	2.0×10^7	2.2×10^7	1.9×10^7	2.7×10^7

The superior physical and electronic properties of SiC make it the foremost semiconductor material for short wavelength optoelectronics, and high-power/high-frequency electronic devices. Particularly because of the excellent heat resistant with high breakdown voltage, SiC is expected to open up a new market of power conversion devices for severe conditions of high-voltage (>10 kV), high temperature (>150 °C), and high-frequency (20 kHz) applications where Si technology is fundamentally inadequate.

The detailed merits of SiC are recited in the following paragraph [6–8, 13–14]:

A. Wide band-gap energy

Due to the wide band-gap over 3eV, electronic devices formed on SiC can operate at elevated temperatures without suffering performance degradation of the intrinsic properties from increasing thermal carriers. Also, this property allows SiC to IGBT for use in electric vehicles, short wavelength optoelectronics.

B. High breakdown voltage

SiC withstands a large voltage gradient (i.e. high electric field) over seven times greater than Si without breakdown (see Table 1.1). This high breakdown electric field enables the fabrication of high-voltage, high-power devices such as diodes, and power transistors, as well as high power microwave devices. Additionally, it allows the devices placed close to each other, providing high density device packing for integrated circuits.

C. High thermal conductivity

The thermal conductivity of SiC is excellent. Heat flows faster through SiC than other semiconductor materials. This property enables SiC devices to handle extremely high power current at severe high-temperature environments. Additionally, the high thermal conductivity is also beneficial

to maximize device packaging density due to efficient thermal dissipation.

D. High saturation velocity of electron

SiC devices can operate at high frequencies (RF and microwave) due to its high saturation electron drift velocity.

As discussed above, the thermo-physical properties allow SiC to offer tremendous benefits over other available semiconductors for a large number of industrial and military applications, such as IGBT for hybrid or electric vehicles, distributed controls for aircraft and so on. Table 1.2 summarizes the advantages and application field of SiC power devices.

Table 1.2 Application field and advantages of SiC power devices.

Device Characteristics	Advantages	Application field
High breakdown voltage	Large power capacity	Electric ships, HEV/EV
High current density	High reliability, downsizing	Space craft, Satellite
High operation temperature	Small cooling system	Power transmission/distribution
High switching speed	Reduced passive components	Energy exploring
Low power losses	High efficiency	HEV/HV, Motor drives

1.1.3 Die-attach technologies

In electronic packaging technology, interconnection materials are commonly categorized into first-level and second-level packaging. The former provides direct interconnection to the integrated circuit (IC) chip, which is generally called as “die”. The latter, in contrast, bonds the components on a printed wiring/circuit board (PWB, PCB) [15–16]. A schematic illustration of typical packaging structure is displayed in Fig. 1.2. Die-attachment to a substrate like PCB is one of the first-level packaging technologies that can be applied to integrated circuits (ICs), insulated gate bi-polar transistors (IGBTs), light emitting diodes (LEDs), quad flat packages (QFPs), and many other device components. It is thus a fundamental and necessary element of any packaging approach of semiconductor devices, as illustrated schematically in Figure 1.3.

In the electronic packaging technology, the die-attach interconnections require sufficiently higher melting point to assure that the bonded interface should not be re-melted during following assembly processes such as reflow soldering. For example, the melting point of die-attachment materials typically need to be above 280 °C when the reflow temperature is 210 – 250 °C. The die-attach layer supplies a major heat dissipation path into the devices, so that the relaxation of thermo-mechanical stress caused by the mismatch of the coefficients of thermal expansion (CTE) between die and substrate is critical issue in the production. The die-attach layer sandwiched between the devices and substrate not only needs to withstand cycled thermal stress, but also to buffer mechanical stress to protect more brittle parts like semiconductor crystals to ensure the proper function of device.

To obtain the aforementioned functions, high temperature solder is the most commonly used for die-attachment. High temperature solder using lead such as Pb-5wt%Sn of which liquidus temperature of 314 °C is one of the typical bonding materials used in die-attachment.

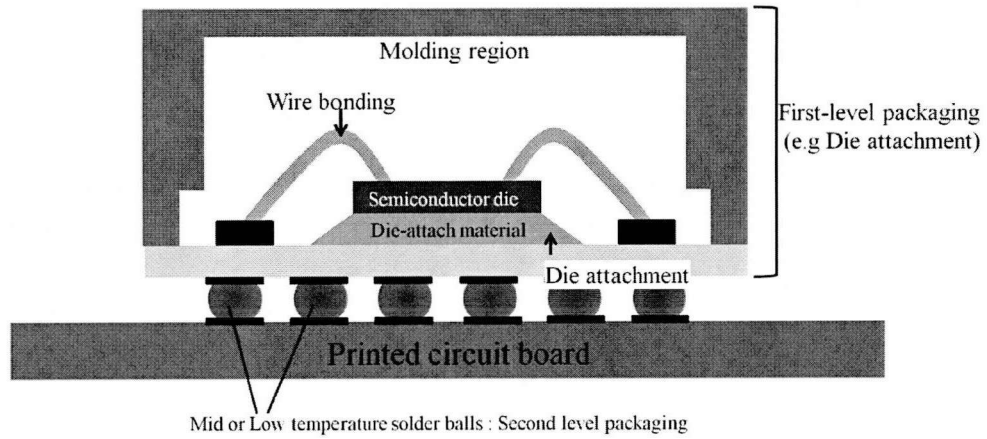


Fig. 1.2 Schematic illustration of a typical package structure [16].

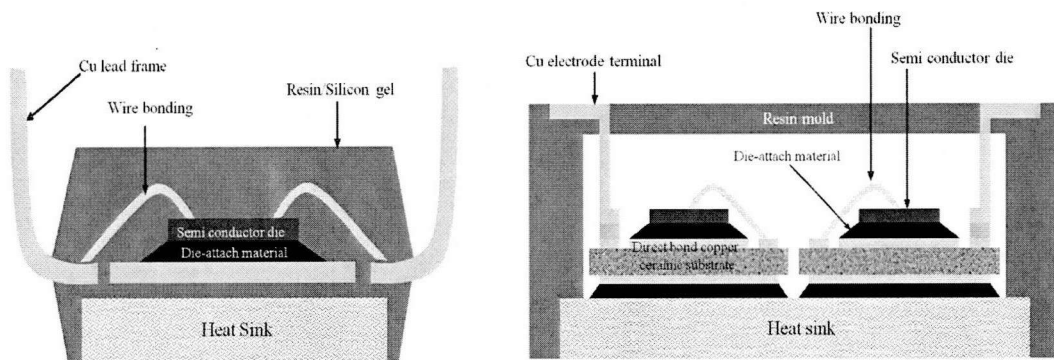


Fig. 1.3 Schematic structure of electronic device with die-attachment.

1.1.4 Conventional die-attach material: High-lead solders

High-lead solders (e.g. Pb–Sn, Pb–Ag, and Pb–In) are widely used in various types of applications in the first-level packaging [17]. High-lead content solders are currently being used as high-temperature solders in power semiconductor packages due to several favorable characteristics such as low cost, excellent wettability, and workability [17, 18]. In particular, Pb–Sn alloys containing 85–97 wt% Pb exhibit superior characteristics to others, with the lowest cost among them [18–20]. Thus, the Sn–Pb solders containing over 85 wt.% of Pb are popularly used as high-temperature solder material for the die-attachments and for bump joints in flip chip packages. Typical compositions of Pb–Sn solders are Pb–5Sn and Pb–10Sn, which have melting ranges of 300 – 314 and 268 – 301 °C, respectively [18–19, 21]. Figure 1.4 shows the binary phase diagram of Pb–Sn alloy.

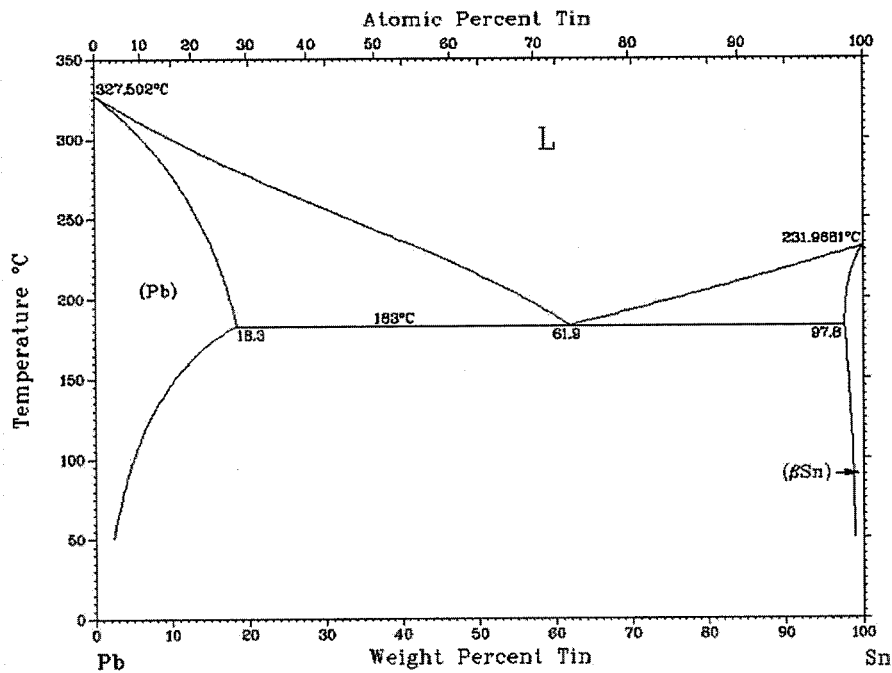


Fig. 1.4 Binary phase diagram of Pb–Sn alloy [21].

Chapter 1
Introduction

These lead-based solders exhibit numerous excellent properties, though they need to be completely eliminated from electronic applications in the near future under the Restriction of Hazardous Substances (RoHS) directive, which claims that Pb causes serious problems relating to both human health and the environment. Despite of the great effort to find lead-free die-attach materials, no replacement with Pb-Sn high temperature solders, partly because most of the researches have focused on developing middle or low temperature lead-free solders. For instance, Sn-37Pb solder has successfully been replaced by Sn-Ag-Cu [22–24] and Sn-Cu [22, 25] alloys with improved mechanical properties. Suitable candidate alloys for high temperature lead-free solder are rarely reported in the literature, and hence Pb-Sn solders are still being used in die-attachment. The establishment of a high-temperature lead-free solder applicable to die-attache has become one of the critical issues in the electronics packaging.

1.1.5 Requirements for lead-free die-attach materials

Solder alloys suitable for semiconductor die-attach need to have numerous characters in their materials properties such as thermal fatigue resistance, electrical/thermal conductivity, and oxidation resistance, as well as the basic mechanical properties of sound joining. In order to replace Si with SiC in power devices, it is necessary to establish a standard die-attachment technology including high-temperature lead-free solder materials. Even SiC has many advantages to Si, they are basically connected to the higher operating temperatures above 300 °C. The packaging of SiC power devices including die-attach need to be improved also to ensure such high temperature operation. Considering the harsh operating environment of SiC power devices, a good alternative die-attachment material should satisfy the following fundamental properties [22, 26–28]:

1. Melting temperature should be higher than 300 °C to withstand at the operating peak temperature approximately 300 °C.
2. Low elastic modulus and certain ductility to maintain a joint structure by relaxation of thermal stress.
3. Small thermal expansion to minimize thermal stress, particularly at reflow treatment.
4. Low electrical resistivity to reduce power loss.
5. High thermal conductivity for thermal dissipation of devices.
6. Thermal and mechanical reliability and durability, especially in fatigue resistance.
7. Sufficient workability to be thin wires or sheets.
8. Environmentally friendly within reasonable economical cost.
9. Airtightness not to break vacuum package.
10. Flux-less process.
11. No alpha ray emission.

1.2 Candidate of lead-free solders for silicon carbide die-attachment

In spite of a wide range of service environments and reliability requirements, only a limited number of solders have been proposed for SiC die-attachment because of the strict requirement of liquidus temperature. Figure 1.5 summarizes alloy systems which have liquidus temperature over 280 °C. In relation to the requirements mentioned above, the candidate materials for SiC die-attach application are briefly reviewed in the following section.

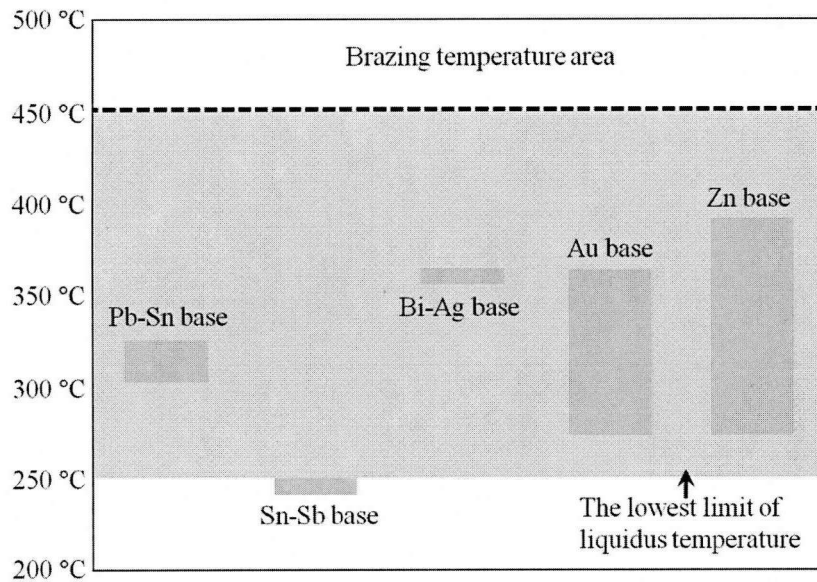


Fig. 1.5 Liquidus temperature of candidate of SiC die-attach materials [17, 21, 29–30].

1.2.1 Au-based die-attach materials

Au based solders are all Au-rich eutectic composition alloys such as Au-20Sn, Au-3Si, and Au-12Ge, and have melting temperature between 278 and 363 °C [17, 21–22]. Their properties are summarized in Table 1.3. Application of these alloys is often limited by the high cost of Au, though three typical Au-base solders are briefly discussed below.

Table 1.3 Au based die-attach materials [22, 29]

Solders (wt%)	Melting point (°C)	Thermal conductivity (W/m·K)	CTE (ppm)	UTS at 25 °C (MPa)	Electrical resistivity (IACS%)*
Au-20Sn	278	57.3	17.5	275	8.0
Au-3Si	363	27.2	14.9	220	15.6
Au-12Ge	361	44.5	13.0	185	7.2

**IACS: International Annealed Copper Standard [A unit of electrical conductivity for metals and alloys]*

A. Au-20Sn eutectic solder

The eutectic Au-Sn alloy that includes 20 wt.% of Sn corresponds to the Au rich eutectic point with a melting temperature of 280 °C (see Fig. 1.6). It has superior properties (e.g. creep resistance, low Young's modulus) to Pb-5Sn that has the similar melting point, so that it is widely used as a solder for high-temperature applications. The high thermal and electrical conductivity is particularly attractive for flip-chip bonding. However, the Au-20Sn solder alloy shows poor workability due to the own hard and moderately brittle nature. These properties mainly arise from the fact that it consists of two coexisting phases: *hcp* substitutional alloy (δ -AuSn) and orthorhombic intermetallic compounds (IMCs). According to the Au-Sn phase diagram [21] in Fig. 1.6, the composite displays

ζ -Au₅Sn + δ -AuSn microstructure at room temperature, and eutectic reaction of $L \leftrightarrow \zeta + \delta$ at 280 °C. The ζ -phase Au₅Sn is stable over a wide range of composition, while the δ phase of Mg-type hexagonal close packed structure (*hcp*) is mostly found at 280 °C. Consequently, the growth of the IMC crystals in the solid phase at lower temperature limits ductility of the *hcp* phase, and affects both the workability and joining property of the solder. In addition to all the problems above, the high cost of Au narrows the application range of Au–20Sn alloy as high temperature solder material.

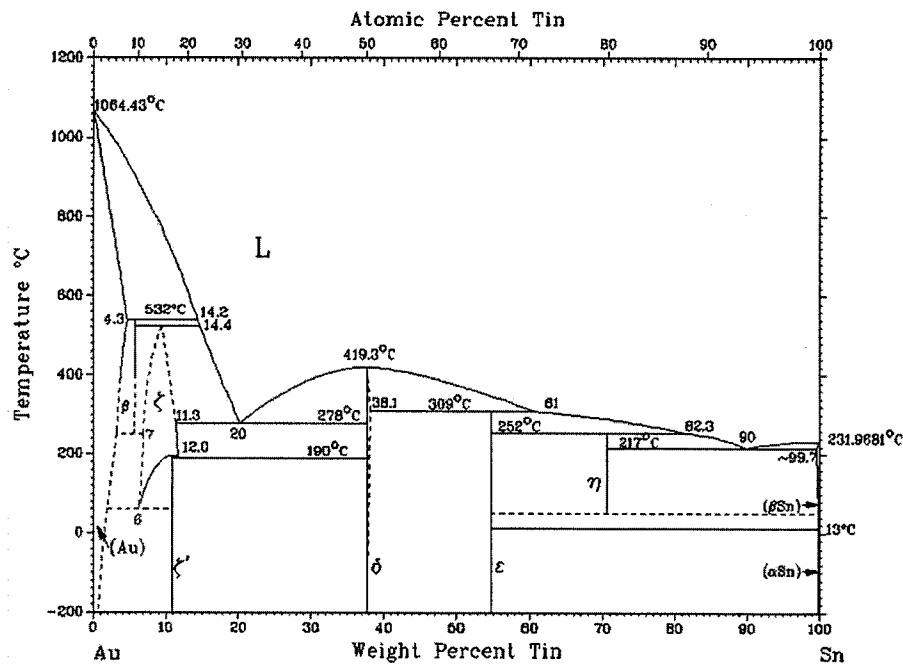


Fig. 1.6 Au–Sn binary phase diagram [21].

B. Au–Ge eutectic solders

Au–Ge eutectic solder (Au–12 wt.% Ge) is one of the most attractive candidate as similar to the Pb–Sn system because of no intermetallic phase found in the alloy, and also because of the adequate eutectic temperature of 360 °C as seen in Fig. 1.7. Au–Ge solders can be used as ternary alloy with a

Chapter 1
Introduction

trace amount of Sb or In [31]. Au-0.24Ge-0.05Sb alloy is a promising candidate for die-attach solder applications, where high ductility of solder alloy is required to relax thermal stresses. Au-0.18Ge-0.10In is also an alternative lead-free solder for optoelectronic packaging because of the high strength, the low elastic modulus, and the stable microstructure at high-temperatures.

The problem of developing Au-Ge based alloys replacing present high-lead solders is the cost associated with the price of Au. The price of Ge is also high so that these alloy systems are less cost-efficient. Furthermore, Au-Ge based alloys tend to form dross than the other Au-base solders.

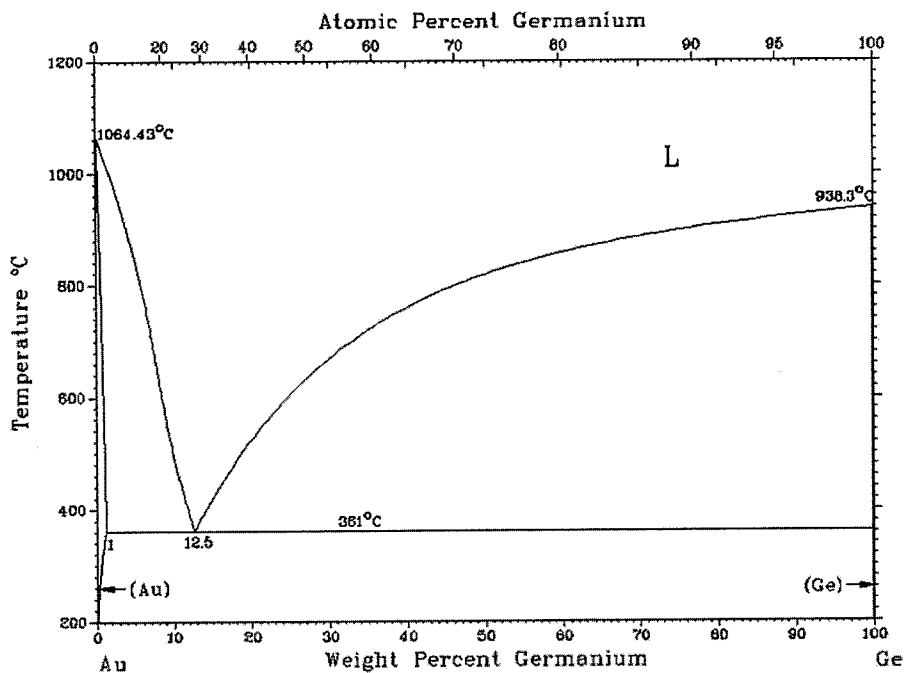


Fig. 1.7 Au-Ge binary phase diagram [21].

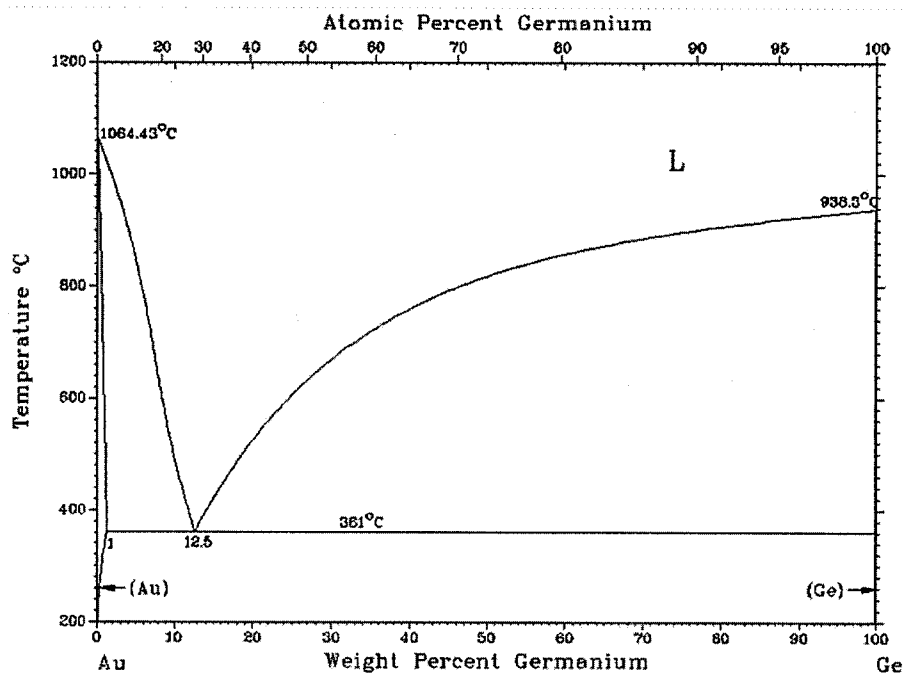


Fig. 1.8 Au–Si binary phase diagram [21].

C. Au–Si eutectic solder and eutectic bonding

Au–Si eutectic alloy has a composition of Au–3 wt.%Si and a melting point of 363 °C. It is a simple eutectic composition, and IMCs do not form in the entire composition of Au–Si alloy as seen in Fig. 1.8. However, Au–Si alloy indicates inter-diffusion and the liquidus line of Au–Si alloy would become dramatically higher with a small increasing of Si content when Au–Si alloy joined with a Si die. Special care should be taken in hot-rolling process of Au–3Si solder due to the high brittleness.

Au–Si eutectic bonding is another method of packaging, but not used as a solder alloy. This is a widely used bonding process for Si die-attach or wafer-to-wafer bonding, particularly in microelectro-mechanical systems (MEMS) packaging [32–34]. However, several problems are reported in the literature such as the formation of air voids and craters [35–37]. Void formation may cause delamination at the interface between a Si die and Au–Si alloy [36]. Hence an adequate barrier layer of metallization is required to avoid the mutual dissolution between a Si die and Au–Si alloy. Otherwise, a new type of high temperature alloy should be developed.

Chapter 1
Introduction

As reviewed above, Au-based solder alloys can be used for flux-less die-attach process of Au metalized chips in the semiconductor packaging. Although these solders possess a proper melting temperature around 300 °C, they have serious drawbacks that make it difficult to replace the high-lead solders in commercialized broad applications. These demerits can be summarized as follows:

- High price of Au: Au is too expensive precious metal to be used in common electronics device packaging. The price of gold has been increasing rapidly about twice during the last four years (see Table 1.4).
- Poor workability: Au–20Sn and Au–3Si solders have brittle nature to fabricate solder products like wires, foils, or powders.
- Massive IMCs formation and inferior wettability

Table 1.4 Average price of pure metal in solder alloys [38, 39]

Metal	Price (USD/kg) on November, 2008	Price (USD/kg) on September, 2012
Gold (Au)	28,646.87	57,531
Silver (Ag)	369.28	1,121
Tin (Sn)	15.10	21.45
Aluminum (Al)	1.98	2.11
Copper (Cu)	3.76	8.28
Bismuth (Bi)	9.86	28.45
Lead (Pb)	1.47	2.32
Zinc (Zn)	1.12	2.14
Antimony (Sb)	4.51	14.99

1.2.2 Bi–Ag based die-attach materials

Owing to Bi having proper melting temperature of 271 °C, Bi and its alloys become candidate die-attach materials for high temperature application. Unfortunately, Bi has brittle nature as common solders, and has poor thermal/electrical conductivity. To improve these drawbacks, Ag was generally adopted for alloying. Bi–Ag eutectic system offers an acceptable melting point as shown in Fig. 1.9. The eutectic temperature is 262.5 °C at the eutectic composition, Bi–2.5 wt.% Ag. Bi–2.5Ag solder does not form IMC, and low solubility of Ag in Bi inhibits solid-solution strengthening. The solder alloy are still under development to improvements the inferior thermal/electrical conductivity as well as poor workability, i.e., brittle Bi phase. Raising Ag content up to about 11 wt.% improves the electrical conductivity, e.g. 86.5 $\mu\Omega\cdot\text{cm}$ for Bi–11Ag alloy, considerably reducing the higher resistivity of 116.5 $\mu\Omega\cdot\text{cm}$ for Bi–2.5Ag eutectic alloy [40, 41]. The thermal/electrical properties of pure Bi, Bi–Ag alloy, conventional Pb–5Sn solder, and Au–20Sn lead-free candidate alloys are summarized in Table 1.5.

Despite the considerable improvements in ductility and thermal/electrical conductivity, Bi–Ag solder alloys show higher electrical resistivity than other solder alloys (e.g. Pb–5Sn, and Au–20Sn). The brittle fracture and poor thermal conductivity are shown in Fig. 1.10 and 1.11, respectively. Bi–Ag based solder alloys thus need more improvements in thermal/electrical conductivity, as well as brittleness for commercial applications.

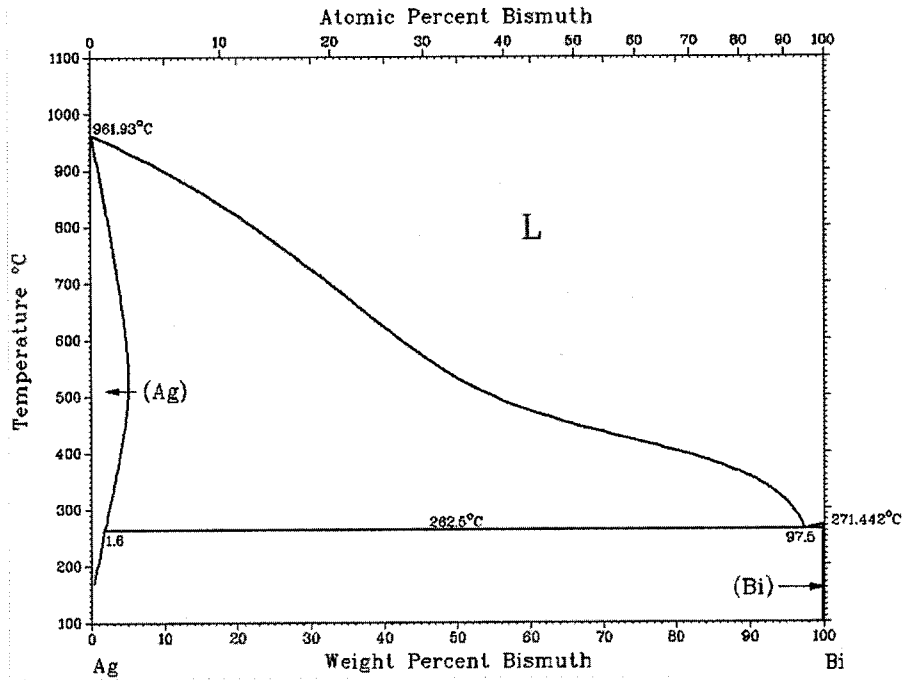


Fig. 1.9 Bi-Ag binary phase diagram [21].

Table 1.5 Pure Bi and Bi-based high temperature solders as compared with other lead-free solder candidate [22, 29, 40].

Solders (wt%)	Liquidus temperature (°C)	Thermal conductivity (W/m·K)	Electrical resistivity ($\mu\Omega/cm$)
Bi	271.4	9.0	117.0
Bi-2.5Ag	263	9.2	116.1
Bi-11Ag	360	10.4	87.3
Pb-5Sn	314	34.7	18.4
Au-20Sn	280	57.3	16.1

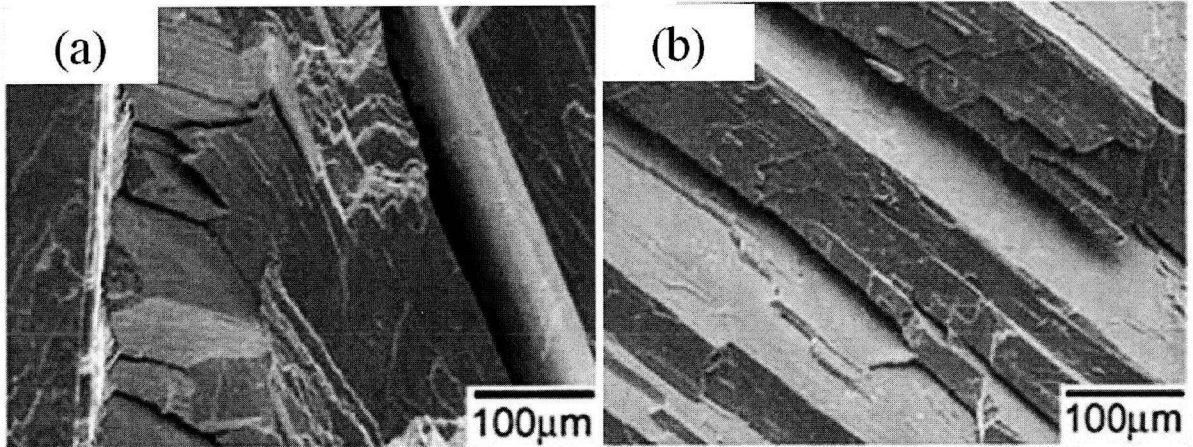


Fig. 1.10 The typical brittle fracture surfaces (SEM):

(a) Pure Bi, (b) Bi-2.5Ag, and (c) Bi-11Ag [42].

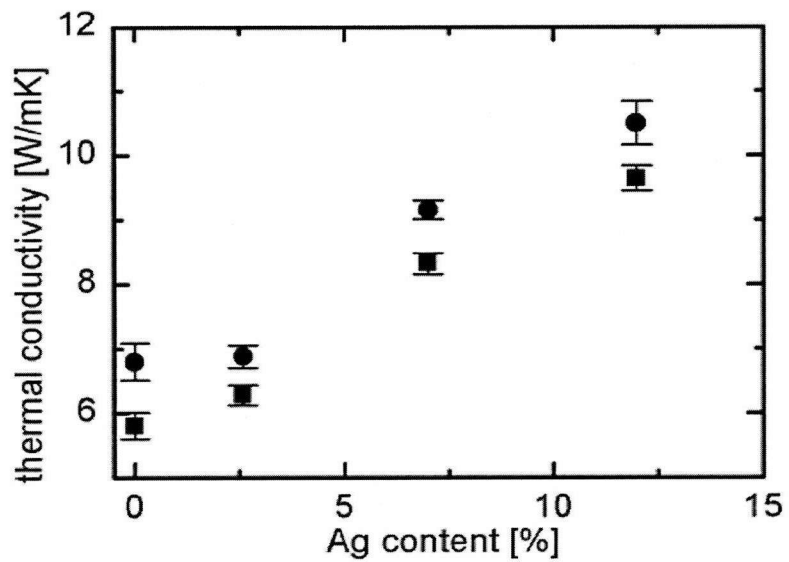


Fig. 1.11 Thermal conductivity of Bi-based solder alloys [43].

1.2.3 Sn–Sb based die-attach materials

Sn has been used as primary element in most of solder alloys due to its excellent workability, wettability, and reasonable cost. Sn-based solders are hence proposed for high temperature lead-free solder. The addition of Sb in Sn assigns the proper melting temperature and more reliability in soldering. As seen in Fig. 1.12, Sn–Sb binary system has no eutectic reaction, and the liquidus temperature increases with increasing Sb content. For this reason, numerous studies have reported the interfacial reactions on metallic substrates, and mechanical properties of Sn–Sb solder alloys [44–46]. Among various Sn–Sb alloys reported, Sn–5Sb is considered to have a great potential to replace high-lead solders in application due to the excellent microstructure stability and mechanical properties of the joining interface obtained by Sn–5Sb solder [47]. Staying at the near-peritectic composition in the phase diagram (see Fig. 1.12), Sn–5Sb alloy has a melting point of 245 °C, which may be too low for SiC die-attach applications.

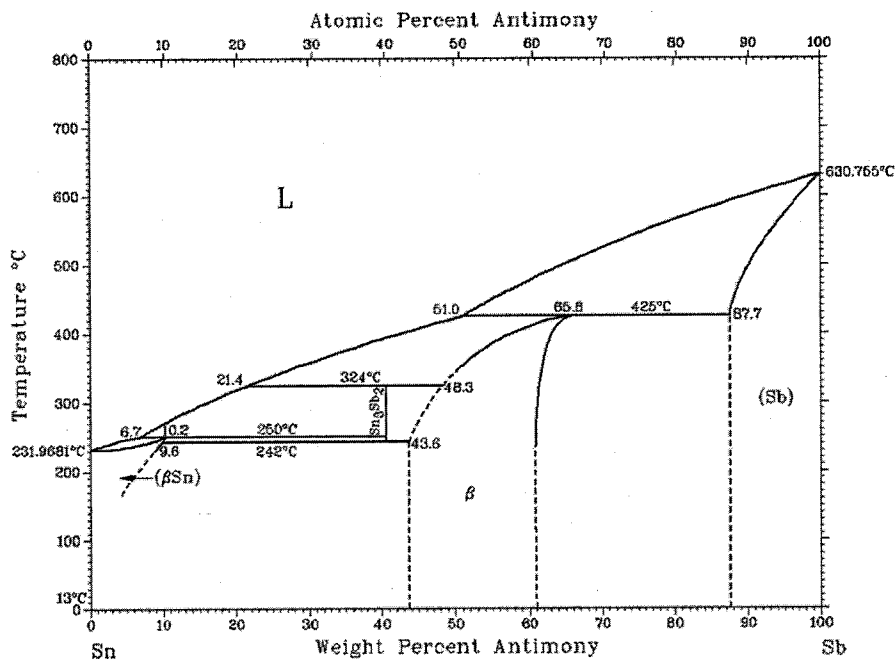
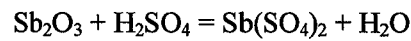
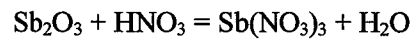
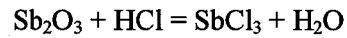
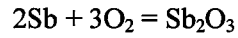


Fig. 1.12 Sn–Sb binary phase diagram [21].

Chapter 1
Introduction

To increase the melting temperature of Sn–5Sb solder some literature proposed Sn–10Sb binary alloy. Although Sn–10Sb alloy has the melting point of 270 °C, the amount of Sb addition beyond 5 wt.% forms hard and brittle IMC phases such as β -SnSb and Sn_3Sb_2 as found in the phase diagram of Fig. 1.12. Moreover, toxic sulfide or chloride of Sb can be produced through the following reaction path [48].



The low melting temperature for high-temperature soldering, high cost of Ag, and toxicity of Sb thus restrict wide application of Sn–Sb solder alloys.

1.2.4 Zn–Al based high temperature lead-free solders

Zn-based solders are one of the attractive candidate alloys due to the beneficial cost, and typically used with alloying Al to improve the poor wettability in the atmospheric conditions. Zn–Al solder alloys have potential merits, as listed below [17, 26, 49].

- The joining strength with Zn-based solders is typically 2-3 times higher than commercial high-lead solders (5-10 MPa).
- They are cost-efficient compared with almost all other solder alloys (see Table 1.4).
- They are light weight materials due to the low density of Zn (7.13 g/cm^3), which is approximately two-thirds of Pb–5Sn solder (11.2 g/cm^3).
- They possess much higher thermal and electrical conductivity.

Zn–6 wt.% Al alloy with a eutectic melting temperature of $381 \text{ }^\circ\text{C}$ is a very interesting candidate for high temperature applications. Zn–6Al alloys are used as high-temperature solders for various applications, especially in die-attaching process. Despite the low cost, there are several drawbacks when considering the use of Zn–6Al alloys as high temperature solder as following [26, 50–52].

- Zn is a corrosive metal and this may severely limit the lifespan under typical service conditions.
- These alloys exhibit relatively poor wetting behavior due to the high oxygen affinity of both Zn and Al.
- Zn–Al eutectic alloy exhibits a dendrite microstructure and is relatively hard in comparison to high lead content solders.

Moreover, Zn–Al solders form and grow some intermetallic compounds (IMCs) such as β

(disordered *bcc*) or β' (ordered *bcc*), γ (Cu_5Zn_8) and ε (disordered *hcp*), when it is used with popular Cu substrate. In particular, the layer thickness of γ -phase rapidly increases above 200 °C.

Therefore, many researchers have discussed methods to improve the drawbacks of Zn–Al solder alloys, and micro-alloying is regarded as one of the most effective ways. The effects of Cu, Sn, Mg and Ga additions into Zn–Al alloys have been investigated, but the data available today is still sparse. The problems of Zn–Al solders thus have not yet been solved as review bellow.

A. Zn–Al–Cu ternary alloys

Cu addition to Zn–4Al solder is observed to suppress the excessive consumption of substrate Cu, and results in decreased activation energy of IMC growth. Therefore, Zn-base solders like Zn–(4–6) wt.% Al–(1–5) wt.% Cu have been developed for ultra-high temperature applications [52, 53]. These solders are designed to have liquidus temperatures between 382 and 402 °C. According to Kang et al.'s report [53], the increase of Al content from 4.0–6.0 wt.% relatively improves the spreadability and electrical resistivity. As the Al and Cu contents increases, the fraction of α - η eutectic/eutectoid phases increases, resulting in higher Vickers hardness and tensile strength. Although Zn–Al–Cu has excellent hardness and tensile strength, its elongation limit is below 10 % [52, 53], which implies that Zn–Al–Cu solder needs to improvement the ductility.

B. Zn–Al–Mg–X quaternary alloys

Zn–4Al–3Mg–3Ga has been investigated by Shimizu et al. [26] to replace Pb–5Sn solder for die-attaching use. According to this research, Zn–4Al–3Mg–3Ga alloy's solidus and liquidus are 309 and 347 °C, respectively. A small amount of voids was achieved at 320 °C or higher in the die-attaching test case of Ag metalized lead-frame and Au plated dummy die. Although this alloy exhibited a sound die-attach status, poor workability and a low capacity for stress relaxation at room temperature may cause a problem. Shimizu et al. reported no failure was observed until 1000 cycles

or until 1000 h of thermal cycle tests between -65 and 150 °C [26]. However, Haque et al. reported the formation of cracks under the same thermal cycle conditions as shown in Fig. 1.13 [54]. Beside, Ga is known to cause liquid metal embrittlement in Al by significantly reducing the cohesion between aluminum grains, and thus lead to severe embrittlement failure [55].

To solve the liquid metal embrittlement of Ga, Cheng et al. proposed another alloy design with the addition of Sn instead of Ga [56]. These Zn–Al–Mg–Sn alloys can reduce the solidus and undercooling. Such Sn addition, however, may deteriorate the ductility of Zn–4Al–3Mg alloy. Thus, the amount of Sn addition should be controlled carefully.

For these reasons, Zn–Al based solders have greatly limited the adoption despite they have the potential benefits.

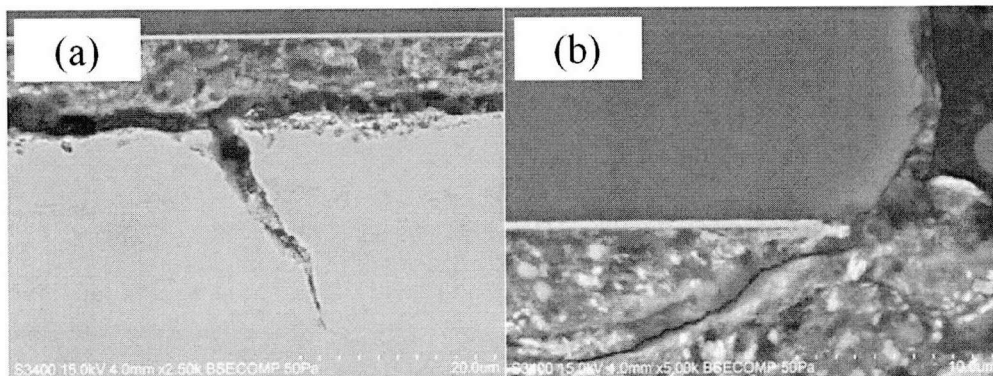


Fig. 1.13 SEM micrograph of die attach samples after 1,000 thermal cycle test with Zn–Al–Mg–Ga solder (a) substrate side, and (b) dummy die side [54].

1.2.5 Zn–Sn based high temperature lead-free solders

As mentioned in the former section, Zn-based alloys possess many potential benefits such as low cost, high strength, proper melting temperature, and thermal/electrical conductivity. Nevertheless, Zn–Al solder alloys are not in practical use due to their serious drawbacks (e.g. brittleness and formation of massive IMCs). Extensive researches have been done in search of alternative Zn-based alloys that do not form IMCs in microstructure with maintaining a sufficient ductility. Zn– x Sn alloys ($x = 20$ – 40 wt.%) have been proposed as a new class of high temperature lead-free solders by the author's research group. Zn–Sn alloy possesses suitable features for high temperature solder applications including relatively high liquidus line (seen Fig. 1.14), along with the fact that IMCs are unable to form in the whole range of composition ratio. Fig. 1.15 shows the typical microstructure of Zn–Sn solders where the dark and bright parts respectively represents the primary α -Zn and eutectic Sn–Zn phases without any formation of IMCs. The alloys also show a much improved ductility compared to other Zn-based alloys, excellent electrical properties, and oxidation resistance at high temperature/humidity [56, 57]. The thermal conductivity of Zn– x Sn ($x = 20, 30, \text{ and } 40$) have been investigated by Kim et al. [58–60], and the results demonstrate that the thermal conductivities of Zn–Sn alloys of 100–106 W/m K are sufficiently high and superior to those of both Au–20Sn (59.1 W/m K) and Pb–5Sn (35.6 W/m K). The shear strength of soldered Cu/Zn–Sn/Cu joint reaches 30–34 MPa, being higher than that of a Pb–5Sn solder (26.2 MPa) [58]. Mahmudi and Eslami have studied the high-temperature shear strength of bulk Zn–Sn solders, and concluded that the yield stress of Zn–Sn solder alloys at 298 and 373 K is much higher than that of a Pb–5Sn solder [61]. Impression creep behavior of Zn–20Sn, Zn–30Sn, and Zn–40Sn solders have been studied by Mahmudi and Eslami as well [62].

Zn–Sn alloys are believed to be one of the most promising lead-free candidates. However, one of the concerns for this alloy as a high-temperature solder is the liquid formation at its eutectic

temperature of 199 °C. Due to this reason, the eutectic Sn–Zn alloy has been used only as a low-temperature solder. This is a critical drawback of the material to be applied for SiC die-attachment, because SiC power devices are supposed to have a maximum operating temperature beyond 300 °C. The operation temperature must be kept below 200 °C when Zn–Sn high temperature solder alloy is used.

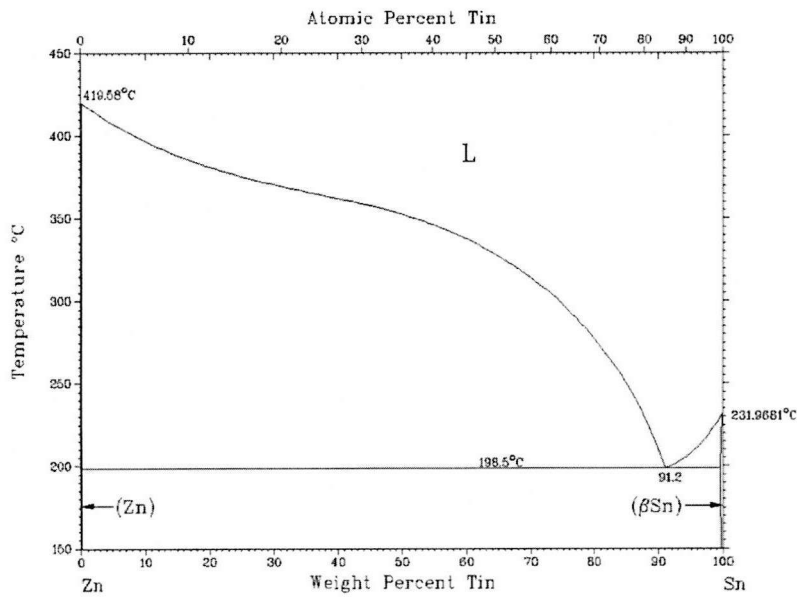


Fig. 1.14 Zn–Sn binary phase diagram [21].

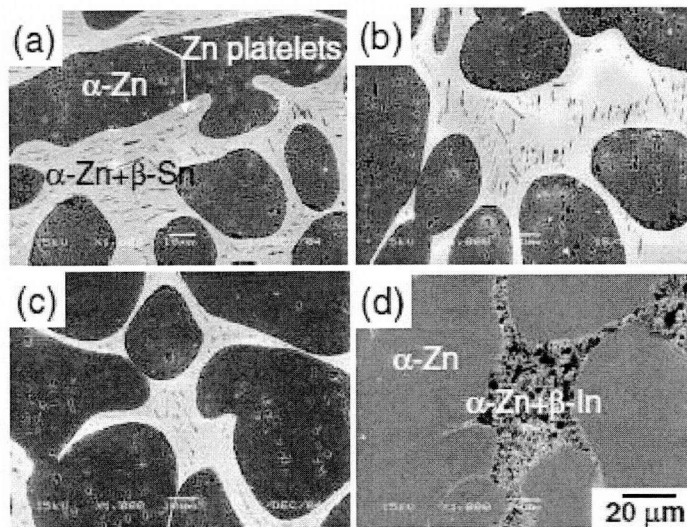


Fig. 1.15 Typical microstructures of the Zn–Sn solders;

Chapter 1
Introduction

(a) Zn-40Sn, (b) Zn-30Sn, (c) Zn-20Sn, and (d) Zn-30In alloys [57].

The die-bonding materials have a key role for device packaging of wide-gap power semiconductor like SiC because of the severe requirements in both reliability and heat management. However, the currently available lead-free materials introduced above do not satisfy the requirements. Therefore, it is necessary to develop new high-temperature die-bonding materials for wide-gap semiconductors packaging.

1.3 Motivation and objective of the thesis

1.3.1 Pure Zn die-attachment

As for the conventional power devices, the maximum temperature in service should be below 150 °C, which can be reached in the engine room of automobiles, it is preferably in the range of temperature below 100 °C. The aforementioned candidates can fulfill this temperature requirement so far. SiC is expected to replace conventional Si power devices, and be used without any cooling system causing high operating temperatures in the range of 250 °C–300 °C, as already introduced in section 1.1.2. Owing to the requirements of excellent reliability and heat management, the interconnection essential to the die attachment in power device has a key role to develop such SiC applications. Unfortunately, none of the current lead-free materials as stated in the former sections is sufficient for SiC power devices operated at high temperatures up to 300 °C. Particularly for automobiles, ceasing the use of radiators is favorable in reducing the total weight and eliminating a fragile part for better reliability.

The author's research group has proposed a new heat-resistant die-attachment structure for SiC on the Si₃N₄ substrate by using pure Zn solder, which has the great advantage of inexpensiveness, and of excellent thermal-shock resistance between –50 and 300 °C, in comparison with conventional Pb–5Sn [63].

However, the crystal structure of Zn is widely known hexagonal close packed (*hcp*), which usually has some brittleness due to the limited numbers of slip/twinning systems. In addition, pure Zn is a relatively active element resulting in easy oxidation at a typical operating temperature of SiC power devices. Pure Zn reserves certain concerns particularly in brittle and oxidation-sensitive features to be used as an ultra-high-temperature solder. Therefore, the author evaluates the effects of adding minor elements on the characteristics of Zn and investigates the interfacial reactions. The author selected Ca, Mn, Cr, and Ti as minor elements because they are active metals, and hence are expected to form fine-grain structures [21], scavenge impurities in the matrix, and form a protective oxide layer on the

surface of Zn [23].

1.3.2 Objective of this thesis

In order to establish a SiC die-attach material, the improvement of some drawbacks pure Zn solder is considered. As described above, pure Zn may have certain drawbacks for use in high-temperature solders, e.g. the brittleness nature and oxidation that come from the crystal structure and low free-energy of oxide formation. To improve such kinds of these properties of metals, many studies have been conducted on the small amount of additives of second elements. In case of lead-free solders or die-attach materials, these researches have been focused mainly for middle temperature Sn-based solders. Moreover, Zn easily forms intermetallic compounds (IMCs) with metal substrates like Cu or Ni, and IMC growth significantly decreases the mechanical properties of the solder joints.

The primary objective of this thesis is thus to enhance the characteristics of pure Zn through minor additions of metal elements toward SiC die-attachment application. To verify relaxation of thermo-mechanical stress and suppression of oxidation during the device operation, the materials properties are investigated by tensile tests and high-temperature accelerated oxidation tests. The interfacial reaction is also studied focusing on the IMC formations which are the major origin of poor strength and reliability in metal joining. Suppression of IMCs growth in solder joints is thus important issue to the electronics industry. In this study, SiC die-attachment with minor element added solders were carried out on a silicon nitride (Si_3N_4) direct bonded copper (DBC) substrate. The joining properties and reliability of die-attach have been examined with thermal cycle tests.

Outline of the thesis

This thesis consists of six chapters including the current chapter 1. This chapter describes the objectives of the research, as well as a brief introduction to the power devices and the die-attach technologies. A limitation of the presently available alloys for SiC die-attachment is also reviewed, particularly for Au, Bi, Sn, and Zn based alloys. The potential of pure Zn is also addressed, on the basis of a new concept for die-attach material.

In chapter 2, minor additions of typical active elements, namely Ca, Mn, Cr, and Ti, are adopted to enhance the ductility and oxidation resistance of pure Zn. The ductility of the modified materials is investigated by tensile tests, and the oxidation resistance evaluated by thermal gravimetric analysis (TGA).

In chapter 3, the interface properties between a Cu substrate and minor elements added Zn alloys is investigated. IMC formations at the interface are scrutinized in connection with the degradation of joining strength and reliability during thermal aging tests.

In chapter 4, the joining property of the SiC die-attachment by soldering with minor elements added Zn is reported. Thermal cycling tests are carried out, and the change in interface structure and joining strength of the solder joints are discussed.

In chapter 5, the attractive application of pure Zn for Si wafer bonding is presented. By using pure Zn as solder, a uniform and void-free bonding process is realized without metallization of Si wafers. The results are compared with conventional Au-20Sn solder.

In chapter 6, the results obtained in the present study are summarized, and suggestions for future works are presented.

REFERENCES

- [1] B.J. Baliga, *"Power Semiconductor Devices"*, PWS Publishing Company, (1995).
- [2] R.R. Tummala, E.J. Rymaszewski and A.G. Klopfenstein, *"Microelectronics Packaging Handbook, Part II, Semiconductor Packaging"*, Chapman & Hall, (1996).
- [3] R.F. Pierret, *"Semiconductor Devices Fundamentals"*, Addison Wesley, (1996).
- [4] http://www.semicon.toshiba.co.jp/eng/prd/pdf_presen/tr_IEGT_200502_e.pdf.
- [5] J.G. Bai, Z.Z. Zhang, J.N. Calata, and G.Q. Lu, *"Low-temperature sintered nanoscale silver as a novel semiconductor device-metallized substrate interconnect material"*, IEEE Trans. Compon. Packag. Technol. 29 (2006) 589.
- [6] P.G. Neudeck, R.S. Okojie, L.Y. Chen, *"High-temperature electronics - A role for wide bandgap semiconductors?"*, Proc. IEEE 90 (2002) 1065.
- [7] H.S. Chin, K.Y. Cheong, A.B. Ismail, *"A Review on Die Attach Materials for SiC-Based High-Temperature Power Devices"*, Metall. Mater. Trans. 41B, (2010) 824.
- [8] W. Wondrak, R. Held, E. Niemann, U. Schmid, *"SiC devices for advanced power and high-temperature applications"*, IEEE Trans. Ind. Electron. 48 (2001) 307.
- [9] M.A. Khan, Q. Chen, M.S. Shur, B.T. Dermott, J.A. Higgins, J. Burm, W.J. Schaff, L.F. Eastman, *"GaN based heterostructure for high power devices"*, Solid-State Electron. 41 (1997) 1555.
- [10] A. Katz, C.H. Lee, K.L. Tai, *"Advanced metallization schemes for bonding of InP-based laser devices to CVD-diamond heatsinks"*, Mater. Chem. Phys. 37(1994) 303.
- [11] L.M. Tolbert, B. Ozpineci, S.K. Islam, M. Chinthavali, *"Wide Bandgap Semiconductors for Utility Applications"*, IASTED International Conference on Power and Energy Systems (2003) 317.
- [12] S. Takashi, *"SiC Power Devices (in Japanese)"*, Toshiba review 59 (2004) 49.
- [13] J.C. Zolper, *"A review of junction field effect transistors for high-temperature and high-power electronics"*, Solid-State Electron. 42 (1998) 2153.

- [14] V.E. Chelnokov and A.L. Syrkin, “*Surface barrier height in metal-SiC structures of 6H, 4H and 3C polytypes*”, Mater. Sci. Eng. B 46 (1997) 248.
- [15] K.J. Puttlize (Ed) and K.A. Stalter, “*Handbook of Lead-free solder Technology for Microelectronic Assemblies*”, Marcell Dekker Inc., USA (2004).
- [16] K. Gilleo (Ed.), “*Area array packaging handbook: manufacturing and assembly*”, McGrawHill, New York, USA (2001).
- [17] G. Humpston and D.M. Jacobson, “*Principles of Soldering and Brazing*”, ASM international, March (1993).
- [18] K.N. Tu and K. Zeng, “*Tin-Lead (Sn-Pb) solder reaction in flip chip technology*”. Mater. Sci. Eng. R34 (2001) 1.
- [19] L.N. Ramanathan, J.W. Jang, J.K. Lin, and D.R. Frear, “*Solid-State Annealing Behavior of Two High-Pb Solders, 95Pb5Sn and 90Pb10Sn, on Cu Under Bump Metallurgy*”, J. Electron. Mater. 34 (2005) L43.
- [20] Chih-ming Chen, Kai-jheng Wang, and Ko-chieh Chen, “*Isothermal solid-state aging of Pb–5Sn solder bump on Ni/Cu/Ti under bump metallization*”, J. Alloys Compd. 432 (2007) 122.
- [21] T.B. Massalski, “*Binary alloy phase diagrams 2nd Ed.*”, ASM international, USA, (1992).
- [22] K. Suganuma, “*Handbook of Lead-free Soldering Technology and Materials (in Japanese)*”, Kougyou-chousakai Ltd., Japan, (2007).
- [23] K.S. Kim, S.H. Huh, and K. Suganuma, “*Effects of intermetallic compounds on properties of Sn–Ag–Cu lead-free soldered joints*”, J. Alloys Compd. 352 (2003) 226.
- [24] K.S. Kim, S.H. Huh, and K. Suganuma, “*Effects of fourth alloying additive on microstructures and tensile properties of Sn–Ag–Cu alloy and joints with Cu*”, Microelectro. Reliab. 43 (2003) 259.
- [25] S.H. Huh, K.S. Kim, and K. Suganuma, “*Effects of Ag Addition on the Microstructural and Mechanical Properties of Sn-Cu Eutectic Solder*”, Mater. Trans. 42 (2001) 739.

- [26] T. Shimizu, H. Ishikawa, I. Ohnuma, and K. Ishida, “*Zn-Al-Mg-Ga Alloys as Pb-free Solder for Die-Attaching Use*”, J. Electro. Mater. 28 (1999)
- [27] J.H. Kim, S.W. Jeong, and H.M. Lee, “*Thermodynamics-Aided Alloy Design and Evaluation of Pb-free Solders for High-Temperature Applications*”, Mater. Trans. 43 (2002) 1873.
- [28] K. Suganuma, “*Lead-Free Soldering in Electronics: Science, Technology, and Environmental Impact*”, Marcel Dekker Inc, (2003).
- [29] E.A. Brandes and G.B. Brook, “*Smithells metals reference book 7th edition*”, Butterworth Heinemann, UK, (1992).
- [30] E.P. Wood, K.L. Nimmo, “*In search of new lead-free electronic solders*”, J. Electron. Mater. 23 (1994) 709.
- [31] V. Chidambaram, J. Hald, and J. Hattel, “*Development of Au-Ge based candidate alloys as an alternative to high-lead content solders*”, J. Alloy. Compd. 490 (2010) 170.
- [32] J.B. Lasky, “*Wafer bonding for silicon-on-insulator technologies*”, Appl. Phys. Lett. 48 (1986) 78.
- [33] M. Shimbo, K. Furukawa, K. Fukuda, and K. Tanzawa, “*Silicon-to-silicon direct bonding method*”, J. Appl. Phys. 60 (1986) 2987.
- [34] R.W. Bower, M.S. Ismail, and S.N. Farrens, “*Aligned Wafer Bonding: A Key to Three Dimensional Microstructures*”, J. Electron. Mater. 20 (1991) 383.
- [35] R.F. Wolfenbittel, “*Low-temperature intermediate Au-Si wafer bonding: eutectic or silicide bond*”, Sens. Actuators A 62 (1994) 680.
- [36] Jin-Wook Jang, Scott Hayes, Jong-Kai Lin, and Darrel R. Frear, “*Interfacial reaction of eutectic AuSi solder with Si(100) and Si(111) surfaces*”, J. Appl. Phys. 95 (2004) 6077.
- [37] Errong Jing, Bin Xiong, and Yuelin Wang, “*The Bond Strength of Au/Si Eutectic Bonding Studied by IR Microscope*”, IEEE Trans. Electron. Packag. Manuf. 33 (2010) 31.
- [38] The public official price in London metal exchange Ltd., <http://www.lme.com> (2012. 10. 04)

- [39] Price report in London metal exchange Ltd., [http:// www.metalprice.com](http://www.metalprice.com) (2012. 10. 08)
- [40] J.M. Song, H.Y. Chuang, and Z.M. Wu, “*Interfacial reactions between Bi-Ag high temperature solders and metallic substrates*”, J. Electron. Mater. 35 (2006) 1041.
- [41] J.M. Song and H.Y. Chuang, “*Faceting Behavior of Primary Ag in Bi-Ag Alloys for High Temperature Soldering Applications*”, Mater. Trans. 50 (2009) 1902.
- [42] J.M. Song, H.Y. Chuang, and T.X. Wen, “*Thermal and Tensile Properties of Bi-Ag Alloys*”, Metall. Mater. Trans. A 38 (2007) 1371.
- [43] M. Rettenmayr, P. Lambracht, B. Kempf, and M. Graff, “*High Melting Pb-Free Solder Alloys for Die-Attach Applications*”, Adv. Eng. Mater. 7 (2005) 965.
- [44] K. Suganuma, “*Advances in lead-free electronics soldering*”, Curr. Opin. Solid State and Mater. Sci. 5 (2001) 55.
- [45] S.W. Chen, P.Y. Chen, and C.H. Wang, “*Lowering of Sn-Sb alloy melting points caused by substrate dissolution*”, J Electron Mater 35 (2006) 1982.
- [46] R.M. Shalaby, “*Influence of indium addition on structure, mechanical, thermal and electrical properties of tin-antimony based metallic alloys quenched from melt*”, J. Alloy. Compd. 480 (2009) 334.
- [47] R. Mahmudi, A.R. Geranmayeh, M. Bakherad, M. Allami, “*Indentation creep study of lead-free Sn-5% Sb solder alloy*” Mater Sci Eng A 457 (2007) 173.
- [48] The Materials Safety Data Sheet from National Fire Protection Association, USA, <http://www.nfpa.org> (2010. 04).
- [49] F. Porter, “*Zinc Handbook – Properties, Processing, and Use in Design*”, Marcell Dekker Inc., USA, (1991).
- [50] V. Chidambaram, J. Hattel, and J. Hald, “*High-temperature lead-free solder alternatives*” Microelectron. Eng. 88 (2011) 981.
- [51] M. Rettenmayer, P. Lambracht, B. Kempf, and C. Tschudin, “*Zn-Al Based Alloys as Pb-Free Solders for Die Attach*”, J. Electron. Mater. 31 (2002) 278.

- [52] S.J. Kim, K.S. Kim, S.S. Kim, C.Y. Kang, and K. Suganuma, “*Characteristics of Zn-Al-Cu alloys for high temperature solder application*”, Mater. Trans. 49 (2008) 1153.
- [53] N.H. Kang, H.S. Na, S.J. Kim and C.Y. Kang, “*Alloy design of Zn-Al-Cu solder for ultra high temperatures*”, J. Alloy. Compd. 467 (2009) 246.
- [54] A. Haque, B.H. Lim, A. S. M. A. Haseeb, H.H. Masjuki, “*Die attach properties of Zn-Al-Mg-Ga based high-temperature lead-free solder on Cu lead-frame*”, J Mater Sci: Mater Electron. 23 (2012) 115.
- [55] F. Cheng, F. Gao, Y. Wang, Y. Wu, Z. Ma, J. Yang, “*Sn addition on the tensile properties of high temperature Zn-4Al-3Mg solder alloys*”, Microelectro. Reliab. 52 (2012) 579.
- [56] J.E. Lee, K.S. Kim, K. Suganuma, J. Takenaka, and K. Hagio, “*Interfacial Properties of Zn-Sn Alloys as High Temperature Lead-Free Solder on Cu Substrate*”, Mater. Trans. 46 (2005) 2413.
- [57] J.E. Lee, K.S. Kim, K. Suganuma, M. Inoue, and G. Izuta, “*Thermal Properties and Phase Stability of Zn-Sn and Zn-In Alloys as High Temperature Lead-Free Solder*”, Mater. Trans. 48 (2007) 584.
- [58] S.J. Kim, K.S. Kim, S.S. Kim, and K. Suganuma, “*Interfacial Reaction and Die Attach Properties of Zn-Sn High-Temperature Solders*”, J. Electron. Mater. 38, (2009) 266.
- [59] S.J. Kim, K.S. Kim, K. Suganuma, and G. Izuta, “*Interfacial Reactions of Si Die Attachment with Zn-Sn and Au-20Sn High Temperature Lead-Free Solders on Cu Substrates*”, J. Electron. Mater. 38, (2009) 873.
- [60] S.J. Kim, K.S. Kim, S.S. Kim, K. Suganuma, and G. Izuta, “*Improving the Reliability of Si Die Attachment with Zn-Sn-Based High-Temperature Pb-Free Solder Using a TiN Diffusion Barrier*”, J. Electron. Mater. 38, (2009) 2668.
- [61] R. Mahmudi and M. Eslami, “*Shear strength of the Zn-Sn high-temperature lead-free solders*”, J. Mater. Sci.: Mater. Electron. 22 (2011) 1168.
- [62] R. Mahmudi and M. Eslami, “*Impression Creep Behavior of Zn-Sn High-Temperature Lead-Free Solders*”, J. Electron. Mater. 39 (2010) 2495.
- [63] K. Suganuma, S. Kim, “*Ultra Heat-Shock Resistant Die Attachment for Silicon Carbide With Pure Zinc*”, IEEE Electr. Device. L. 31 (2010) 1467.

Chapter 2

Enhanced ductility and oxidation resistance of Zn by the addition of minor elements for use in SiC die-attachment

Abstract

Pure Zn is one of the best die-attachment candidates for use in next-generation wide-gap semiconductor power devices operating at temperatures up to 300 °C. However, it has certain drawbacks when used at high operating temperatures: poor ductility and limited oxidation resistance. In this chapter, we investigate the effect of adding minor elements — Ca, Mn, Cr, and Ti — for better ductility and oxidation resistance of Zn. These additions have found to reduce the grain size in their microstructure, enhancing the tensile strength and the elongation limit of the material. Oxidation resistance of pure Zn is significantly improved as well. The enhanced ductility and oxidation resistance consequently increases the interconnection ability of Zn alloys as die-attachment candidates.

2.1 Introduction

From the viewpoint of energy conservation, wide-gap semiconductors, especially silicon carbide (SiC) have been receiving considerable attention as an alternative technology to replace Si power semiconductor devices. These new wide-gap SiC semiconductors possess excellent physical and electrical properties, such as a higher breakdown voltage, low power loss and higher thermal conductivity. The wide-gap SiC semiconductor devices were prospected the high operating temperature because they can reduce the size of or eliminate the cooling system. Therefore, die bonding materials of wide-gap semiconductors have to need the high-melting temperature and high thermal conductivity [1, 2]. High-lead solders have been widely used for power-device packaging owing to their beneficial characteristics [3, 4]. Although these solders exhibit numerous excellent properties, they need to be completely eliminated from electronic applications in the near future under the Restriction of Hazardous Substances (RoHS) directive. This is because they lead to serious problems relating to both human health and the environment owing to lead toxicity. Therefore, several alternatives to high-lead solders—including Au–Sn/Si/Ge alloys [5–8], Bi–Ag alloys [9, 10], Zn–Al-based alloys [11, 12], and Zn–Sn alloys [13, 14]—have been proposed. However, lead-free alloys currently used for die attachment have several serious problems—such as the formation of massive intermetallic compounds (IMCs) [5, 6], their brittle nature [9–12], and their eutectic reaction at about 200 °C [13]. These drawbacks make it difficult to replace conventional high-lead solders, especially in high-temperature operation above 200 °C, and thus limit their applications.

In wide-gap power semiconductor devices, the die-bonding materials are a key role to applications owing to the requirements of excellent reliability and heat management. However, the current die-attachment lead-free materials could not be applied to wide-gap SiC semiconductor devices. For these reasons, it is necessary to develop new high temperature die-bonding materials for wide-gap semiconductors attachment.

In a previous study, the author's research group proposed a new die-attachment structure using a

pure Zn solder for SiC die attachments, which possessed the merits of being inexpensive and exhibiting excellent thermal shock resistance between -40 and 300 °C [15]. However, pure Zn still has certain drawbacks for use in high-temperature solders, e.g., brittle nature due to hexagonal close packed (HCP) structure (see Table 2.1) and sensitivity to oxidation stem from low free energy oxide formation.

Although many studies have been conducted to improve the mechanical and chemical properties of Zn through the addition of trace amounts of other elements [21–24], this has been done only for Sn-based solders. However, there is no study to increase the ductility and oxidation resistance of pure Zn for use as a die-attachment material by the addition of minor elements. In this chapter, the author evaluated the effects of adding minor elements on the microstructure, tensile properties, and oxidation resistance of Zn. The author selected Ca, Mn, Cr, and Ti as minor elements because they are active metals, and hence are expected to form fine-grain structures [21], scavenge impurities in the matrix, and form a protective oxide layer on the surface of Zn [23].

Table 2.1 Slip system and critical resolved shear stress (CRSS) of single crystal metals at room temperature [16–20]

	Crystal structure	Purity (%)	Slip plane	Slip Direction	CRSS (MPa)	Ref.
Zn	HCP	99.999	(0001)	[11-20]	0.18	16
Mg	HCP	99.996	(0001)	[1120]	0.77	17
Ti	HCP	99.99	(1010)	[11-20]	13.7	18
Ag	FCC	99.99	(111)	[110]	0.48	19
Cu	FCC	99.999	(111)	[110]	0.65	19
Ni	FCC	99.8	(111)	[110]	5.7	19
Mo	BCC	-	(110)	[111]	49.0	20

2.2 Experimental procedures

Preparation of minor element added Zn

The minor alloying elements were added to pure Zn (>99.99%), with the amount of each element addition being fixed at around 0.1 mass%. Hereafter, the composition unit “mass%” is omitted and these alloys are simply referred to as Zn–X alloys (X = Ca, Mn, Cr, and Ti). The experimental Zn alloys were melted with the minor alloying elements in an arc-melting furnace and allowed to cool in the furnace. Table 2.2 shows chemical composition of prepared die-attach materials which were analyzed using inductively coupled plasma (ICP) mass spectroscopy.

Table 2.2 Chemical composition of pure Zn and minor elements added Zn

	Composition (mass%)				
	Pure Zn	Zn–Ca	Zn–Mn	Zn–Cr	Zn–Ti
Pb	0.001				
Cd	<0.001				
Cu	<0.001				
Ag	<0.005				
Ca	<0.001	0.086			
Mn	<0.001		0.092		
Cr	<0.001			0.087	
Ti	<0.001				0.089

Tensile test of minor element added Zn

The ingot specimens were cold rolled into 1.2-mm sheets and were cut by an electro-spark machine for use as specimens in tensile tests. The gauge length and width of the specimens were 24

and 4 mm, respectively. The specimens were homogeneously heat treated at 180 °C for 3 h to remove residual stress and defects. Then, they were polished using 3 μm Al₂O₃ powder. Tensile tests were performed at room temperature at a strain rate of $7.0 \times 10^{-4} \text{ s}^{-1}$. Figure 2.1 shows the illustration of a tensile specimen and the tensile test status.

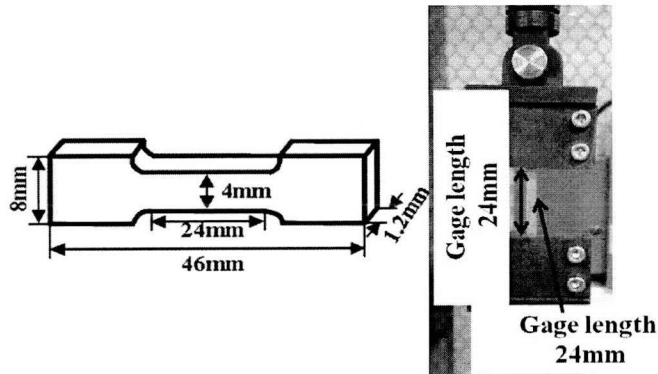


Fig. 2.1 Schematic and photo image of tensile test specimen.

Microstructure analysis

The microstructure changes were observed using a scanning electron microscope (SEM, JEOL, JSM-5510S). For observation of microstructure, specimens were polished with 0.05 μm Al₂O₃ powders and were etched with dilute hydrochloric acid (5 vol.% HCl in C₂H₅OH). The fracture surfaces of bulk specimens, and oxidation surface after TGA were also examined by SEM. Microstructure analysis were carried out using X-ray diffraction (XRD, Rigaku, Rint-2500). An electron probe microanalysis (EPMA, JXA-8800R, JEOL) was conducted to confirm the formation of intermetallic compounds.

High temperature oxidation test

The high-temperature oxidation resistance of the alloys was investigated by conventional thermal gravimetric analysis (TGA), which enabled measuring the weight changes at 400 °C up to 150 min in a standard air environment.

2. 3 Results and discussion

2. 3. 1 Enhancement of ductility

In order to investigate the improvement of ductility, tensile test is generally selected method. Figure 2.2 shows the nominal stress–strain curves of each specimen during the tensile test. The ultimate tensile strength (UTS) and elongation of pure Zn were 48 MPa and 5%, respectively. The results of UTS and elongation shows the similar value compared with ref. 26. In the present study, two significant effects due to the use of additives were identified: (1) compared with pure Zn, the elongation of the alloys, Zn–X (X = Ca, Mn, and Cr), dramatically increased from 5% to approximately 40% and strength increased to around 90 MPa; and (2) the Zn–Ti alloy showed the highest strength at about 125 MPa whereas the elongation of 25% was lower than that of the other additives. The serrated flow curve of pure Zn is shown in the inset of Fig. 2.2. This is a well-known phenomenon in which the ductility of a metal decreases because of twinning. A twinning occurs in a definite direction on a specific crystallographic plane for each crystal structure. Although the twinning is not a dominant deformation mechanism in metal which possess many possible slip systems, while pure Zn has few slip system resulting in twinning. Liu *et al.* reported the inhibition of the serration on high-purity Zn through the grain size control [25]. Their results show the improvement of ductility on high-purity Zn. The addition of minor elements can suppress this serration and enhance ductility, as shown in Fig. 2.3. These tensile strength and elongation data results are summarized Fig. 2.3.

Fracture specimens of pure Zn and Zn–X (X = Cr and Ti) alloys are shown in Fig. 2.4(a). Pure Zn does not show any significant increase in length or reduction in width. In contrast, the Zn–X alloys exhibit necking and tearing as ductile fractures. The micrographs show the cross-sectional views of the fracture sides. The decrease in width for pure Zn, Zn–Ti, and Zn–Cr were 0.2, 0.6, and 1 mm, respectively. While pure Zn showed a little width decline because pure Zn did not arise the necking, Zn–X alloys showed a considerable decrease in width because of the necking. Thus, Fig. 2.4(b–d) also explain the existence of necking with decreasing specimen width.

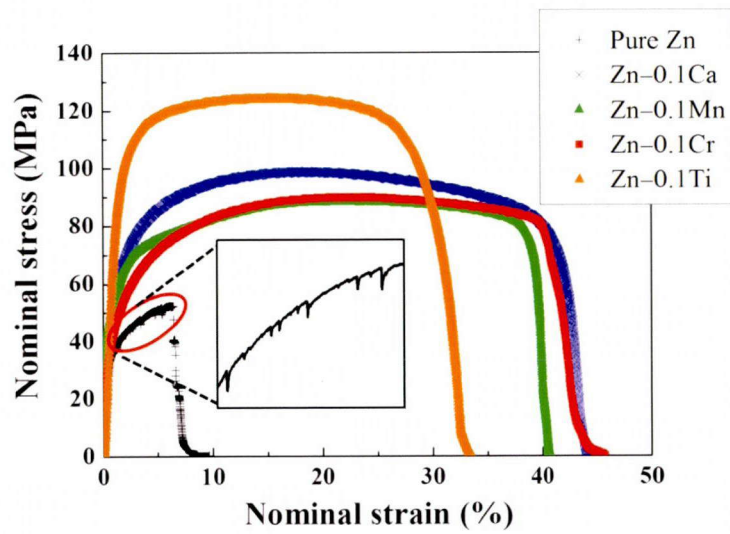


Fig. 2.2 Nominal stress–strain curves of pure Zn and Zn–X alloys (X = Ca, Mn, Cr, and Ti).

Inset shows the serrated flow of pure Zn.

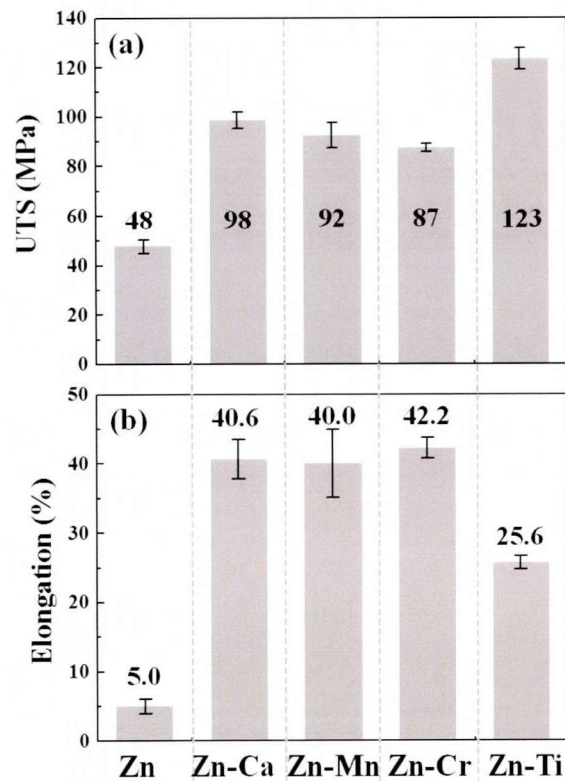


Fig. 2.3 Tensile properties of pure Zn and Zn–0.1X alloys (X= Ca, Mn, Cr and Ti)

(a) ultimate tensile strength, (b) Elongation.

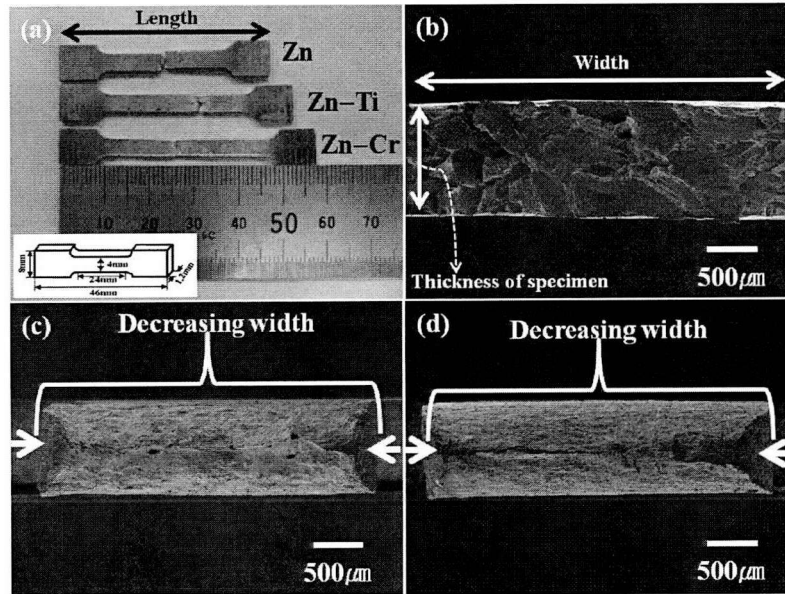


Fig. 2.4 (a) Photographs of tensile tests specimens for observing change in length.

Top-view SEM images of each material: (b) pure Zn, (c) Zn–Cr alloy, and (d) Zn–Ti alloy.

Figure 2.5(a1–c2) shows the fracture patterns of pure Zn, Zn–0.1Cr, and Zn–Ti after tensile tests as the delegate of each fracture pattern. Pure Zn shows typical brittle fracture patterns such as a cleavage plane occurring along the crystallographic plane $\{0001\}$ and river markings due to a limited slip system or twinning, as shown in Fig. 2.5(a2). On the other hand, the Zn–X alloys exhibit substantially different fracture patterns. Fig. 2.5(b1) and (b2) displays aspects of dimple patterns, and fine voids are observed in parts of the fracture surfaces in the Zn–Cr alloy. The Zn–Ti alloy shows a fracture pattern slightly different from those of pure Zn and the Zn–Cr alloy, as shown in Fig. 2.5(c1) and (c2). Although micro voids were also observed in the Zn–Ti alloy, they were few in number. Thus, the addition of the minor elements, except for Ti, to pure Zn has an excellent effect on enhancing pure Zn ductility.

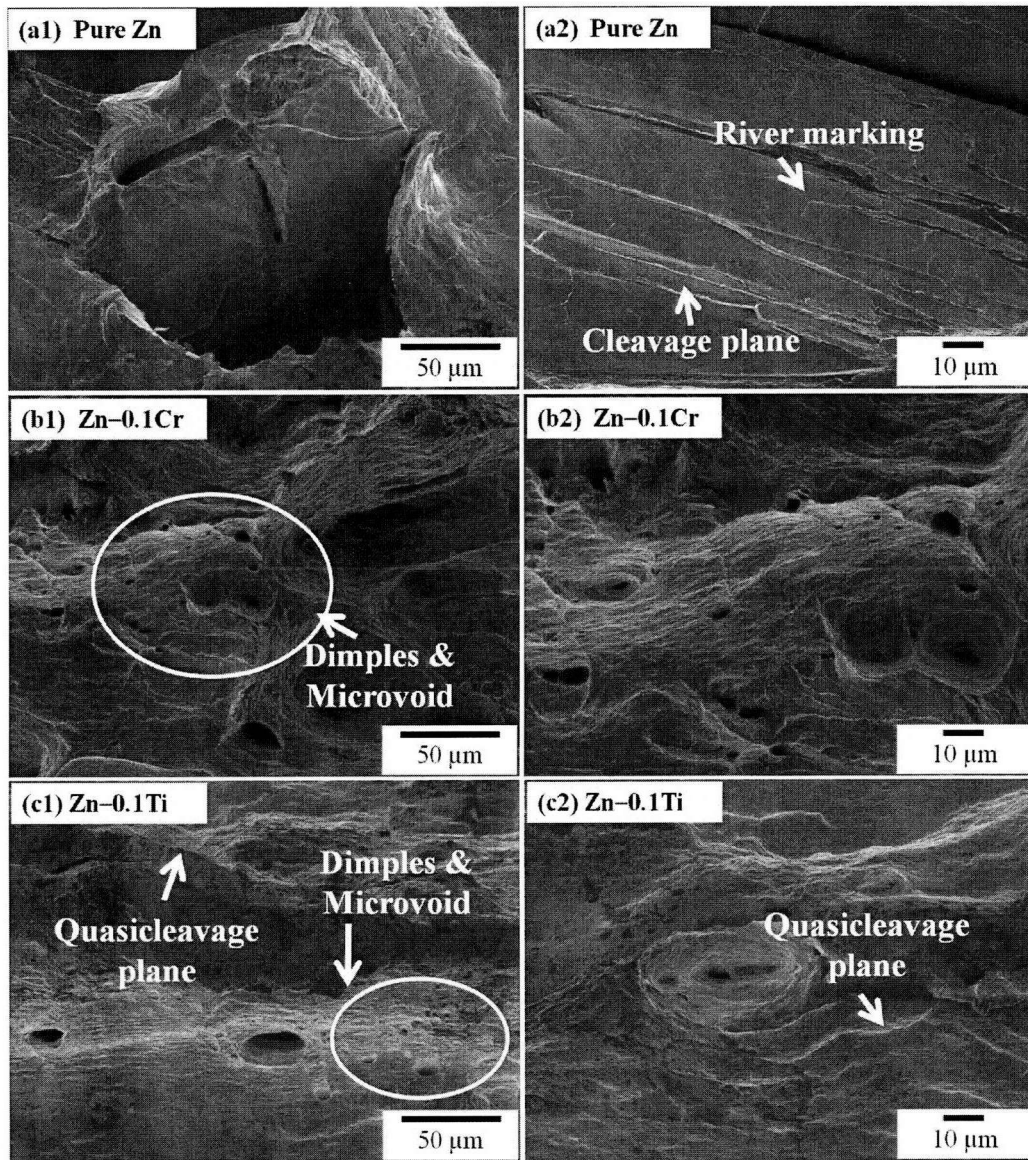


Fig. 2.5 SEM fracture surfaces: (a-1) cleavage fracture of pure Zn, (a-2) arrows in the enlarged image of pure Zn show a cleavage plane and river markings as typical brittle fracture patterns. (b-1) Dimples and microvoid patterns of Zn-Cr are observed as ductile fracture patterns, (b-2) enlarged fracture of the Zn-Cr alloy. (c-1) The Zn-Ti alloy shows a mixed fracture such as a quasicleavage plane and microvoids and (c-2) the quasicleavage plane of Zn-Ti at high magnification.

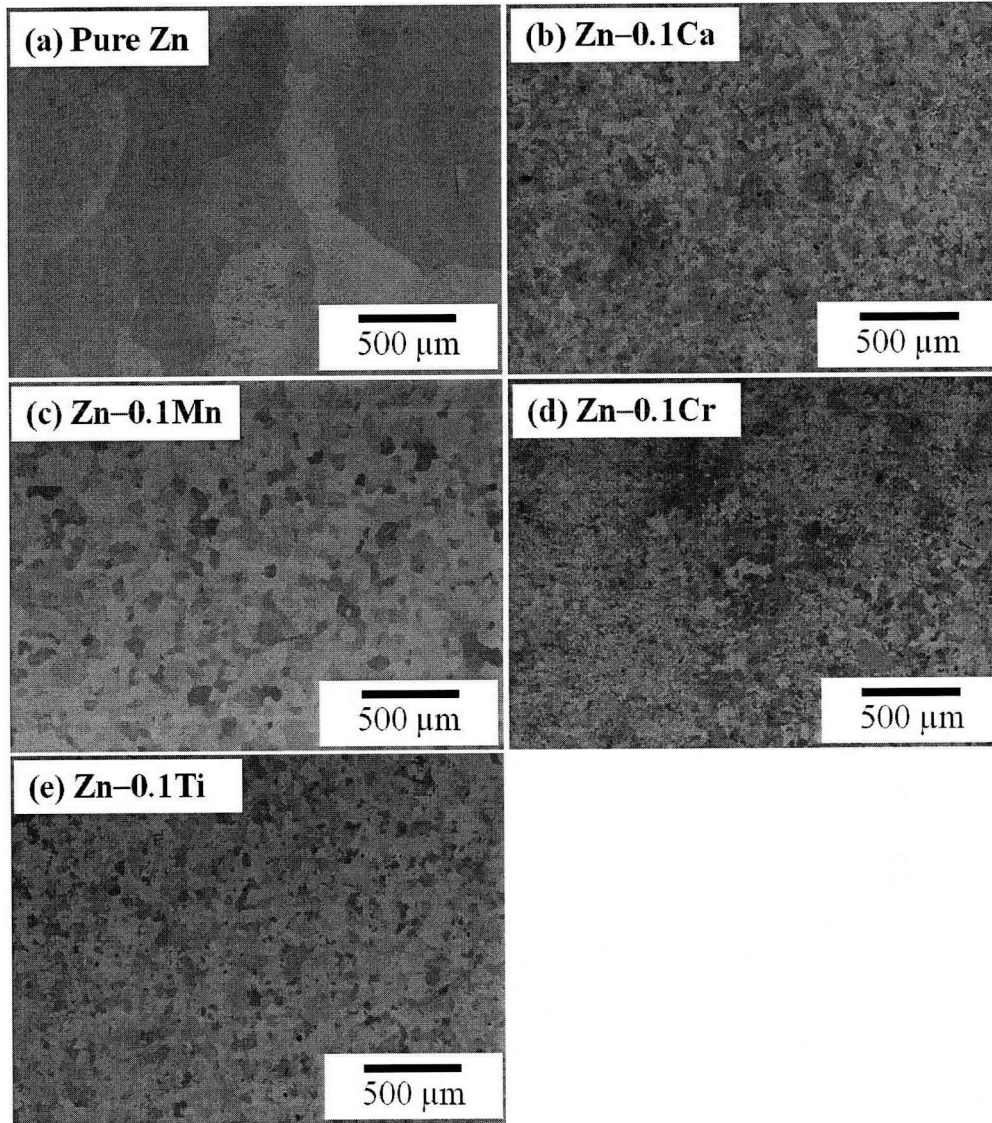


Fig. 2.6 SEM images of microstructures: (a) pure Zn exhibits a coarse grain size (over 800 μm). The addition of minor elements refines the grain size to less than 100 μm : (b) Zn-Ca, (c) Zn-Mn, (d) Zn-Cr, and (e) Zn-Ti alloys.

2. 3. 2 Microstructure change

To better understand the significant improvements in the mechanical properties of the alloys, their microstructures were observed. Fig. 2.6(a–e) shows the microstructures of each material prior to conducting tensile tests. Pure Zn exhibits a relatively coarse grain structure whereas all Zn–X alloys show a finer grain structure, as shown in Fig. 2.6(a–e). The average grain size of pure Zn was significantly large at approximately 800 μm , whereas those of the Zn–X alloys were less than 100 μm (see the Fig. 2.7).

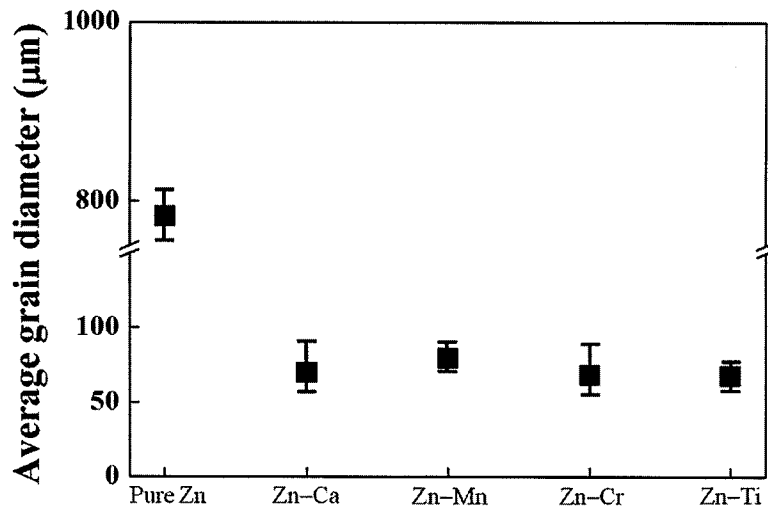


Fig. 2.7 Average grain size of each material.

Thus, all minor elements exhibited efficiency as grain refiners. There are several reports on the grain refinement effects of Mg alloys resulting from grain growth restriction caused by the dispersion of intermetallic or nucleant fine particles [26, 27]; however, the grain refinement mechanism of Zn by the addition of minor elements such as Ca, Mn, Cr, and Ti has scarcely been reported. As is well known through the general theory of metals, the effect of adding minor elements on grain refinement can be attributed to the restriction on grain growth resulting from grain boundary solidification, which

Chapter 2

Enhanced ductility and oxidation resistance of Zn by the addition of minor elements for use in SiC die-attachment

results in solidification-front pinning mainly due to the growth restriction effect. The effect of minor elements on growth kinetics can be understood by the restriction of the solidification front caused by the minor elements ahead of the solid–liquid interface. Their relatively small solid solubility in Zn (0.58 at.%) causes a rapid enrichment of the solute in the liquid ahead of the growing solid surface during solidification. In particular, the addition of Cr and Ti has a considerable effect on grain refinement because their solid solubility is negligible (0.01–0.04 at.%) compared with other elements. In brief, the minor elements are considered to stabilize the formation of fine grains and inhibit recrystallization. Although Fig. 2.3 shows that the stress–strain curve patterns of the Zn–X alloys (X = Ca, Mn, and Cr) are different from that of the Zn–Ti alloy, there are no substantial differences among the microstructures in Fig. 2.6(b–e). To clarify the difference between the stress–strain curve patterns of Zn–X (X = Ca, Mn, Cr) and Zn–Ti in Fig. 2.3, the Zn–Ti alloy was observed using SEM at high magnification. Figure 2.8 (a) shows the fine precipitates along grain boundaries. X-ray diffraction analysis could not detect the composition of the precipitate, whereas an electron probe micro analyzer could detect a Ti-rich area. Figure 2.8 (b)–(d) present to the EPMA mapping results. The Ti-rich precipitates are assumed to be IMCs such as a Zn_xTi_y combination [28]. The existence of these IMCs along grain boundaries has been considered the cause of brittleness, thus resulting in the lower elongation of the Zn–Ti alloy as shown in Fig. 2.3.

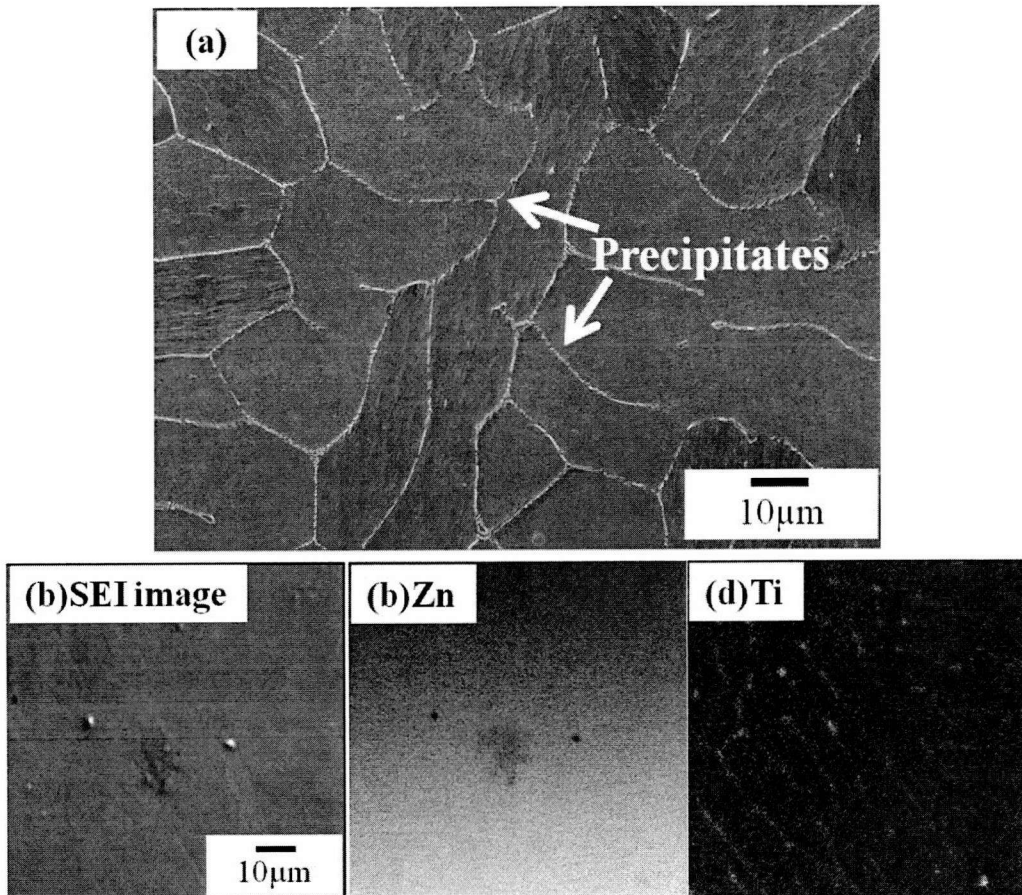


Fig. 2.8 (a) SEM image of precipitates (Zn_xTi_y IMCs) of the Zn–Ti alloy, (b)–(d) EPMA element mapping analysis image of a Zn–Ti alloy.

2. 3. 3 Improvement of oxidation resistance

To investigate the effect of adding the minor elements on high temperature oxidation behavior, the alloys were evaluated by TGA to measure any increase in weight. Although wide-gap semiconductor power devices operate at temperatures up to 300 °C, in this study, oxidation experiments were conducted at 400 °C to ascertain oxidation behavior more rapidly and clearly. The relationship between weight gain and oxidation time at 400 °C in air is shown in Fig. 2.9 (a). The curve for pure Zn follows a rapid linear-rate law and a final weight gain of 0.2% was attained after 150 min. The weight gain rate of pure Zn slowed at around 90 min. Although the weight gain of the Zn–X alloys increased with oxidation time, the weight gain rate is much slower than that of pure Zn. The final weight gains of the Zn–Ca, Zn–Mn, and Zn–Ti alloys are about half that of pure Zn, which is approximately 0.1%. In addition, the rate of weigh-gain declined about 60 min. Among the alloys, the Zn–Cr alloy showed least change in weight of about 0.03%, and the stabilized time against oxidation was much lower than that of the other specimens. These results imply that the oxidation resistance of the Zn–X alloys is better than that of pure Zn. Figure 2.9(b) shows the final weight change results at 400 C.

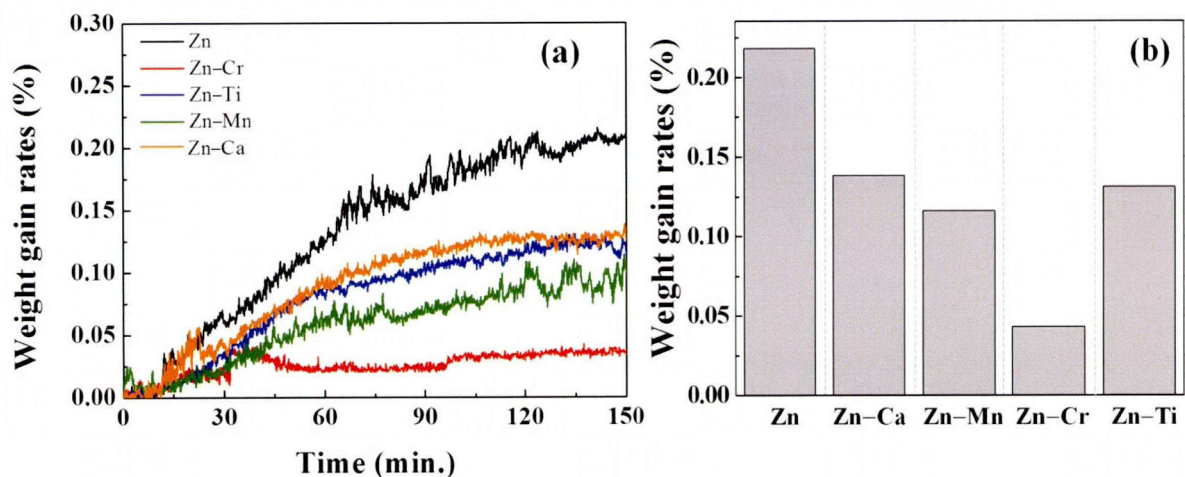


Fig. 2.9 Results of a high-temperature oxidation test (a) TGA weight gain curves

and (b) the final weight gain changes at 400 °C for 150 min.

It has been assumed that the minor elements are concentrated at the surface or subsurface of Zn and form a compact and stable oxidation barrier, thus protecting materials from further oxidation due to the penetration of oxygen. Several studies have explained the protection mechanism by the addition of elements to steels [29]. This theory has been generally interpreted as oxidation behavior suppressed by the addition of elements to metals. All minor elements indicate oxidation suppression because they form a compact and stable oxidation barrier. In particular, the addition of Cr shows the best inhibition effect on oxidation behavior. Figure 2.10 shows the oxidation surface of each specimen. All of specimens exhibited severely oxidized surface. The morphology of oxide products is similar to whiskers, though they are very short about 200nm and thin about sub-nanometer, as shown in inset of Fig. 2.10. In case of the Zn-0.1Cr alloy, the density of needle-shaped oxide is the lowest because of less oxidation as shown Fig. 2.10(c). From the results of high temperature oxidation, it can be concluded that the Zn-0.1Cr alloy can effectively prevent oxidation.

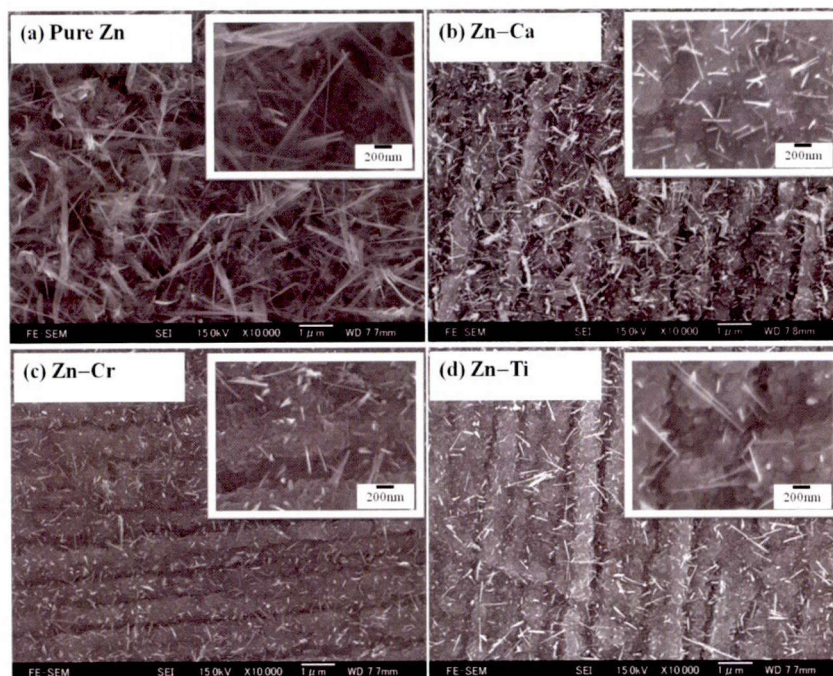


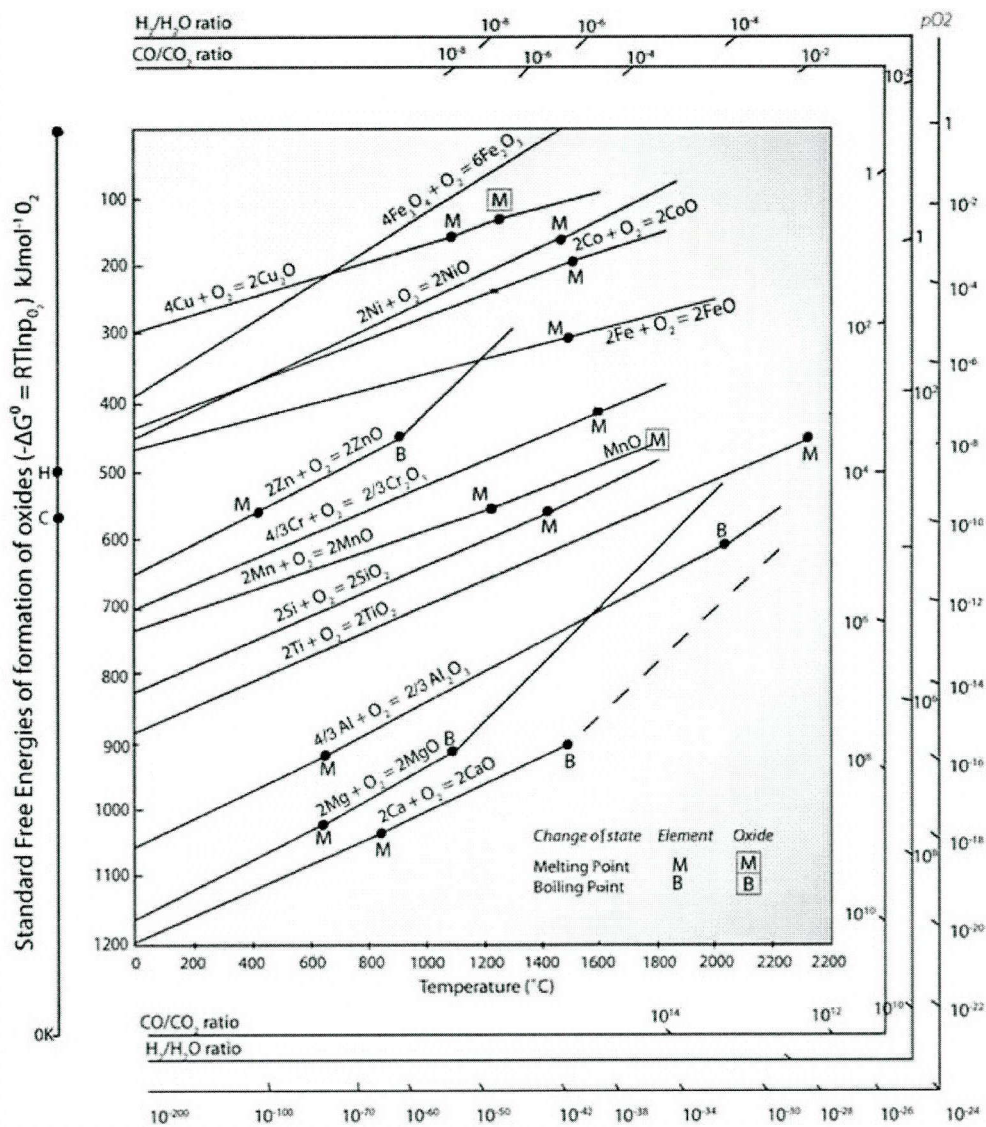
Fig. 2.10 SEM images of oxidation surface (a) pure Zn, (b) Zn-Ca alloy, (c) Zn-Cr alloy, and (d) Zn-Ti alloy. The inset images are high magnification SEM image of oxidation products.

2. 4 Conclusions

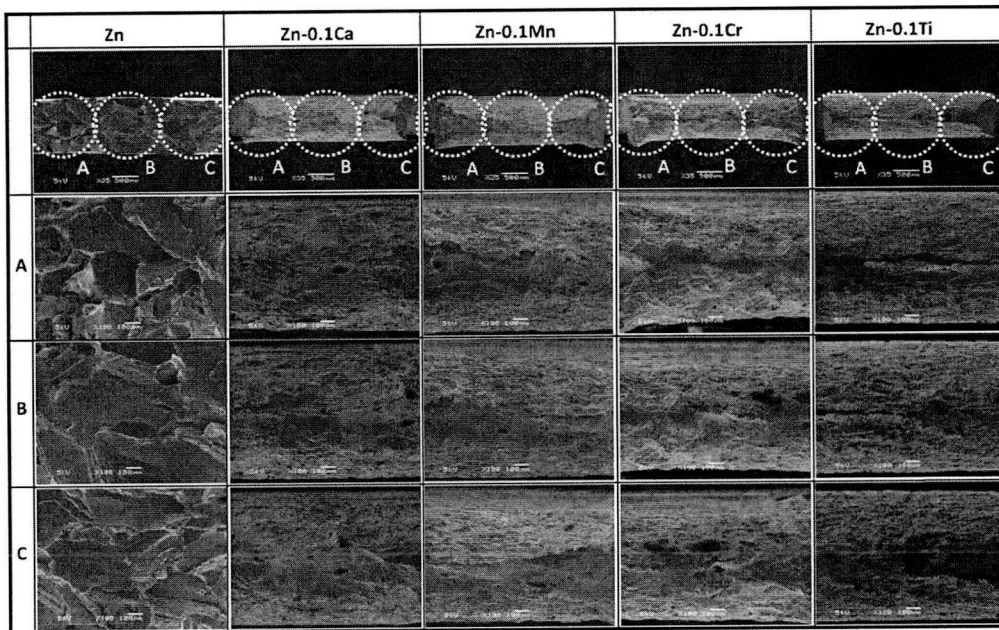
The interconnection technologies, such as die-bonding, ductility is the very important characteristics because the ductility is relaxing external and thermal expansion stress. In addition, the oxidation resistance has relation to durability and reliability in high-temperature operation beyond 200 °C. Owing to its brittleness and poor oxidation resistance, pure Zn has been a concern for use in interconnection technologies. Therefore, the present chapter sought to enhance the ductility and oxidation resistance of pure Zn by the addition of minor elements for use in die-bonding materials. From the obtained tensile data and microstructure information, this chapter concluded that the addition of minor elements effectively improved ductility without degrading strength. Moreover, the formation of coarse grain structures was suppressed and the brittleness of pure Zn was reduced. The addition of Ti resulted in lower elongation than that for other additives because fine precipitates exist along grain boundaries as brittle Zn_xTi_y intermetallic compounds. The addition of all minor elements to pure Zn results in oxidation resistance improvement. It is possible that minor elements preferentially form a compact and stable barrier layer at the surface or subsurface of Zn, and that these layers inhibit oxidation. Among the alloys obtained by adding minor elements, the Zn–Cr alloy showed the slowest oxidation ratio.

From these results, improvement of ductility by inhibition of serration and oxidation resistance by a compact and stable barrier layer with the addition of the minor element Cr is superior to that with all other elements. Therefore, the addition of minor elements to fabricate new Zn-based die-bonding materials is expected to be applicable to the interconnectivity of wide-gap semiconductor devices for use at high operating temperatures.

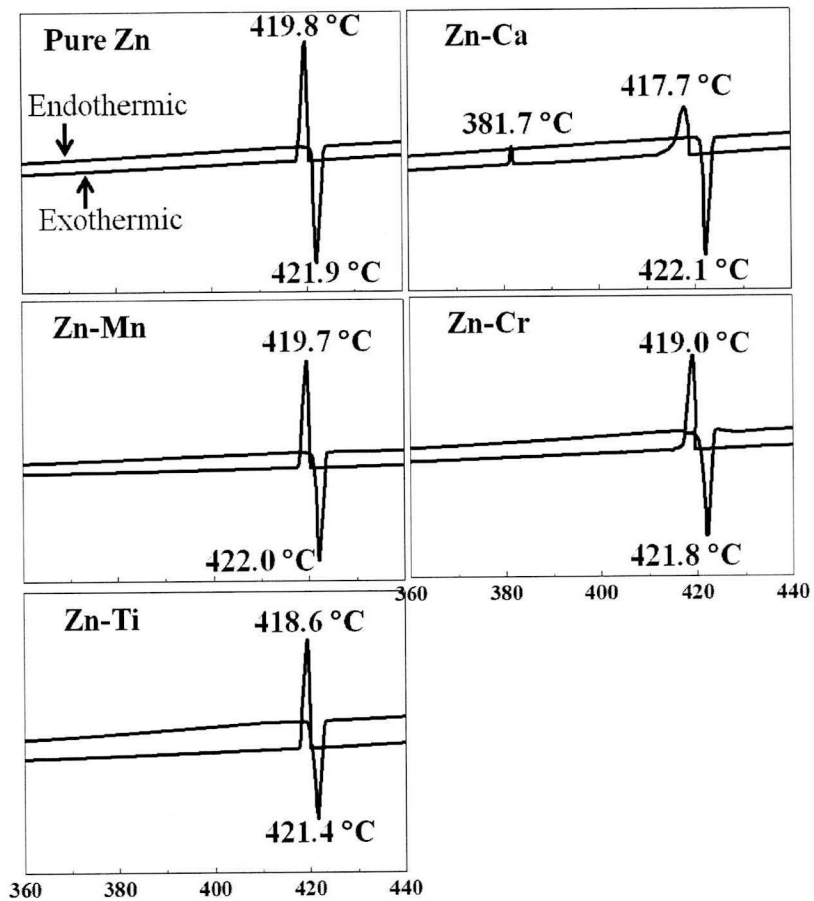
Appendix



A. Elingam diagram of metals for selection of the additive minor elements [30].



B. Wide range of fracture surfaces of all specimens.



C. DSC curves of all specimens for investigation of melting temperature change.

REFERENCES

- [1] W. Wondrak, R. Held, E. Niemann, and U. Schmid, “*SiC devices for advanced power and high-temperature applications*”, IEEE Trans. Ind. Electron. 48 (2001) 307.
- [2] M. Asif Khan et al., “*GaN BASED HETEROSTRUCTURE FOR HIGH POWER DEVICES*”, Solid-State Electron. 41, (1997) 1555-1559.
- [3] G. Humpston and D.M. Jacobson, “*Principles of Soldering and Brazing*”, ASM international, March (1993).
- [4] K.N. Tu and K. Zeng, “*Tin-Lead (Sn-Pb) solder reaction in flip chip technology*”. Mater. Sci. Eng. R34 (2001) 1.
- [5] H.G. Song, J.P. Ahn, and J.W. Morris Jr., “*The Microstructure of Eutectic Au-Sn Solder Bumps on Cu/Electroless Ni/Au*”, J. Electron. Mater. 30 (2001) 1083.
- [6] J.Y. Tsai, C. W. Chang, Y.C. Shieh, Y.C. Hu, and C.R. Kao, “*Controlling the Microstructures from the Gold-Tin Reaction*”, J. Electron. Mater. 34 (2005) 182.
- [7] Jin-Wook Jang, Scott Hayes, Jong-Kai Lin, and Darrel R. Frear, “*Interfacial reaction of eutectic AuSi solder with Si(100) and Si(111) surfaces*”, J. Appl. Phys. 95 (2004) 6077.
- [8] V. Chidambaram, J. Hald and J. Hattel, “*Development of Au-Ge based candidate alloys as an alternative to high-lead content solders*”, J. Alloys Compd. 490 (2010) 170.
- [9] M. Rettenmayer, P. Lambracht, B. Kempf, and M. Graff, “*High Melting Pb-Free Solder Alloys for Die-Attach Applications*”, Adv. Eng. Mater. 7 (2005) 965.
- [10] J.M. Song, H.Y. Chuang, and T.X. Wen, “*Thermal and Tensile Properties of Bi-Ag Alloys*”, Metall. Mater. Trans. A 38 (2007) 1371.
- [11] T. Shimizu, H. Ishikawa, I. Ohnuma, and K. Ishida, “*Zn-Al-Mg-Ga Alloys as Pb-free Solder for Die-Attaching Use*”, J. Electro. Mater. 28 (1999)
- [12] M. Rettenmayer, P. Lambracht, B. Kempf, and C. Tschudin, “*Zn-Al Based Alloys as Pb-Free Solders for Die Attach*”, J. Electron. Mater. 31 (2002) 278.

Chapter 2

Enhanced ductility and oxidation resistance of Zn by the addition of minor elements for use in SiC die-attachment

- [13] J.E. Lee, K.S. Kim, K. Suganuma, M. Inoue, and G. Izuta, “*Thermal Properties and Phase Stability of Zn-Sn and Zn-In Alloys as High Temperature Lead-Free Solder*”, Mater. Trans. 48 (2007) 584.
- [14] S.J. Kim, K.S. Kim, S.S. Kim, K. Suganuma, and G. Izuta, “*Improving the Reliability of Si Die Attachment with Zn-Sn-Based High-Temperature Pb-Free Solder Using a TiN Diffusion Barrier*”, J. Electron. Mater. 38, (2009) 2668.
- [15] K. Suganuma, and S. Kim, “*Ultra Heat-Shock Resistant Die Attachment for Silicon Carbide With Pure Zinc*”, IEEE Electr. Device. L. 31 (2010) 1467.
- [16] D.C. Jillson, “*Institute of Metals Division - Quantitative Stress-Strain Studies on Zinc Single Crystals in Tension*”, Trans. AIME, 188 (1950) 1129.
- [17] E.C. Burke and W.R. Hibbard, “*Plastic Deformation of Magnesium Single Crystals*”, Trans. AIME, 194 (1952) 295.
- [18] A.T. Churchman, “*The Slip Modes of Titanium and The Effect of Purity on Their Occurrence during Tensile Deformation of Single Crystals*”, Proc. R. Soc. London Ser. A 226A (1954) 216.
- [19] F.D. Rosi, “*Stress-strain Characteristics and Slip-band Formation in Metal Crystals - Effect of Crystal Orientation*”, Trans. AIME, 200 (1954) 1009.
- [20] N. K. Chen and R. Maddin, “*Plasticity of Molybdenum Single Crystals*”, Trans. AIME, 191 (1951) 937.
- [21] A.G. Ramirez, H. Mavoori, and S. Jin, “*Bonding nature of rare-earth-containing lead-free solders*”, Appl. Phys. Lett. 80 (2002) 398.
- [22] S.K. Das, A. Sharif, Y.C. Chan, N.B. Wong and W.K.C. Yung, “*Influence of small amount of Al and Cu on the microstructure, microhardness and tensile properties of Sn-9Zn binary eutectic solder alloy*”, J. Alloys Compd. 481 (2009) 167.
- [23] X. Chen, A. Hu, M. Li, and D. Mao, “*Study on the properties of Sn-9Zn-xCr lead-free solder*”, J. Alloys Compd. 460 (2008) 478.

- [24] M. McCormack, G.W. Kammlott, H.S. Chen, and S. Jin, “*Significantly improved mechanical properties in Pbfree, SnZnIn solder alloy by Ag doping*”, Appl. Phys. Lett. 65 (1994) 1100.
- [25] J.H. Liu, C.X. Huang, S.D. Wu, and Z.F. Zhang, “*Tensile deformation and fracture behaviors of high purity polycrystalline zinc*”, Mat. Sci. Eng A-Struct. 490 (2008) 117.
- [26] M. Easton and D. StJohn, Metall. “*Grain Refinement of Aluminum Alloys: Part I. The Nucleant and Solute Paradigms—A Review of the Literature*”, Mater. Trans. A 30 (1999) 1613.
- [27] D.H. StJohn, M. Qian, M. Easton, P. Cao, and Z. Hildebrand, “*Grain Refinement of Magnesium Alloys*”, Metall. Mater. Trans. A 36 (2005) 1669.
- [28] J.L. Murray, “*The Ti-Zn (Titanium-Zinc) System*”, Bull. Alloy Phase Diagrams 5 (1984) 52.
- [29] K. Hauffe, “*Oxidation of Metals*”, Plenum Press, New York, (1965).
- [30] The web site of Dissemination of IT for the Promotion of Materials Science, University of Cambridge, <http://www.doitpoms.ac.uk> (2011. 04)

Chapter 3

Effects of minor elements on the reaction between Zn and Cu substrate during thermal aging

Abstract

In the present chapter, the minor elements added Zn alloys is scrutinized when applied as a high temperature lead-free solder based on the finding in the previous chapter. Since the thickness of IMC layers at joining interface has an apparent relation to the joint reliability, understanding IMC growth mechanisms is an important key for die-attach bonding. Hence the properties of interface between a Zn alloy and Cu substrate are investigated in detail, focusing on IMC growth and shear strength degradation by thermal aging tests. At every solder/Cu interface, the reaction layers are confirmed to include two types of Cu–Zn intermetallic compounds: γ -Cu₅Zn₈ and ε -CuZn₅ phases identified at the Cu side. The joint interface with minor elements added Zn reduces the growth rate of IMCs. In particular, 0.1 wt.% Cr addition in pure Zn solder remarkably suppresses the IMC growth, and improves the shear strength after thermal aging at 150 °C. This effect appears more clearly at the higher aging temperature of 250°C. During the aging test at 250 °C for 100 h, a considerable number of cracks has been developed inside the γ -Cu₅Zn₈ phase at Cu/Zn joining interface. On the other hand, no crack has been confirmed at Zn–0.1Cr/Cu interface. After the thermal aging tests at 250 °C for 500 h, the specimens with pure Zn lose the original shape of bonding interface due to the excessive consumption of Cu atoms by IMC forming reaction. In contrast, the interface with Zn–0.1Cr remains the solder structure even after the thermal aging due to the suppressed IMC growth. Since the IMC are brittle material with a much different density from the solder alloys, the excessive thickness of IMC layer is the major source to hinder the solder joint reliability. In sum, the additive Cr shows beneficial effects for suppressing IMC growth and improves shear strength after the thermal aging. Zn–0.1Cr solder alloy is hence expected to enhance the joining reliability in SiC die-attachment.

3. 1 Introduction

In a previous chapter, the ductility and oxidation resistance of Zn die-attach materials were enhanced its drawbacks e.g. poor ductility and limited oxidation resistance through the addition minor of elements such as Ca, Mn, Cr, and Ti. Consequently, because of improved ductility and oxidation resistance, the interconnection ability of Zn alloys as die-attachment candidates was significantly enhanced. However, Zn based solders still has certain drawbacks for die-attachment, e.g., formation of slightly thicker intermetallic compounds (IMCs) with metal substrate [1–3]. Among the metal substrate, the Cu substrate is the most widely used as the thermal interfacial material (TIM) in the die attach bonding, which plays the important functions as the heat transfer and keeping of the construction. Therefore, to establish the die-attach materials, an understanding of the interfacial properties and IMC growth with substrate are very important. The thickness of IMCs between a solder and a Cu substrate has relationship on the strength and joint reliability. For instance, excessively thick IMCs layers can significantly degrade the physical and mechanical properties of the solder joints, particularly in harsh environment [4]. The suppression of IMCs growth in solder joints is important issue to the electronics industry. The several reports carried out for suppressing the IMCs growth only for the Sn-base solders [5–7]. There are scarcely reports the inhibition of IMCs growth between pure Zn solder and Cu substrate by element doping as SiC die-attach materials. Therefore, to apply die-attach process, the newly designed minor elements added Zn (Zn–0.1X, X= Ca, Mn, Cr, and Ti) should be evaluated interfacial properties and IMCs growth.

The growth rates of IMC and the interdiffusion coefficients of atomic species in them have been widely determined by estimating the thickness change of the IMC layer [8–10]. The objective of present chapter is to study and evaluate the effect of different minor elements on interfacial reaction, particularly growth of IMCs layer between Zn die-attach material and Cu substrate during thermal aging.

3. 2 Experimental procedures

The die-attach materials used in this chapter, Zn–0.1wt.%M (M = Ca, Mn, Cr, and Ti) and pure Zn were fabricated using the same procedures of the arc melting in Ch. 2. The alloy ingots were prepared as solder sheets (4 mm × 4 mm × 0.2 mm) by cold rolling, and their faces were polished with 3 μm alumina powder. Hereafter, the composition unit of “wt.%” is omitted in the notation. The copper substrates and copper dummy chips were prepared, and their surfaces were degreased in a 5 vol.% aqueous HCl solution. After pickling, these substrates were cleaned in ethanol and dried in air. The alloys were soldered under H₂ reduction atmosphere. The soldered specimens were heated at peak temperature 430 °C which was 20 °C higher than melting temperatures for 120s (Heating rate of 85 °C/min). Figure 3.1 shows the schematic soldering structure and temperature profile.

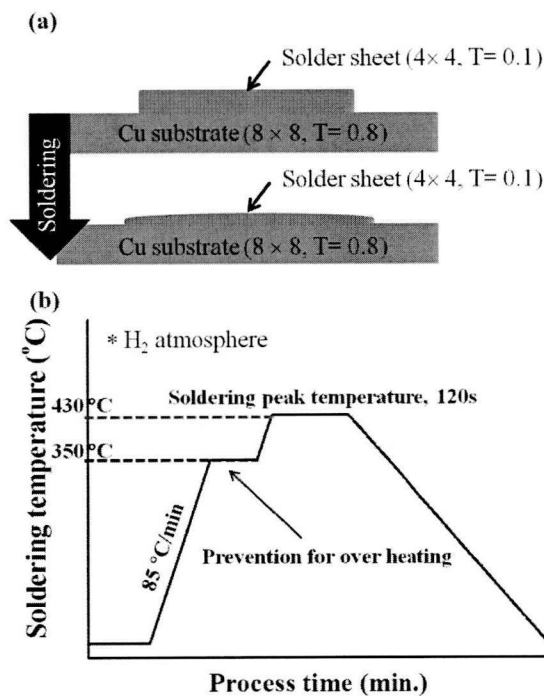


Fig. 3.1 (a) Schematic of the present bonding structure, and (b) soldering temperature profile.

To investigate the rate of IMCs growth, we carried out thermal aging at 150 and 250 °C for 100 – 500 hours. In order to observe the growth of IMCs, the specimens were etched by using 2 vol.% HCl–98 vol.% C₂H₅OH solution for 1–3 s after polishing. Then, the interfacial reaction layer was observed using scanning electron microscopy (SEM; JEOL, JSM-5510S instrument). The interface layers and reaction products were analyzed by x-ray diffraction (XRD) spectroscopy (Rigaku, Rint-2500) and electron probe microanalysis (EPMA; JEOL, JXA-8800R). The shear tests was carried out performed at a head speed of 1 μm/s and a height of 200 μm as shown in Fig. 3.2. Five specimens were tested for each data point.

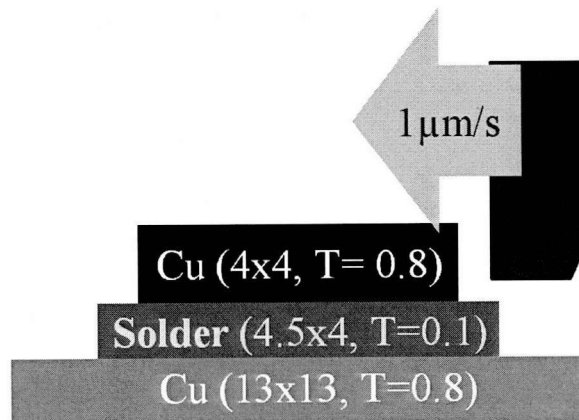


Fig. 3.2 Schematic diagram of the shear tests with Cu/solder/Cu joints.

3. 3 Results and discussion

3. 3. 1 Bonding interface as soldered

To investigate of the interfacial reaction, the microstructures of Zn/Cu and Zn-0.1X/Cu interfaces are observed by SEM. Figure 3.3 displayed the Back scattered (BS)-SEM micrographs of the intermetallic layers formed between the solders and Cu substrate after soldering at 430 °C for 120s. Generally, the Cu substrate is consumed by Zn and the formation and growth of the intermetallic compounds (IMC) formed simultaneously at the soldered interface during the soldering [1, 2]. An interfacial reaction layer is observed in all specimens, and the interfacial reaction layer has irregular interface (like scallop shape interface) with the solders side while the interface with Cu substrate side is relatively flat, as shown in Fig. 3.3 and enlarge images are displayed Fig 3.4. Three white broken lines are superimposed on the BS-SEM micrograph as shown in Fig. 3.4; the lower one corresponds to the initial surface of the Cu substrate, central one displays boundary of scallop type and flat type IMC phase, and the upper one indicates the interface of Zn solder/IMC phase. The total thicknesses of Zn/Cu reaction layer is about 35 μ m while minor element added Zn/Cu reaction layer is significantly thinner than Zn/Cu interface about 15 μ m. To clarify their reaction layer phases, polished surfaces of the interface were examined by X-ray diffraction analysis (XRD). A typical result is illustrated in Fig. 3.5; this result indicates that ϵ -CuZn₅ and γ -Cu₅Zn₈ are mainly formed by solder. From the binary Cu-Zn phase diagram, three intermetallic compounds, i.e., β' -CuZn, γ -Cu₅Zn₈, and ϵ -CuZn₅, can be expected for this reaction system. Suganuma *et al.* also reported that two Cu-Zn intermetallic compound layers, such as γ -Cu₅Zn₈ and β' -CuZn, are formed at reflow temperature for the Sn-Zn eutectic solder/Cu interface [9]. The β' -CuZn phase cannot be identified in the XRD due to the reaction thickness of β' -CuZn is very thin, less than 1 μ m as seen in Ref. 11. The amount of Zn is much larger than in the Sn-Zn eutectic alloy/Cu reaction system, which can easily promote the formation of ϵ -CuZn₅.

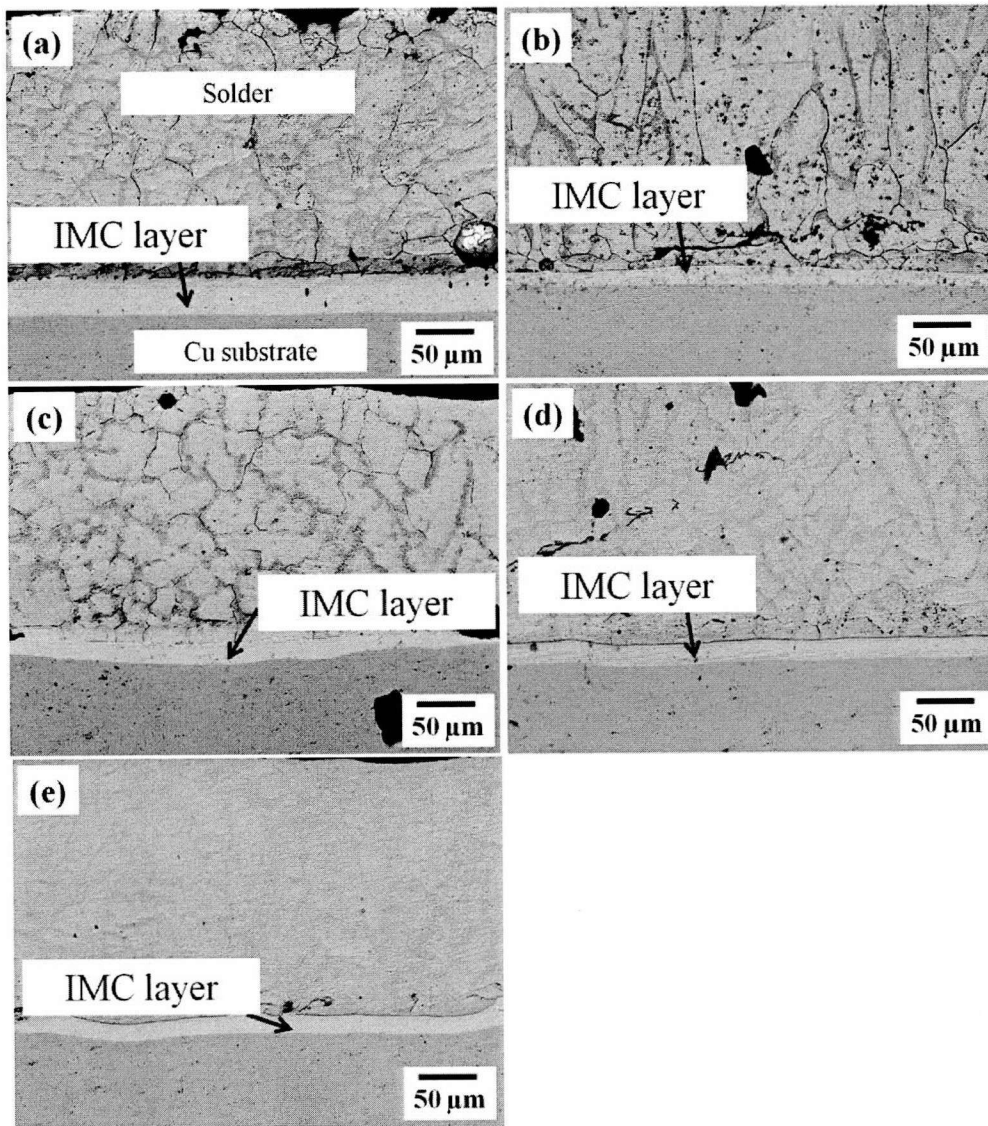


Fig. 3.3 SEM micrographs of reaction interface as soldered on a Cu substrate; (a) with pure Zn, (b) with Zn-0.1Ca, (c) with Zn-0.1Mn, (d) with Zn-0.1Cr, and (e) with Zn-0.1Ti.

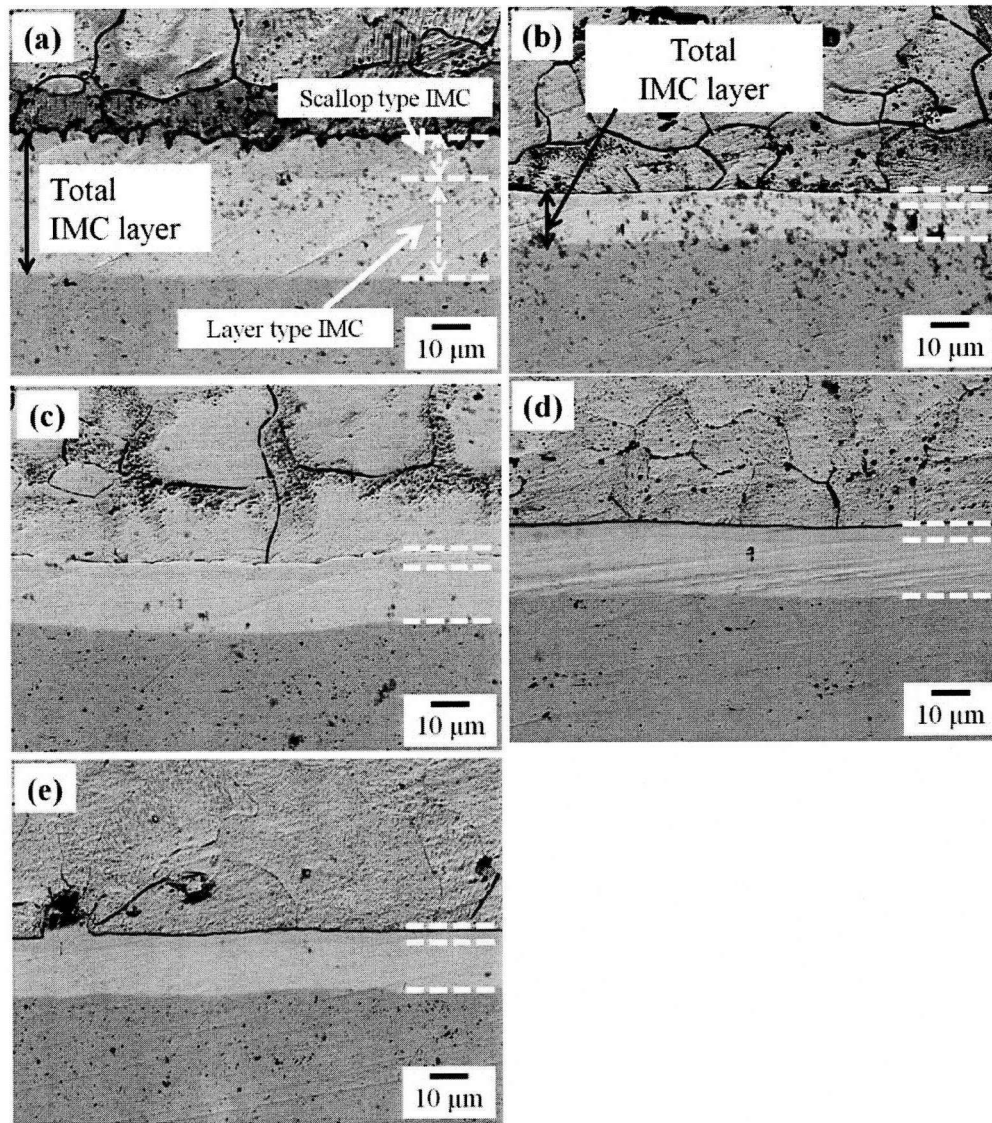


Fig. 3.4 Enlarged SEM micrographs of Fig.3.3; (a) with pure Zn, (b) with Zn-0.1Ca, (c) with Zn-0.1Mn, (d) with Zn-0.1Cr, and (e) with Zn-0.1Ti.

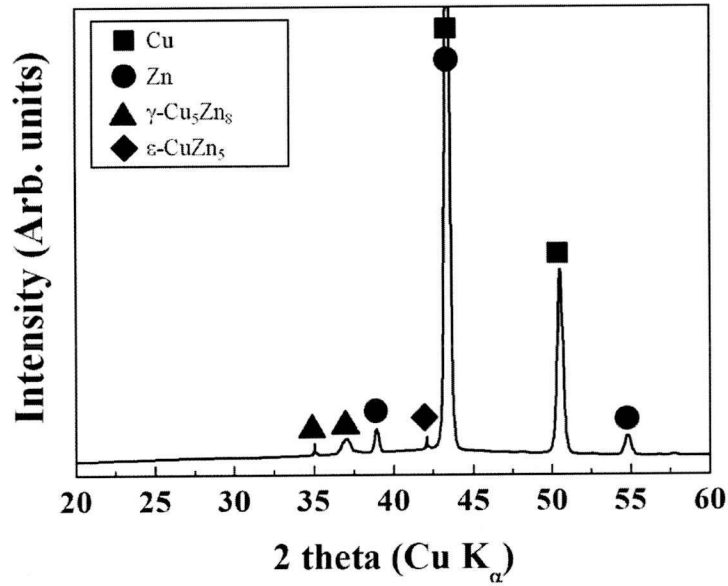


Fig. 3.5 Typical X-ray diffraction patterns of the soldered interface.

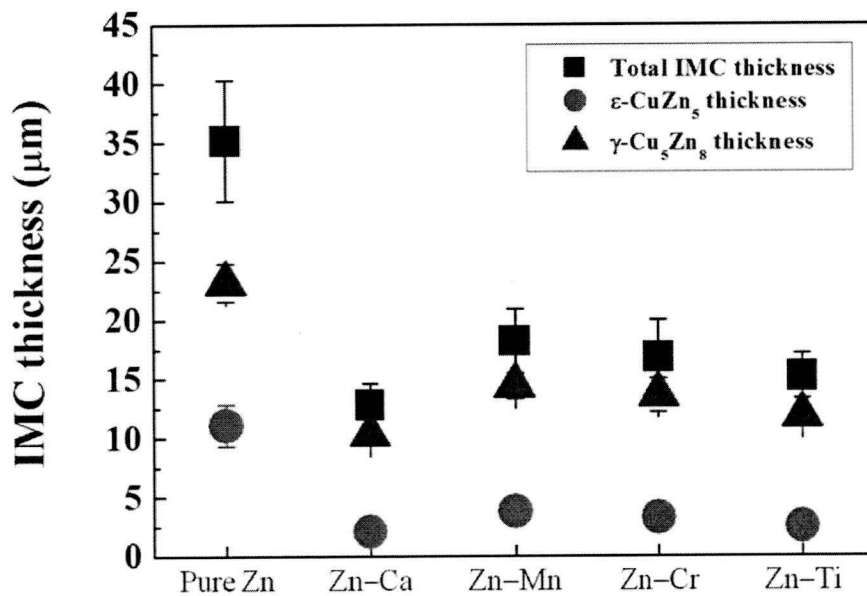


Fig. 3.6 Comparison of the IMC thickness as soldered interface.

For the present reaction system, it can be said that Cu dissolution into the liquid solder forms the scallop-shaped ϵ -CuZn₅ layer. Moreover, the growth of scallop-shaped ϵ -CuZn₅ is expected that the Cu is predominantly transported to molten solder along the ϵ -CuZn₅ grain boundaries during soldering. This reaction shows the same tendency of Sn–Pb solder/Cu interface [11–15]. Figure 3.6 shows the thickness change of the reaction layers following addition elements. The γ -Cu₅Zn₈ reaction layer was thicker formed as compared with ϵ -CuZn₅ compound. In case of the pure Zn, the thickness of the γ -Cu₅Zn₈ reaction layer is over twice that of the ϵ -CuZn₅ one, i.e., about 6 to 11 μm for ϵ -CuZn₅ and 23 to 27 μm for γ -Cu₅Zn₈ layer. On the other hand, Zn–0.1X/Cu reaction layer is significantly thinner than Zn/Cu interface. The thickness of reaction layer is about 2 to 4 μm for ϵ -CuZn₅ and 10 to 15 μm for γ -Cu₅Zn₈ layer.

To confirm the reaction layers at the interface, EPMA was also carried out for all samples. Figure 3.7 shows a typical EPMA element mapping results of the soldered joints with pure Zn and Zn–0.1Cr solder, respectively. Zn–0.1Cr/Cu interface clearly indicates the significantly thinner IMC thickness than Zn/Cu interface. Although BS-SEM images could not observed the β' -CuZn phase, EPMA mapping image shows the very thin (less than 1 μm) β' -CuZn phase as marked in the Fig. 3.7(a-2), accordingly the report of Suganuma *et al.* [9]. From the results of the EPMA element mapping, however, it was found that these reaction layers contain only Cu and Zn and not minor elements as shown in Fig. 3.7(b1 – b3), Combining the results of XRD analysis and quantitative EPMA, as summarized in Table 3.1, the thinner reaction layer was confirmed as ϵ -CuZn₅ and the thicker reaction layer was confirmed as γ -Cu₅Zn₈. The atomic percentage ratio between Cu and Zn is approximately 1:5 (points 1 - 3) and 5:8 (points 4 - 5) for both Zn/Cu and Zn–0.1X/Cu couples. Thus, there is only γ -Cu₅Zn₈ and ϵ -CuZn₅ in interfacial reaction layer, which is consistent with the XRD results.

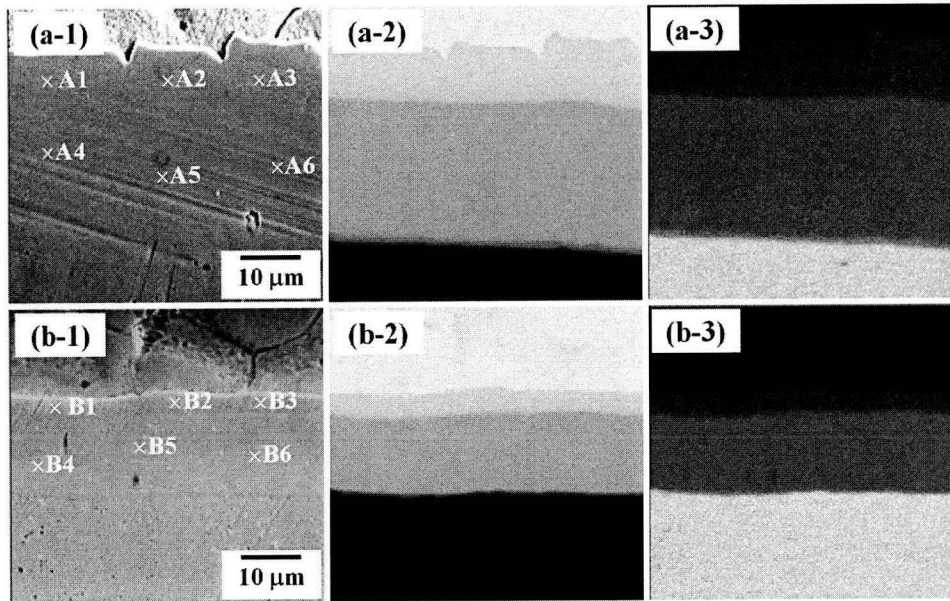


Fig. 3.7 EPMA mapping analysis of the interface (a) between pure Zn and Cu substrate: (a-1) SEI image and mapping images of (a-2) Zn, and (a-3) Cu. (b) between Zn-0.1Cr and Cu substrate: (b-1) – (b-3) have the same means to (a-1) – (a-3).

Table 3.1 EPMA quantitative analysis of reaction layers.

	Point	Average Zn atomic%	Identified phase
Pure Zn/Cu	A1 – A3	82.32 ± 1.31	ϵ -CuZn ₅
	A4 – A6	64.43 ± 0.69	γ -Cu ₅ Zn ₈
Zn-0.1Cr/Cu	B1 – B3	81.34 ± 0.94	ϵ -CuZn ₅
	B4 – B6	61.27 ± 0.57	γ -Cu ₅ Zn ₈

3.3.2 IMC growth during thermal aging

Due to the high operation temperature, thermal exposure test (e.g. thermal aging) is an important. To investigate the growth rates of IMC, therefore, thermal aging was carried out at 150 °C and 250 °C for 100–500 hours. In this session, the solid-state annealing behavior of pure Zn solder and minor elements added Zn (Zn–0.1X, X=Ca, Mn, Cr, Ti) were compared.

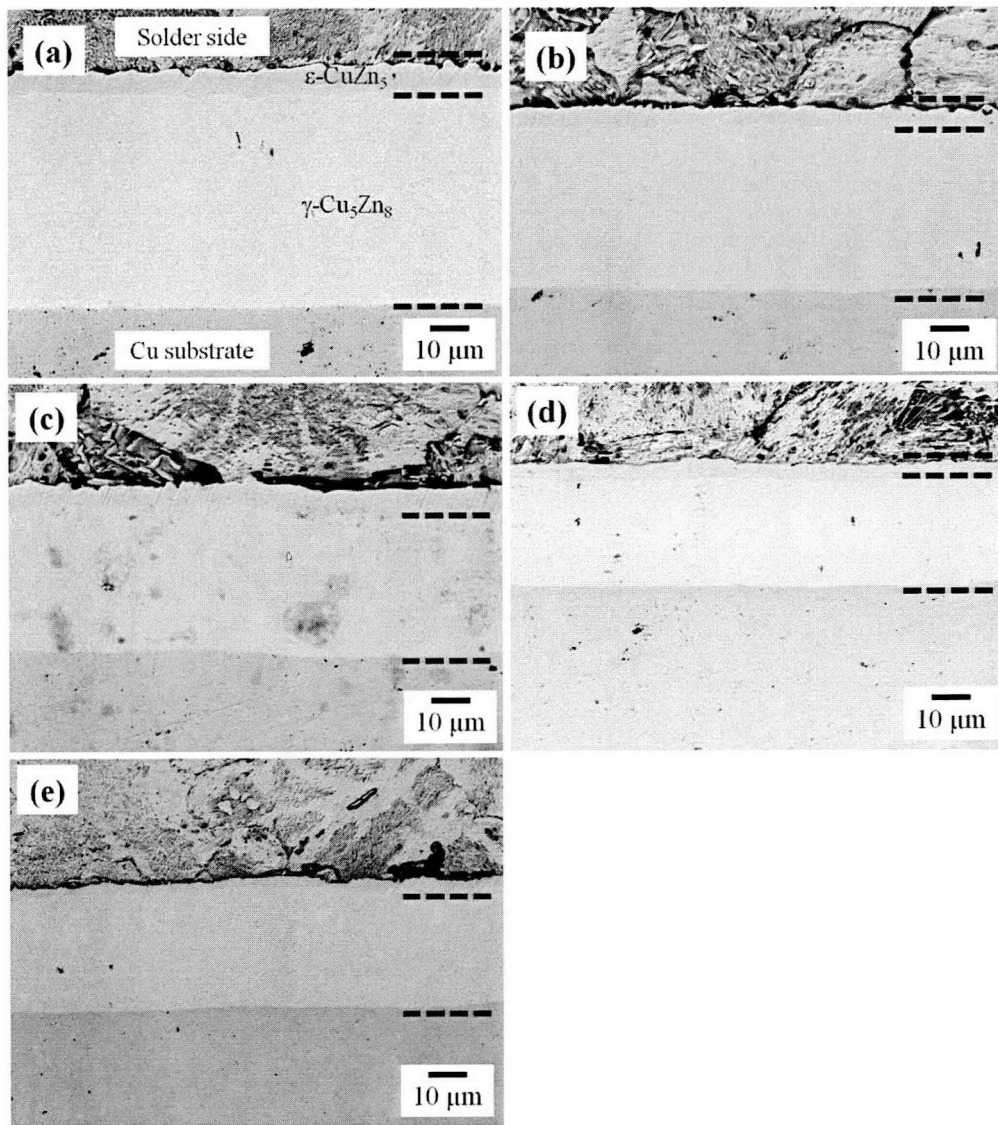


Fig. 3.8 SEM micrographs of reaction interface on a Cu substrate after thermal aging at 150 °C for 100h; (a) with pure Zn, (b) with Zn–0.1Ca, (c) with Zn–0.1Mn, (d) with Zn–0.1Cr, and (e) with Zn–0.1Ti.

For aging 100h at 150 °C, as shown in Fig. 3.8, IMC layer at the interface was much thicker than (about twice) as soldered interface. The total thicknesses of Zn/Cu reaction layer is about 65 μm , and Zn-0.1X/Cu reaction layers are about 40 μm , respectively. The interfacial reaction between the solder and Cu substrate continues during isothermal aging, which can be evidenced by thickness increase of the IMC. The morphology of the scallop type $\epsilon\text{-CuZn}_5$ gradually transforms to flat type $\gamma\text{-Cu}_5\text{Zn}_8$ phase. The minor element added solders, on the other hand, the $\gamma\text{-Cu}_5\text{Zn}_8$ layer exhibited a slower growth. Figure 3.9 shows the comparison of IMC thickness for Zn/Cu, Zn-0.1Mn/Cu and Zn-0.1Cr/Cu couples after isothermal aging at 150 °C for 200 h, and 500 h. The IMC thickness of Zn/Cu interface after aging for 200h, and 500h is about 84 μm , and 130 μm , respectively. In case of minor elements added Zn such as Zn-0.1Mn (59, and 92 μm) and Zn-0.1Cr (48, and 63 μm) displayed thinner IMC layer, it imply the minor element addition shows the depressing effect on the IMC growth. Among the addition element, Cr addition indicates the slowest growth rate during the thermal aging because the assumed Zn_xCr_y IMC phase existing in solder matrix, which can block diffusion. These IMC formations can be explained from the Cr-Zn binary phase diagram [16]. According to the phase diagram, Cr-Zn IMC formation occurs for 0.03 wt.% of Cr concentration. Although the Zn-0.1Ca and Zn-0.1Ti with Cu interfaces show the thinnest IMC layer, it causes the delamination after aging 200h between solder and IMC layer as shown in Fig. 3.10.

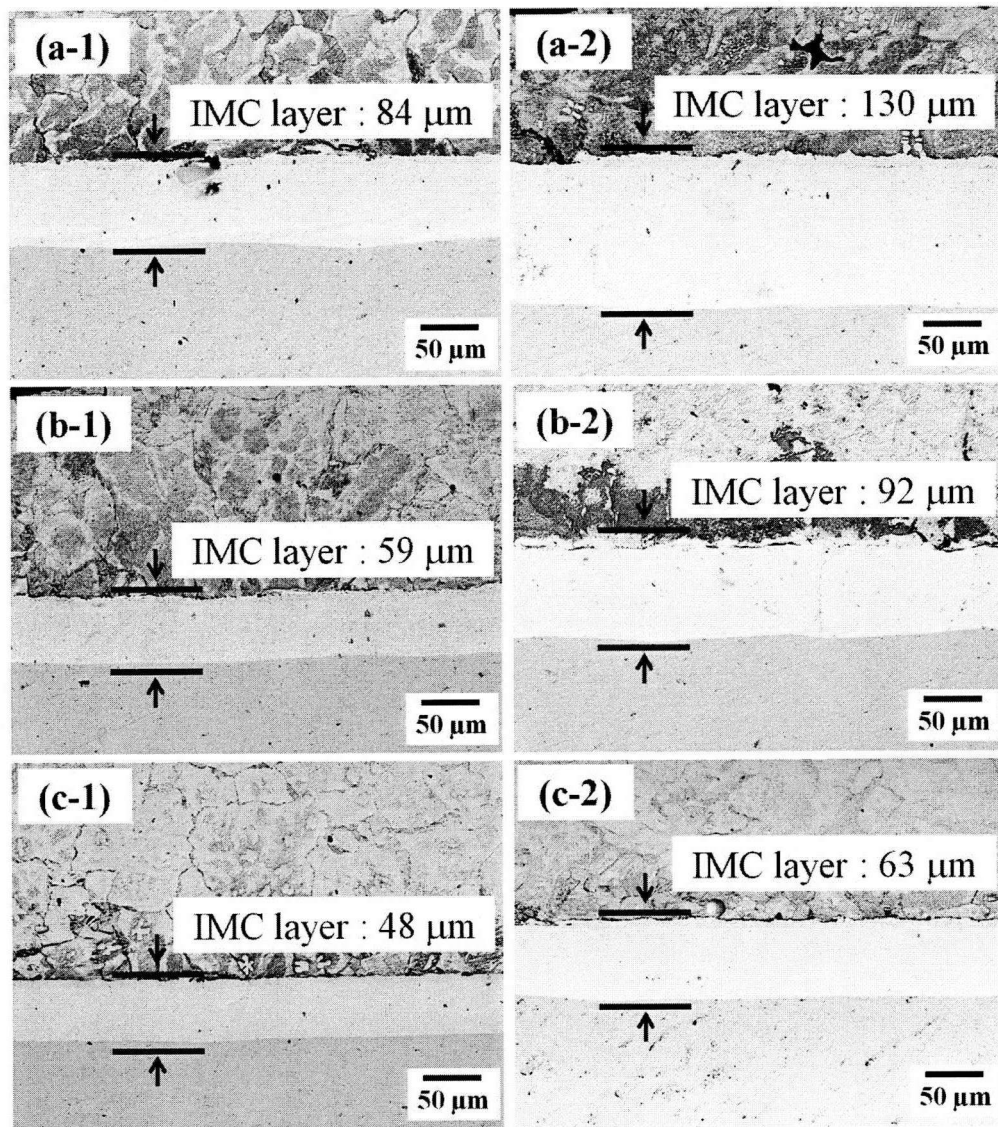


Fig. 3.9 SEM images of joint interface after thermal aging at 150 °C: (a-1) Zn/Cu interface aging for 200h, (a-2) Zn/Cu interface aging for 500h, (b-1) Zn-0.1Mn/Cu interface aging for 200h, (b-2) Zn-0.1Mn/Cu interface aging for 500h, (c-1) Zn-0.1Cr/Cu interface aging for 200h, and (c-2) Zn-0.1Cr/Cu interface aging for 500h.

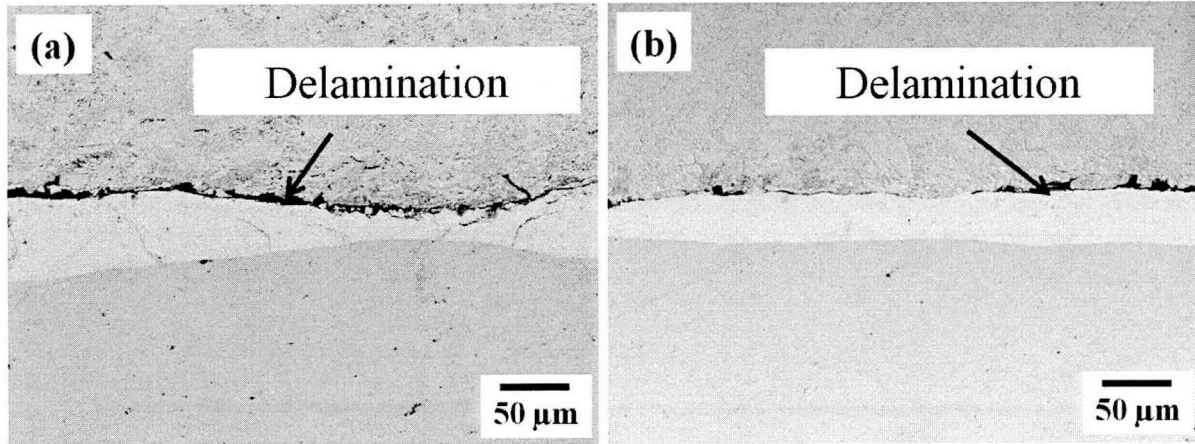


Fig. 3.10 Delaminated interface between solder and IMCs during thermal aging at 150 °C for 200h: (a) Zn-0.1Ca/Cu interface, and (b) Zn-0.1Ti/Cu interface.

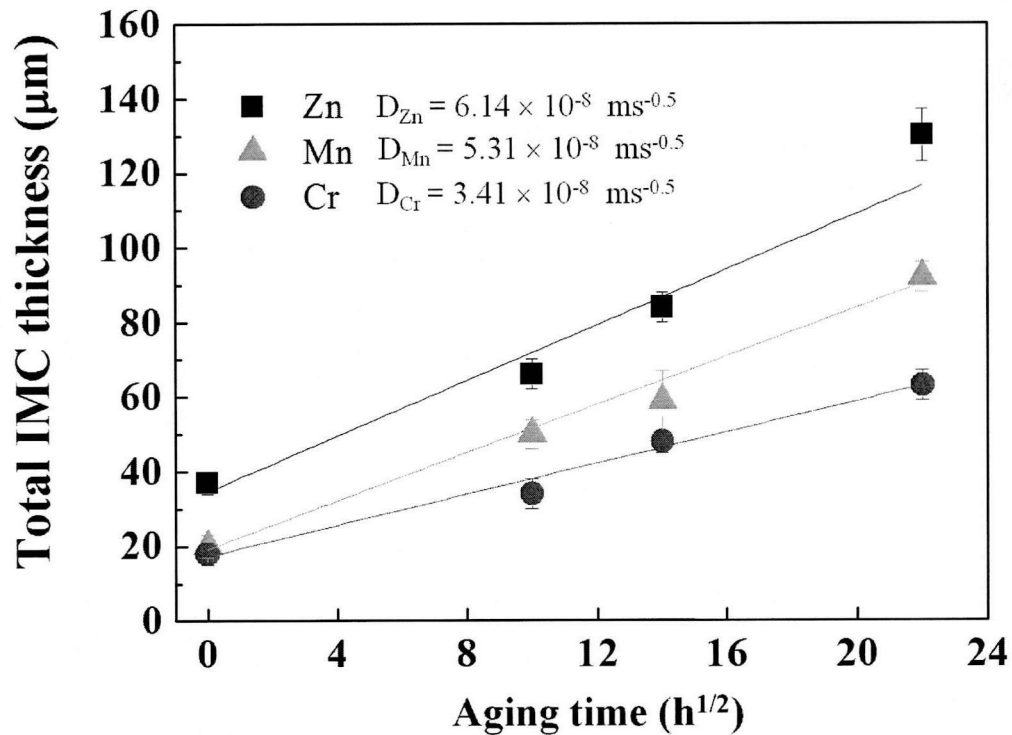


Fig. 3.11 The relationship curves between IMC thickness and aging time ($h^{1/2}$).

The IMC thickness of solder/Cu interface is plotted as a function of aging time and temperature, as illustrated in Fig. 3.11. It is found that the IMC thickness increases monotonically with aging time at 150 °C. To realize the effect of minor elements addition on growth rate, the IMC growth rates were calculated by the following Arrhenius equation [2, 7, 17–19].

$$X = X_0 + At^n \exp(-Q/RT) \quad (1)$$

where X and X_0 are the IMC thickness at t time and the initial IMC thickness as-soldered, respectively. Q is the activation energy, R denotes the gas constant, T and t mean the aging temperature and aging time, respectively. A means a constant and n is growth exponent. n was defined as 0.5 because the process is diffusion-controlled reaction as reported by Subbarayan [20]. Consequently, Equation (1) can be simplified as followed Equation (2):

$$X = X_0 + \sqrt{Dt} \quad (2)$$

where T is the aging time, X denotes the IMC thickness at t time, X_0 means the initial IMC thickness as-soldered, D is the coefficient of IMC growth rate. The values of IMC growth rate, D , were calculated by the slope of experimental results in Fig. 3.11. In this study, the growth rates were determined as $3.77 \times 10^{-15} \text{ m}^2/\text{s}$, $2.82 \times 10^{-15} \text{ m}^2/\text{s}$, and $1.16 \times 10^{-15} \text{ m}^2/\text{s}$ for Zn/Cu, Zn-0.1Mn/Cu, and Zn-0.1Cr/Cu, respectively. From the results of diffusion rate calculation, it is noteworthy that the IMC growth rate of Zn-0.1Cr exhibits only a-third of pure Zn/Cu couple.

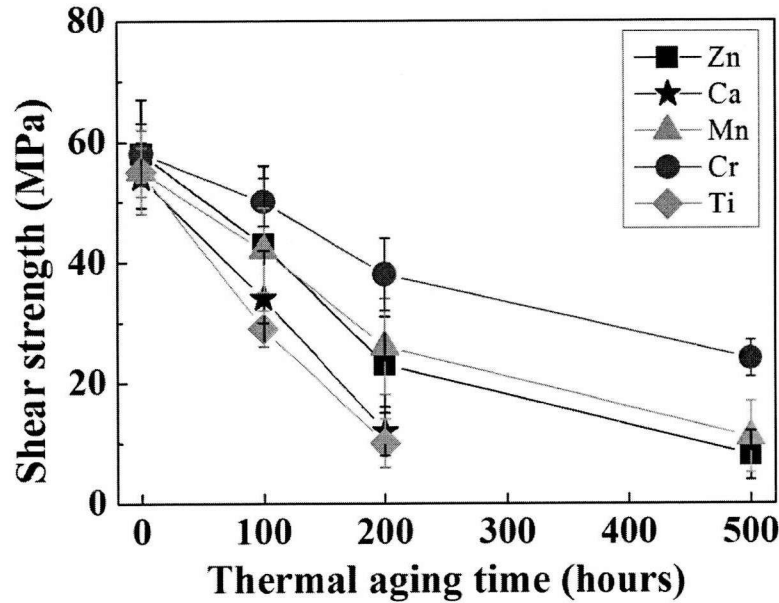


Fig. 3.12 Joining strength change of the Cu/solder/Cu joints during the thermal aging.

Figure 3.12 shows the result of shear strength testing for the Cu/solder/Cu joints with Zn and minor elements added Zn solders during the thermal aging. The shear strength of a joint with all solders is about 60 MPa, which is significantly higher than that of reported Au-20Sn solder (41.8 MPa) [3, 21] or that of Pb-5Sn solder (26.2 MPa) [3, 21, 22]. With an increase in aging time, the shear strength of the joint with all solders decreases sharply, except with Zn-0.1Cr. The decline of shear strength with Zn-0.1X (X = Ca, Mn, Ti) after aging causes the brittle nature of IMC layer, which gradually grow during aging time. During the aging time, the higher shear strength of the Zn-0.1Cr alloy can be attributed to its thinner IMC thickness. In case of the joints with Zn-0.1Ca and Zn-0.1Ti, they show the lowest shear strength aging for only 200h, it could agree the delaminated interface microstructure as shown in Fig. 3.10.

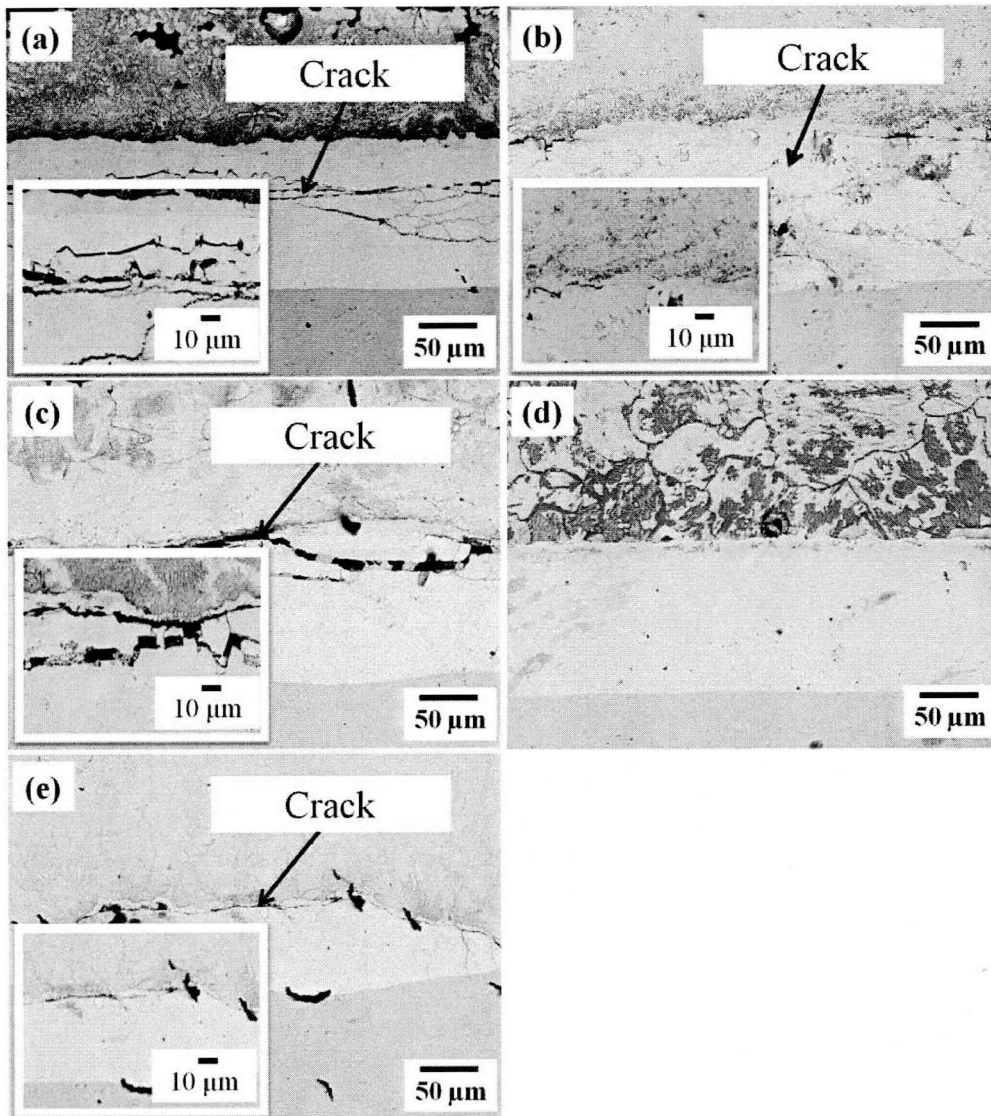


Fig. 3.13 SEM micrographs of reaction interface on a Cu substrate after thermal aging at 250 °C for 100h; (a) with pure Zn, (b) with Zn-0.1Ca, (c) with Zn-0.1Mn, (d) with Zn-0.1Cr, and (e) with Zn-0.1Ti. The insets indicate the enlarged images.

To describe the high temperature environment i.e. SiC power device operating temperature, thermal aging at 250 °C was carried out. During aging treatment at higher temperatures for 100h, the formation of a considerable crack was observed inside the γ -Cu₅Zn₈ IMC phase, except Zn-0.1Cr/Cu interface as shown in Fig. 3.13. To investigate the duration of Zn-0.1Cr/Cu interface, thermal aging was carried out continuously until 500h compared with Zn/Cu joining specimen. Figure 3.14 shows

the interface images after thermal aging for 500h at 250 °C. For aging 500h at 250 °C, the pure Zn loses its own shape as solder due to completely consume the reaction with Cu atom. Although the Zn-0.1Cr shows the crack at the γ -Cu₅Zn₈ layer, it can retain the structure as solder. In case of Zn/Cu specimen, the Cu atom migration occurs to a whole of the solder side as mentioned above but the Cu was not reached at a top of solder side in the minor Cr addition specimen during solid-state aging process. A too-thick IMC layer deteriorates the solder joint reliability because the IMC are brittle and have different densities from the solder alloys [1, 3]. It is imply that the addition of Cr is benefit for restraining interfacial IMCs. It is quite reasonable to consider that reliability of Zn-0.1Cr/Cu joint would be better than Zn/Cu joint because of thinner intermetallic compound layer. From the result of thermal aging, it is concluded that the usage of Zn-0.1Cr alloy has more improved characteristics than pure Zn as a high temperature solder on Cu substrates from the present session. Therefore, the joints reliability of SiC die-attach could be anticipated to improve. In order to establish more reliable solder alloys, further works are required to assess the compatibility various plating or metallization substrates.

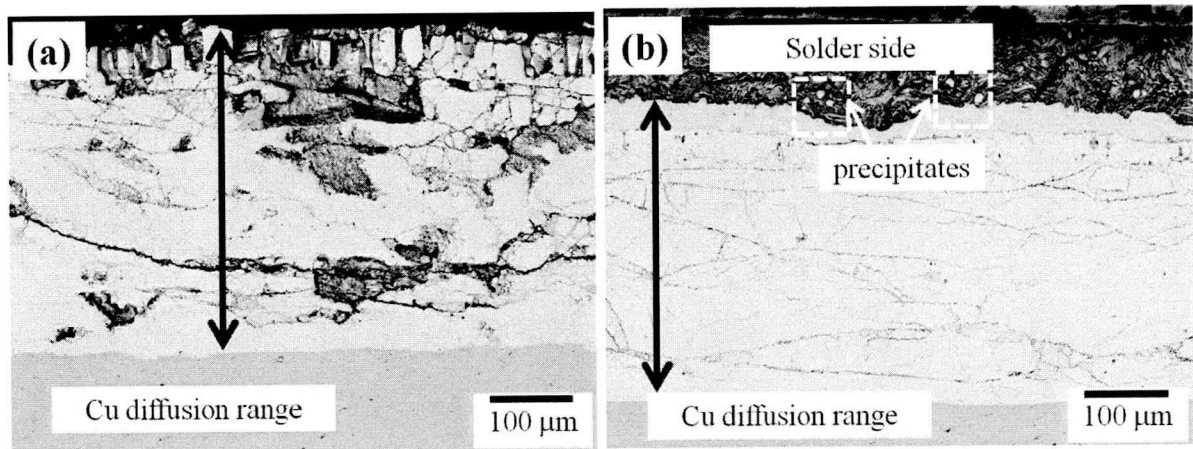


Fig. 3.14 Different appearance after thermal aging at 250 °C for 500h; (a) with pure Zn, and (b) with Zn-0.1Cr.

3. 4 Conclusions

In the present chapter, pure Zn and Zn-0.1X (X = Ca, Mn, Cr, and Ti) alloys were joined on Cu substrate, especially to focus on the growth of intermetallic compounds during the thermal aging. The results can be summarized as follows:

1) The thicknesses of Zn/Cu IMC layer is about 35 μ m, and Zn-0.1X/Cu reaction layers are about 15 μ m, respectively, after soldering at 430 °C. Two reaction layers were formed at the solder/Cu interface, and identified as scallop shape ϵ -CuZn₅ phase adjacent to the solder, and layer type γ -Cu₅Zn₈ formed facing to the Cu substrate, respectively.

2) For aging 100h at 150 °C, the total thicknesses of Zn/Cu reaction layer is about 65 μ m, and Zn-0.1X/Cu reaction layers are about 40 μ m, they are much thicker than (about twice) as soldered interface. However, the growth rate of the scallop type ϵ -CuZn₅ is significantly slower than layer type γ -Cu₅Zn₈ due to gradual transition from γ -Cu₅Zn₈ phase to the scallop type ϵ -CuZn₅. With aging time for 100h, the joints interface with minor element added solders exhibited a slower growth than Zn/Cu joining specimens.

3) The IMC thickness of Zn/Cu interface after aging at 150 °C for 200h, and 500h is about 84 μ m, and 130 μ m, respectively. In contrast, joint interface of minor elements added Zn such as Zn-0.1Mn and Zn-0.1Cr displayed thinner IMC layer. The calculated IMC growth rates during thermal aging indicated as 3.77×10^{-15} m²/s, 2.82×10^{-15} m²/s, and 1.16×10^{-15} m²/s for Zn/Cu, Zn-0.1Mn/Cu, and Zn-0.1Cr/Cu, respectively. The minor Cr exhibited the slowest growth rate during the thermal aging due to the formation of small Zn_xCr_y IMC phase in solder matrix, which can block diffusion. It implies the minor Cr has an effect of the depressing on the IMC growth.

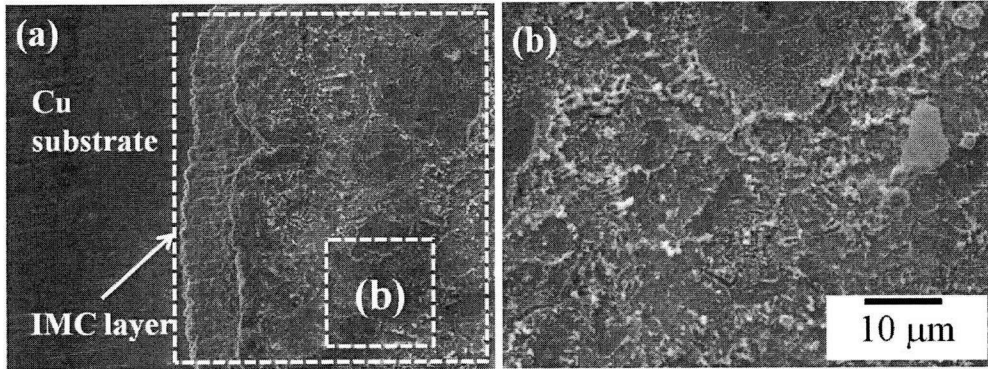
4) The shear strength of an as solder joints with all solders (Cu/solder/Cu) exhibited about 60 MPa. With an increase in aging time at 150 °C, the shear strength of the joint with all solders significantly

decreases except with Zn-0.1Cr. The shear strength drop with Zn-0.1X (X = Ca, Mn, Ti) after aging stem from the thick IMC layer, which has a brittle nature. During the aging time, the higher shear strength of the Zn-0.1Cr alloy can be attributed to its thinner IMC thickness.

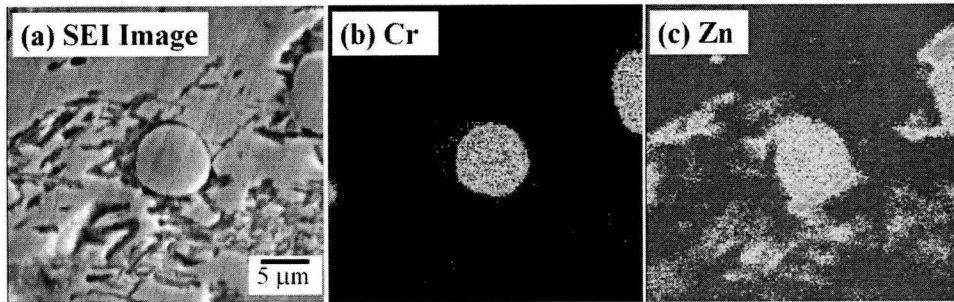
5) For aging at 250 °C, the formation of a considerable crack was observed inside the γ -Cu₅Zn₈ IMC phase, except Zn-0.1Cr/Cu interface. The interface after thermal aging for 500h at 250 °C, the pure Zn joining specimens lost its own shape as solder due to completely consume the reaction with Cu atom. The interface with Zn-0.1Cr could remain the solder structure due to, but the inevitable crack was observed. A too-thick IMC layer is the well-known state to hinder the solder joint reliability because the IMC are brittle and have different densities from the solder alloys. In the present chapter, the additive Cr shows a benefit for restraining interfacial IMCs.

Thus, it is concluded that the usage of Zn-0.1Cr alloy has more improved characteristics than pure Zn as a high temperature solder on Cu substrates and the joints reliability of SiC die-attach could be anticipated to improve. In order to establish more reliable interconnection, further works are required to assess the compatibility between improved alloys and various metalized substrates and to attach SiC die to substrates.

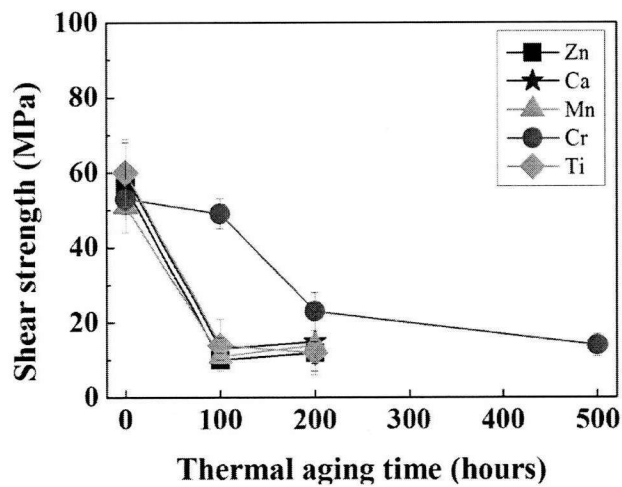
Appendix



A. Fracture surface of Zn-0.1Cr/Cu joints;
(a) low magnification x100 and (b) high magnification image.



B. EPMA mapping images of the precipitates inside solder.



C. Joining strength change of the Cu/solder/Cu joints during the thermal aging at 250°C.

REFERENCES

- [1] J.E. Lee, K.S. Kim, K. Suganuma, J. Takenaka, and K. Hagio, “*Interfacial Properties of Zn–Sn Alloys as High Temperature Lead-Free Solder on Cu Substrate*”, Mater. Trans. 46 (2005) 2413.
- [2] Y. Takaku, L. Felicia, I. Ohnuma, R. Kainuma, and K. Ishida, “*Interfacial Reaction Between Cu Substrates and Zn–Al Base High-Temperature Pb-Free Solders*”, J. Electron. Mater. 37 (2008) 314.
- [3] S.J. Kim, K.S. Kim, S.S. Kim, and K. Suganuma, “*Interfacial Reaction and Die Attach Properties of Zn–Sn High-Temperature Solders*”, J. Electron. Mater. 38 (2009) 266.
- [4] J.M. Kim, S.W. Woo, Y.S. Chang, Y.J. Kim, J.B. Choi, and K.Y. Ji, “*Impact reliability estimation of lead free solder joint with IMC layer*”, Thin Solid Films 517 (2009) 4255.
- [5] M. Ghosh, Abhijit Kar, S.K. Das, and A.K. Ray, “*Aging Characteristics of Sn–Ag Eutectic Solder Alloy with the Addition of Cu, In, and Mn*”, Metall. Mater. Trans. A 40 (2009) 2369.
- [6] WenXue Chen, SongBai Xue, and Hui Wang, “*Wetting properties and interfacial microstructures of Sn–Zn–xGa solders on Cu substrate*”, Mater. Des. 31 (2010) 2196.
- [7] Yu-hua Hu, Song-bai Xue, Huan Ye, Zheng-xiang Xiao, Li-li Gao, and Guang Zeng “*Reliability studies of Sn–9Zn/Cu and Sn–9Zn–0.06Nd/Cu joints with aging treatment*”, Mater. Des. 34 (2012) 768.
- [8] T. Sasaki, M. Tanaka, and Y. Ohno, “*Intermetallic compound formation between lead-free solders (Sn) and Cu or Ni electrodes*”, Mater. Lett. 61 (2007) 2093.
- [9] K. Suganuma, K. Niihara, T. Shoutoku, and Y. Nakamura, “*Wetting and interface microstructure between Sn–Zn binary alloys and Cu*”, J. Mater. Res. 13, (1998) 2859.
- [10] K. Suganuma, T. Murata, H. Noguchi, and Y. Toyada, “*Heat resistance of Sn–9Zn solder/Cu interface with or without coating*”, J. Mater. Res. 15, (2000) 884.
- [11] H.K. Kim, H.K. Liou and K.N. Tu, “*3-dimensional morphology of a very rough interface formed in the soldering reaction between eutectic SnPb and Cu*”, Appl. Phys. Lett. 66 (1995) 2337.

- [12] H.K. Kim and K.N. Tu, “*Kinetic analysis of the soldering reaction between eutectic SnPb alloy and Cu accompanied by ripening*”, Phys. Rev. B 53 (1996) 16027.
- [13] K.N. Tu, T.Y. Lee, J.W. Jang, L. Li, D.R. Frear, K. Zeng and J.K. Kivilahti, “*Wetting reaction versus solid state aging of eutectic SnPb on Cu*”, J. Appl. Phys. 89 (2001) 4843.
- [14] K.N. Tu and K. Zeng, “*Tin-Lead (Sn-Pb) solder reaction in flip chip technology*”. Mater. Sci. Eng. R34 (2001) 1.
- [15] A.M. Gusak and K.N. Tu, “*Kinetic theory of flux-driven ripening*”, Phys. Rev. B 66 (2002) 115403.
- [16] T. B. Massalski, “*Binary alloy phase diagrams 2nd Ed.*”, ASM international, USA, (1992).
- [17] S. Chada, W. Laub, R.A. Fournelle, and D. Shangguan, “*An improved numerical method for predicting intermetallic layer thickness developed during the formation of solder joints on Cu substrates*”, J. Electron. Mater. 28 (1999) 1194.
- [18] M. Schaefer, R.A. Fournelle, and J. Liang, “*Theory for intermetallic phase growth between Cu and liquid Sn-Pb solder based on grain boundary diffusion control*”, J. Electron. Mater. 27 (1998) 1167.
- [19] Christopher Fuchs, Timo Schreck, and Michael Kaloudis “*Interfacial reactions between Sn-57Bi-1Ag solder and electroless Ni-P/immersion Au under solid-state aging*”, J. Mater. Sci. 47 (2012) 4036.
- [20] G. Subbarayan, “*A procedure for automated shape and life prediction in flip-chip and BGA solder joints*”, J. Electron. Pack. 118 (1996) 127.
- [21] S.J. Kim, K.S. Kim, K. Suganuma, and G. Izuta, “*Interfacial Reactions of Si Die Attachment with Zn-Sn and Au-20Sn High Temperature Lead-Free Solders on Cu Substrates*”, J. Electron. Mater. 38, (2009) 873.
- [22] K. Suganuma, and S. Kim, “*Ultra Heat-Shock Resistant Die Attachment for Silicon Carbide With Pure Zinc*”, IEEE Electr. Device. L. 31 (2010) 1467.

Chapter 4

Joining properties and thermal shock reliability of SiC die-attached joints

Abstract

In the present chapter, SiC die-attachment with using Zn-0.1Cr solder is evaluated by thermal shock resistance, in comparison with the conventional Pb-5Sn solder joining. The pure Zn and Zn-0.1Cr solders exhibit excellent heat-cycle resistance for the DBC die-attach structure in the temperature range from $-50\text{ }^{\circ}\text{C}$ to $300\text{ }^{\circ}\text{C}$. In spite of the apparent thermal cycle resistance confirmed by the experiments, the enhancement mechanism has not yet been clarified in the Cr added Zn solder. Further study to clarify the reason of the improved thermal cycle reliability is suggested to establish the solder application in future.

4. 1 Introduction

In die-attach applications to power devices, the selection of solder material is crucial for reliable mechanical integrity of the metal-semiconductor joint and packaging [1–3]. Because of considerable thermo-mechanical stresses resulting from a mismatch in the coefficients of thermal expansion (CTE) on both sides of the solder layer seriously affect the thermal and mechanical reliability of the solder joints [3, 4]. Due to the power device applications are usually subjected to temperature variation in a wide range during the operation, new high-temperature Pb-free solders are required to have greater joint reliability at higher operating temperature, as compared with the present high-Pb-content solders. SiC semiconductor power devices, the required considerable wider operating temperature ranges from -50 to 300 °C than Si power devices (from -40 to 150 °C) [5, 6]. Thermal cycling (or thermal shock) reliability test are commonly used to evaluate the thermo-mechanical fatigue reliability of electronic assemblies. The thermal cycling test is uniformly heated up and cooled down in order to induce thermo-mechanical strains and stresses in interconnections and interfaces of the devices.

The previous chapter, pure Zn was improved through minor elements addition. Among the minor elements added Zn, Zn–0.1Cr solder is one of the best choice because it improves the ductility, oxidation resistance, and intermetallic compounds growth as explained in the Ch. 2 and 3. In the present chapter, for confirming the potential of die-attach material, SiC die-attachment is carried out and evaluated the thermal fatigue reliability of joints minor using minor Cr added Zn. These results were compared pure Zn and those of the currently used high-temperature solders, i.e., Pb-5Sn.

4. 2 Experimental procedures

SiC die attachment on direct bond copper (DBC) substrate

The solder alloys used in this chapter, Zn–0.1Cr, pure Zn, and Pb–5Sn were prepared as sheets (4×4 mm, $t=0.2$ mm), and the sheet faces were polished with 3 μm alumina powders. SiC dies (4 mm x 4 mm, $t=1$ mm) were coated with 800 nm titanium nitride (TiN) and 200 nm Au layer using a radio frequency (RF) sputter. Silicon nitride (Si_3N_4) direct bonded copper (DBC) was used as substrate because Si_3N_4 has excellent high temperature stability, high thermal conductivity and a coefficient thermal expansion (CTE) (CTE=3.5 ppm/K) closely matching that of SiC. A TiN diffusion barrier was adopted to increase the reliability of die attachment to a Cu substrate, and its efficacy was evaluated. Because titanium nitride is a stable compound, there was no reaction phase between titanium nitride and zinc, while zinc and copper formed two intermetallic compound layers as the reaction products, i.e., $\eta\text{-Cu}_5\text{Zn}_8/\varepsilon\text{-CuZn}_5$, which is identical to the Zn–Sn/Cu interface.

For SiC die attachment, the prepared solder sheets and a SiC die were set up on a DBC substrate as shown in Fig. 4.1. The die-attached specimens for the Zn based solders were heated to soldering temperatures of 450 °C, which are 30 °C higher than their melting temperatures, and held for 120 s. The die was attached with the Pb-5Sn solder at 340 °C, which is 26 °C higher than its liquidus temperature of 314 °C, and held for 120 s. The SiC die was soldered at peak temperature 450 °C in an atmosphere of formic acid reflow. The temperature profile of soldering illustrated Fig. 4.2.

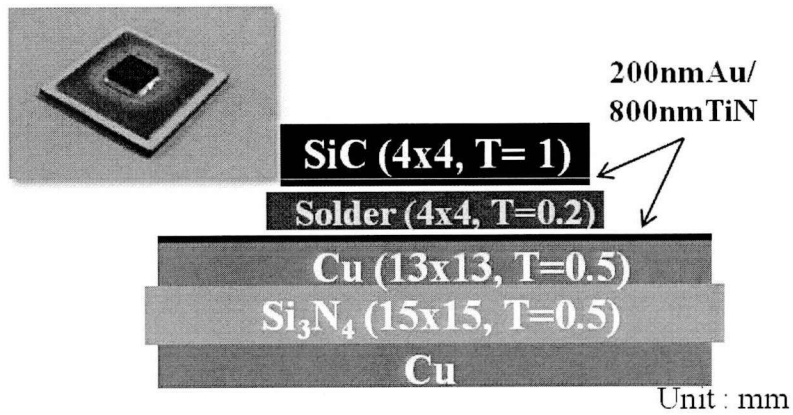


Fig. 4.1 Schematic structure of SiC die-attach structure and its photo.

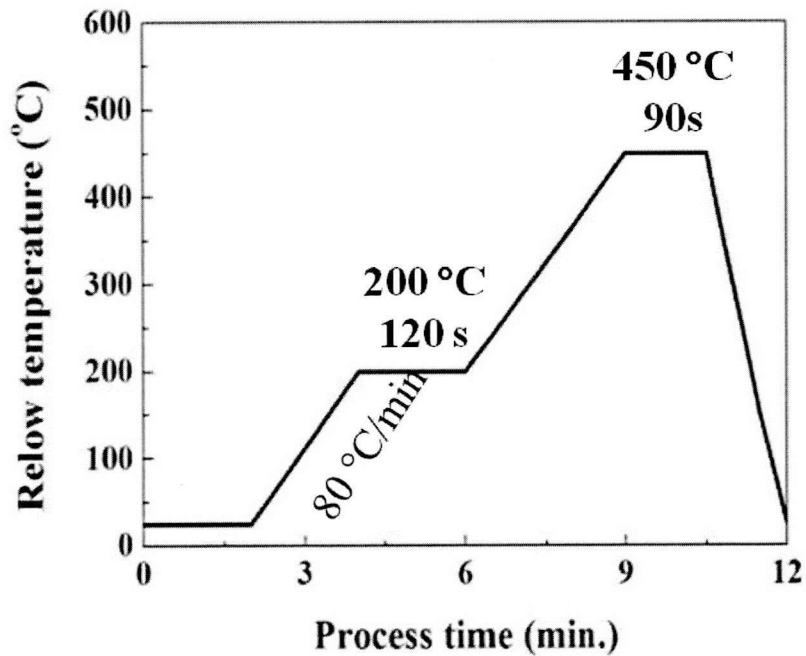


Fig. 4.2 Temperature profiles of the die-attach soldering.

Thermal shock reliability test

In a thermal cycling test, the SiC die-attached joints were put into a thermal cycling chamber and exposed to a temperature range of $-40\text{ }^{\circ}\text{C}$ to $300\text{ }^{\circ}\text{C}$ with a heating/cooling rate of $\pm 1\text{ }^{\circ}\text{C/s}$ and a holding time of 30 min at each peak temperature. The thermal cycling profile presented Fig. 4.3. Figure 4.4 shows the schematic image of the shear test using a bond tester (Dage-4000) for evaluating the joining strength. The shear test was performed at a head speed of $1\text{ }\mu\text{m/s}$ and a height of $200\text{ }\mu\text{m}$.

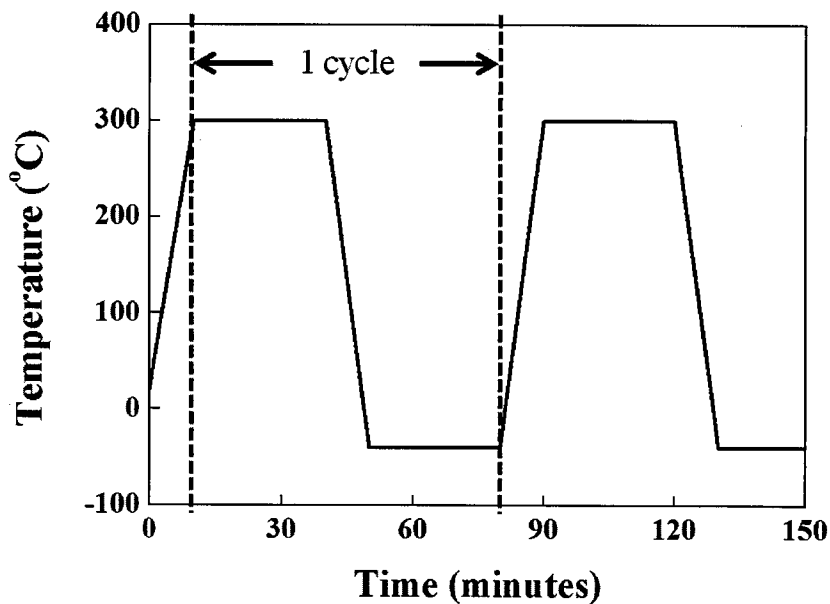


Fig. 4.3 Temperature profile of thermal cycling for the evaluation of SiC joint reliability.

4. 3 Results and discussion

4. 3. 1 Interfacial reaction of the SiC die-attached joints

Figure 4.4 shows the typical interfacial microstructures of the SiC die-attachment to a DBC substrate with Zn-0.1Cr solder that was soldered at 450 °C for 120s. Zn-0.1Cr solder wetted both the SiC die and DBC substrate well. The interface microstructure observations confirm that a sound die attachment on a Si₃N₄-DBC substrate can be achieved with the prepared solders.

To establish Zn-0.1Cr solder as a SiC die-attach material, understanding of interfacial reactions with a substrate is required. In this chapter, however, the basis of interfacial reaction is insufficient. Therefore, the analysis of interfacial microstructure using a transmission electron microscope (TEM), and electron probe X-ray microanalyzer (EPMA) for could be carried out. In the observation of TEM, the interface between TiN and α -Zn phase and the effect of minor Cr could be investigated. From the EPMA results are expected the definition of reaction layer composition and the migration or transition of interfacial microstructure during the die-attach process.

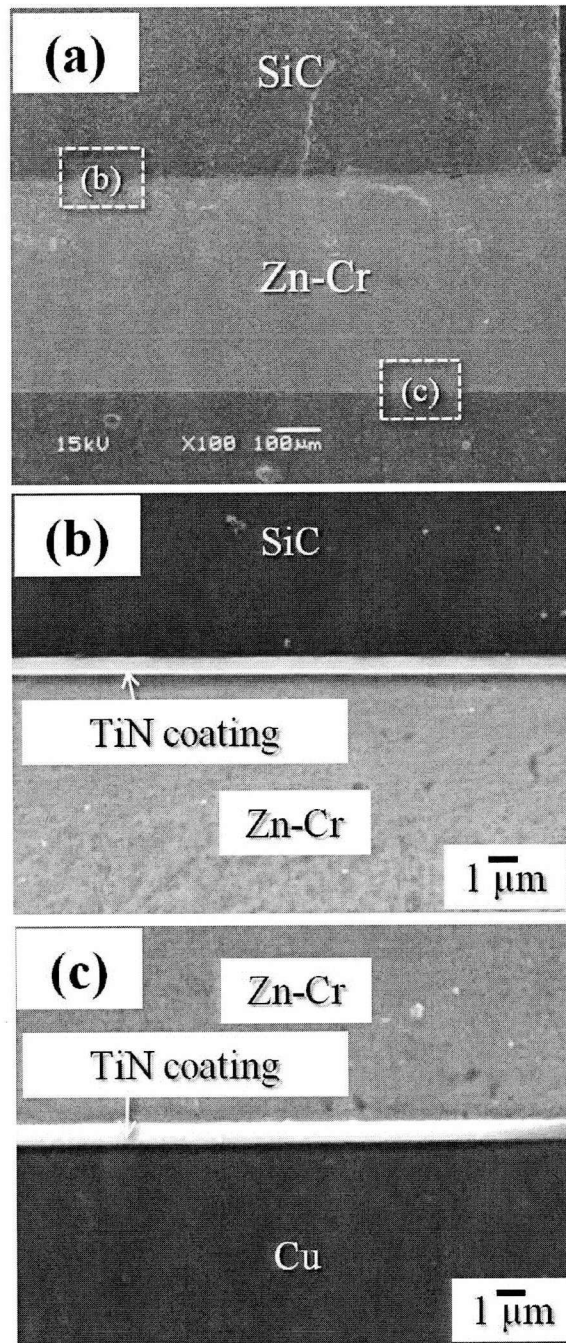


Fig. 4.4 SEM micrographs of SiC die-attachment on a DBC substrate: (a) a low magnification image of die-attach interface, (b) the interface of SiC die side, and (c) the interface of DBC substrate side.

4. 3. 2 Thermal cycle reliability

Fig. 4.5 shows the changes of the die-shear strength of the SiC/DBC joints as a function of thermal cycling time, where the joint strength with Zn-0.1Cr solder was compared with that with conventional Pb-5Sn, and pure Zn. The initial strength of the joints with Zn-0.1Cr and pure Zn was about three times higher than that with Pb-5Sn. The joints with Zn-0.1Cr and pure Zn maintain their high strength up to 500 cycles without serious degradation. Thus, the excellent thermal shock resistance of the current die-attach structure was proved by the fact that high shear strength of the die attach can be maintained even after severe thermal shocks. In contrast, the joint with Pb-5Sn decreased its strength to half of the initial strength, about 12 MPa. It is much lower strength than those with other solders.

Figure 4.6 shows the interface of the die-attached joints with pure Zn, Zn-0.1Cr, and Pb-5Sn solders on the TiN coated DBC substrate after 500cycles. In the die-attached joints with pure Zn and Zn-0.1Cr, it is noteworthy that no crack as shown in Fig. 4.6(a) and (b). Although the joint with pure Zn was not observed the crack, a little deformation of microstructure was observed due to thermo-mechanical stresses resulting from a mismatch in the CTE. The joints with Zn-0.1Cr solder showed no change of microstructure even after 500 cycles but just a small IMC growth inside the solder layer as shown inset of Fig. 4.6(b). In case of the Pb-5Sn solder joint (Fig. 4.6(c)), severe vertical and horizontal thermal fatigue cracking were observed inside solder layer. The cracks are link together to form a network on the entire joint region.

Although the present chapter presents a thermal cycle resistance SiC die-attachment with Zn-0.1Cr solder, the mechanism is not cleared. In the further study, the reason for the improvement of thermal cycle reliability will be investigated and established suggested.

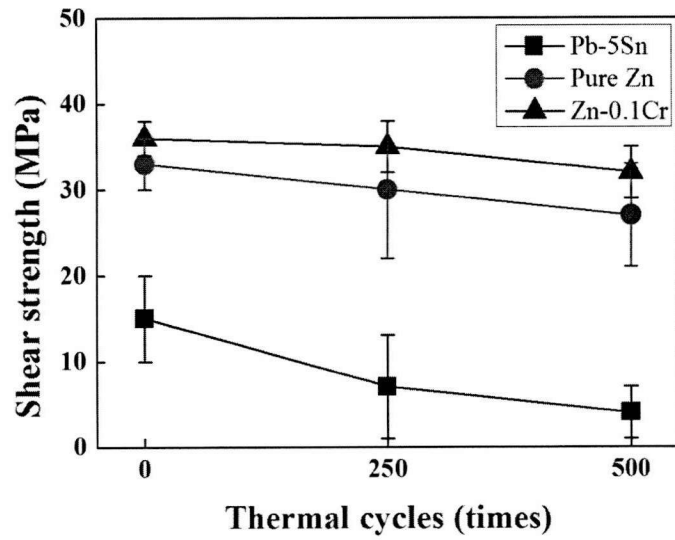


Fig. 4.5 The relationship between the number of thermal cycles and joint strengths of the SiC die-attachment.

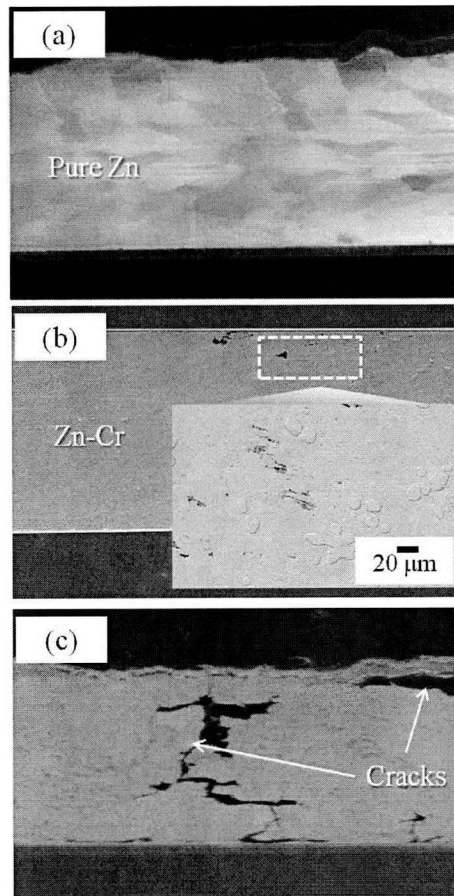


Fig. 4.6 The interface of SiC die-attachments after 500cycles of thermal cycling: (a) pure Zn, (b) Zn-0.1Cr, and (c) Pb-5Sn. The inset image shows the high magnification of solder layer.

4. 4 Conclusions

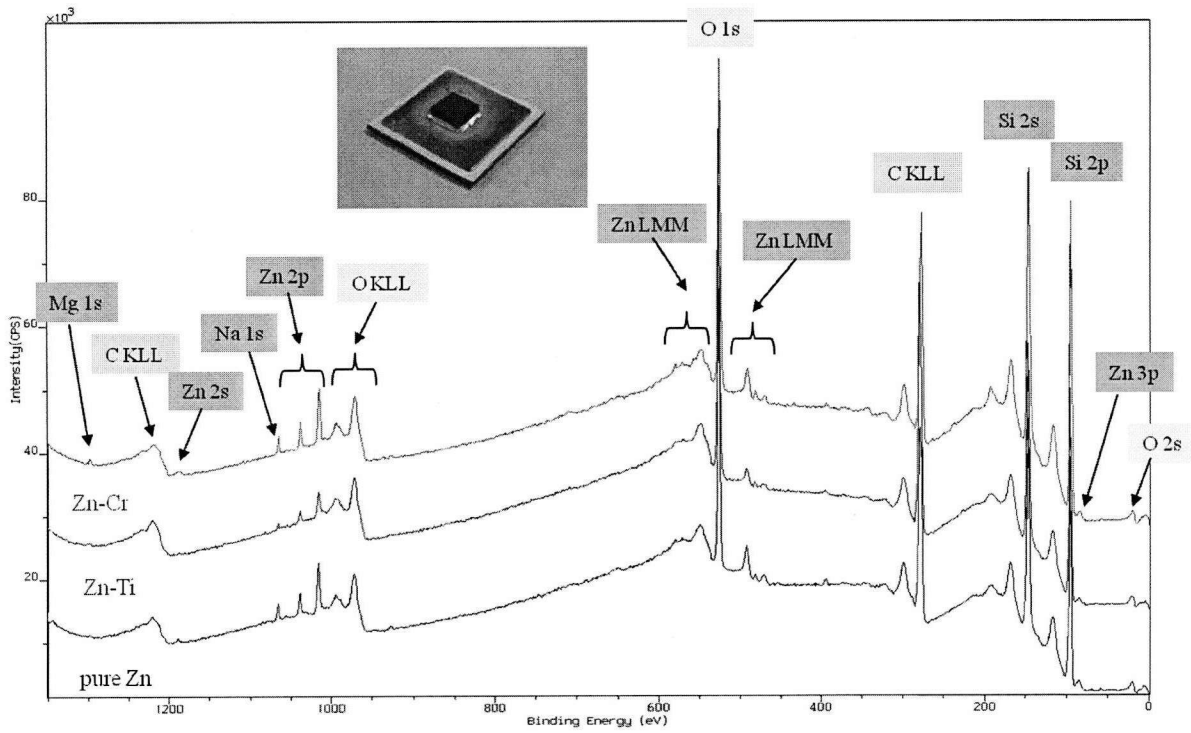
In the present chapter, some properties of pure Zn based high temperature solders and thermal shock resistance of the DBC die-attach structure were evaluated. The results are summarized as follows:

1) Although the SiC die-attachment to a DBC substrate with Zn-0.1Cr solder shows a sound bonding interface, the reaction mechanism of die-attachment is not cleared. Therefore, the interfacial reaction can be investigated in the further study.

2) Pure Zn and Zn-X solders provide excellent heat-cycle resistance for the DBC die-attach structure between $-50\text{ }^{\circ}\text{C}$ and $300\text{ }^{\circ}\text{C}$ without cracking. The die-attach structure with minor Cr added Zn and the TiN metallization interfaces has potentially the relaxation of thermo-mechanical stress. Thus, Zn-0.1Cr solder with Si_3N_4 -DBC exhibits quite excellent thermal shock resistance as compared with the conventional Pb-5Sn solder. Pure Zn based solder (minor Cr added Zn) has the great advantages of inexpensiveness compared with other candidates such as Au-based alloy solders or silver nano-particles.

Although the new process and thermal cycle reliability of SiC die-attachment have been studied, a mechanism of enhanced reliability is a necessary aspect for future study. Moreover, to optimize the packaging, the tradeoff considerations among materials selection (DBC substrate change to DBA), thermal dissipation design, electrical performance test (power cycle), and manufacturability should be introduced into the further evaluation.

Appendix



A. XPS result to investigate possible surface Zn contamination outside the SiC.

B. XPS quantitative analysis of reaction layers.

	Pure Zn	Zn-Ti	Zn-Cr
Mg	0.06	0.04	0.11
Na	0.51	0.12	0.46
Zn	0.72	0.35	0.65
O	18.35	18.55	16.30
C	53.75	57.85	51.59
Si	26.60	23.09	30.88

REFERENCES

- [1] R.R. Tummala, E.J. Rymaszewski and A.G. Klopfenstein, "*Microelectronics Packaging Handbook, Part II, Semiconductor Packaging*", Chapman & Hall, (1996).
- [2] K. Suganuma, "*Advances in lead-free electronics soldering*", *Curr. Opin. Solid State and Mater. Sci.* 5 (2001) 55.
- [3] H.S. Chin, K.Y. Cheong, and A.B. Ismail, "*A Review on Die Attach Materials for SiC-Based High-Temperature Power Devices*", *Metall. Mater. Trans.* 41B, (2010) 824.
- [4] Bo. Liou, C.M. Chen, R. Horng, Y. Chiang, and D. Wu, "*Improvement of thermal management of high-power GaN-based light-emitting diodes*", *Microelectro. Reliab.* 52 (2012) 861.
- [5] J.S. Karppinen, J. Li, T.T. Mattila, and Mervi Paulasto-Kröckel, "*Thermomechanical reliability characterization of a handheld product in accelerated tests and use environment*", *Microelectro. Reliab.* 50 (2010) 1994.
- [6] K. Suganuma, and S. Kim, "*Ultra Heat-Shock Resistant Die Attachment for Silicon Carbide With Pure Zinc*", *IEEE Electr. Device. L.* 31 (2010) 1467.

Chapter 4
Joining properties and thermal shock reliability of SiC die-attached joints

Chapter 5

Non-metallization Si wafer bonding by self-regulated eutectic reaction with pure Zn

Abstract

The present chapter introduces a world-first application of pure Zn used as interconnection material for Si wafer bonding. This bonding process can be carried out in the atmospheric pressure without metallization of Si surface. Resulting shear strength of the bonding exceeds 50 MPa, significantly higher than the typical strength of conventional Au–20Sn solders. The superior results are ascribed to uniform and void-free interface created by self-regulated Si–Zn eutectic reaction. In addition to the scientific finding of the unique eutectic reaction, the cost-efficient wafer bonding method has a wide range of applications in Si based devices.

5.1 Introduction

Si wafer-to-wafer bonding is recognized as a key technology for three dimensional system integrations, such as multi-tip large-scale integration (LSI) devices, stacked memories, and micro-electromechanical systems (MEMS) [1–3]. Considerable number of Si wafer bonding methods have been proposed in the literature [4–8], classified into two categories: direct fusion, and intermediate layer bonding [6]. The former process requires heat treatment at high temperature about 1000 °C to create a fusion layer between directly contacted Si wafers [1, 2]. The latter, in contrast, can be processed at considerably lower temperature by adopting an intermediate bonding layer of polymeric [4] or metallic [5–8] material inserted between Si wafers under certain pressure. In this category, Au–Si eutectic bonding has been used for integrated circuits packaging and MEMS applications [5–7]. The typical drawbacks of this method, however, are the formation of air voids and facet pits caused by uncontrolled Si dissolution into the Au layer in the Au–Si eutectic reaction [5–7, 9]. These typical defects show the Fig. 5.1 and 2. A sound bonding interface with high strength, i.e. uniform interface without any voids/defects formation, is rarely achieved by the Au–Si eutectic method, and may usually require more metallization layers on Si wafer, such as Ni, Pt, or Cr. Nevertheless, the high cost of Au causes another drawback of the Au–Si bonding in application to commercial products. The high demand for establishing a substantial but cost-efficient wafer-to-wafer bonding technique in the vast field of Si technologies has motivated us to develop an ideal bonding process based on our recent achievements particularly on lead-free solder materials [10,11]. In this letter, we hence propose a novel bonding process of Si wafers by utilizing self-regulated Si–Zn eutectic reaction. Using pure Zn as intermediate solder material, our bonding method is processed in air, at the atmospheric pressure, without surface metallization of Si wafers. The self-regulated Si–Zn eutectic reaction provides a thin and uniform bonding layer, resulting in a higher bonding strength

than that achieved by other competing techniques. As well as the low cost of the process, the present method demonstrates promising interconnection features of bonded Si wafers.

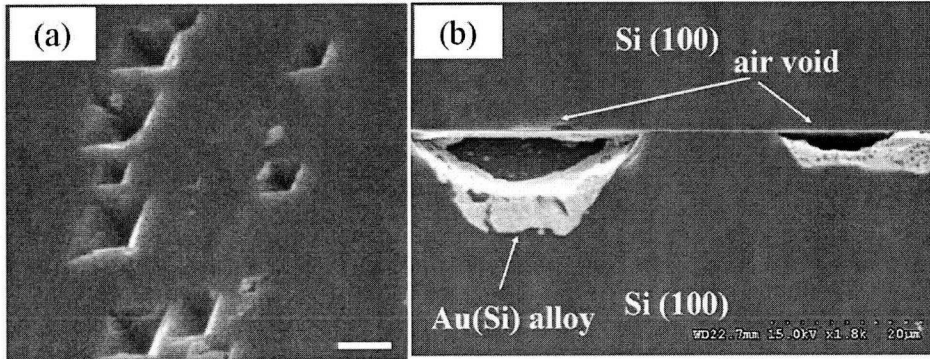


Fig. 5.1 Typical defects of Si wafer bonding using Au or Au-Si [7, 9].

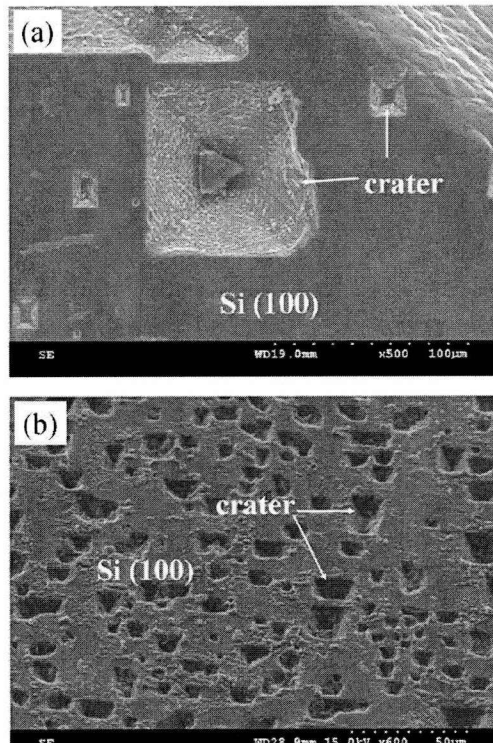


Fig. 5.2 Morphology of reacted Si surfaces:

(a) Au/Si bonding and (b) Au/amorphous Si bonding [12].

5.2 Experimental procedures

Pure Zn (> 99.99%) cold-rolled into 100 μm thick sheet, and a mirror polished 525 μm thick Si (100) wafer were prepared for the present study. The Zn sheet was cut into 10×10 mm specimens. Each surface of them was then mechanically polished, and finished using 0.1 μm Al_2O_3 abrasive powders. The final dimensions of the Zn sheets were $10 \times 10 \times 0.05$ mm. Two types of Si specimens of 10×10 mm (top) and 15×15 mm (bottom) were cut from the prepared Si (100) wafer. Before bonding, these Si and Zn specimens were degreased in acetone, and 20 vol.% aqueous HCl solution, and then rinsed in ethanol, de-ionized water, and dried in high pressure air. The prepared Zn sheet was inserted between two Si wafers (larger one at bottom), and held under the slight pressure (~ 2 kPa) of 20 g Ni weight block, as schematically shown in the Fig. 5.2. The prepared specimens were heated in an oven for 20 min. at 450 $^\circ\text{C}$, which is 30 $^\circ\text{C}$ higher than the melting point of pure Zn ($T_m = 419.58$ $^\circ\text{C}$). For comparison, Si wafer bonding tests with using commercial Au–20Sn solder were carried out with the similar processing conditions, but at the lower bonding temperature of 310 $^\circ\text{C}$, which is also 30 $^\circ\text{C}$ higher than the liquidus temperature (280 $^\circ\text{C}$) of the eutectic solder.

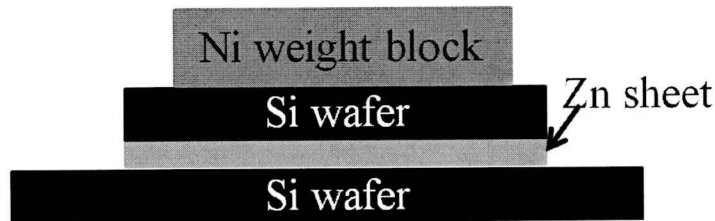


Fig. 5.3 Schematic of the present bonding structure.

5.3 Results and discussion

5.3.1 Bonding strength

Quality of a wafer bonding can generally be evaluated by the mechanical properties since high bond strength is the fundamental issue for device packaging. Hence we first evaluate the mechanical properties of the bonded specimens by shear tests using Dage 4000 where the head speed is set to 5 $\mu\text{m/s}$ and the fly height to 50 μm from the base tip surface. As displayed in Fig. 5.3, the typical shear strength of pure Zn bonding exceeds 50 MPa, significantly higher than other methods compared with; the conventional Au–20Sn eutectic solder gives below 8 MPa, and Au–Si about 20 MPa reported in the literature [7]. The measurements may even underestimate the bonding strength of pure Zn because Si wafer always exhibits fractures around 50 MPa during the tests (see the picture presented in the inset of Fig. 5.3). The breakage of Si wafer implies that pure Zn bonding exhibits sufficient mechanical strength as a soldering material for Si wafer. It is noteworthy that the process using pure Zn as an intermediate material does not require any metallization layer on Si surface to achieve such a high bonding strength.

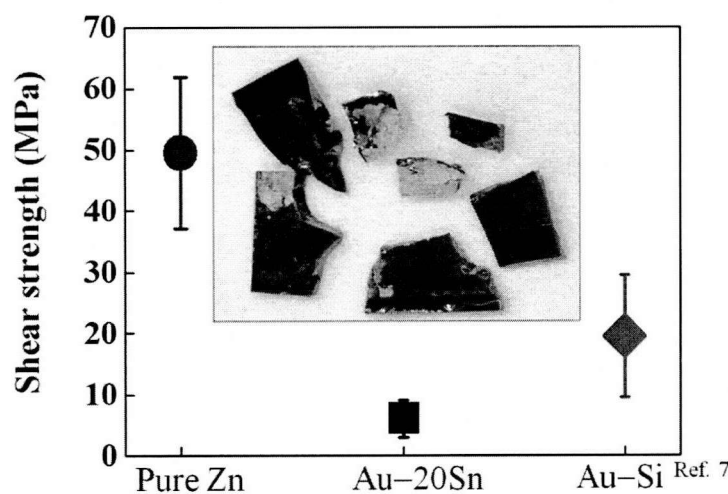


Fig. 5.4 Shear strengths of wafer bonding by pure Zn, Au–20Sn, and Au–Si[7]. The inset

image shows a typically broken specimen of pure Zn by fracture during the shear tests.

5.3.2 Microstructure of wafer bonding interface

To reveal the origin of the high bonding strength of Si/Zn interface, we have observed the cross-section microstructure of the bonding interface by field-emission scanning electron microscopy (FE-SEM). The SEM images in Fig.5.4 present a typical interface microstructure of Si and pure Zn bonding, and that of Au–20Sn soldering. The interface morphology resulting from the two bonding methods is different each other; pure Zn appears to wet well on the wafer surfaces of the both sides, and creates uniform and void-free reaction layers with Si (see Fig. 5.4(a)). In contrast, no reaction layer is found at the Au–20Sn/Si interface as shown in Fig. 5.4(b). Instead, massive air void, and delamination area are observed at the place. Higher magnification images in Fig. 5.4(c) and (d) confirm that the reaction layer at the Zn/Si interface is about 500 nm thick, but no reaction layer formed at Au–20Sn/Si interface. In the literature, similar air void formation at bonding interface between Si and intermediate materials have been reported, and those air voids are considered due to excessive Si dissolution into Au layer, particularly when Au–Si eutectic reaction occurs [9, 12]. The differences of interface morphologies observed seen in SEM images may explain the variation of joining strength registered in the shear tests. The uniform reaction layer between pure Zn and Si causes the high shear strength, while the absence of such a reaction layer in Au–20Sn solder results in poor mechanical bonding. These FE-SEM cross-section observations in Fig. 2(a) – 2(d) thus conclude that the presence of an intact reaction layer is essential to achieve high joining strength of wafer bonding processes.

Transmission X-ray imaging was utilized to observe air void formation at the Si and intermediate material interfaces of the bonding test specimens in the present study. However, there was no detectable void or defect confirmed in the pure Zn bonded wafer specimens (see Fig. 5.5(a)). In contrast, the specimens of Au–20Sn bonding typically display many defects as shown in Fig. 5.5(b), supporting the poor connection areas of the bonding interface as observed in the FE-SEM image of

Fig. 5.4(d). The void-free interface recorded by X-ray transmission imaging again demonstrates the superior feature of our Si wafer bonding with pure Zn. To examine the reacted Si surfaces with pure Zn, dilute HCl solution was used to remove the pure Zn bonding layer on bonded Si wafers. Figure 5.6(a) shows the exposed Si surface for the pure Zn bonding. The craters could not be seen on the bonding surface. Although Fig. 5.5 (c) displayed a small crater, it is very small size ($10\mu\text{m}$) and few while the big craters was reported using Au-Si [12]. We supposed that Si (100) planes are the most resistant to dissolving in Zn and have slower dissolution rate than Au. Due to a slow dissolution rate did not have enough time to form the craters, the interface of non-metallization bonding with pure Zn could obtain few or no craters wafer surface.

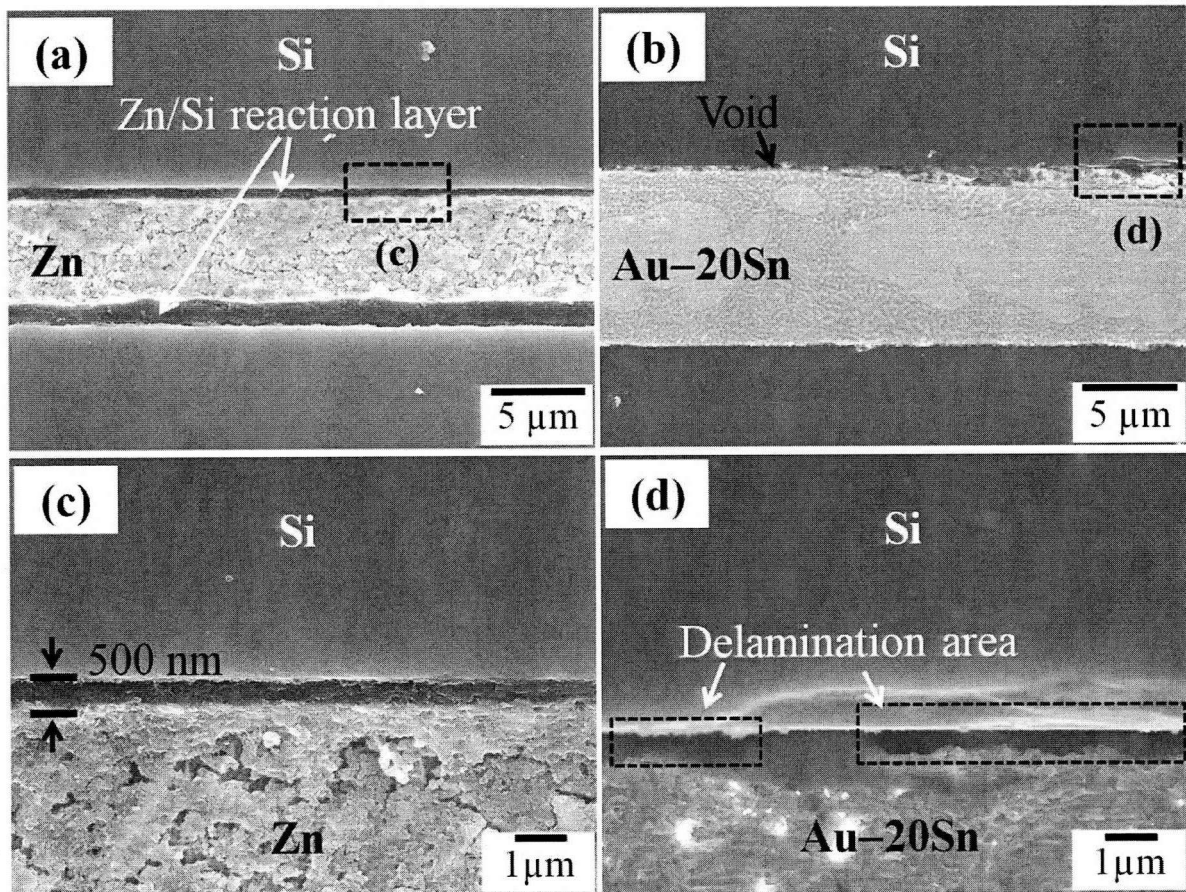


Fig. 5.5 Cross-section images of bonding interface (a) with pure Zn, and (b) with Au-20Sn.

(c) and (d) are the magnified images of (a) and (b), respectively.

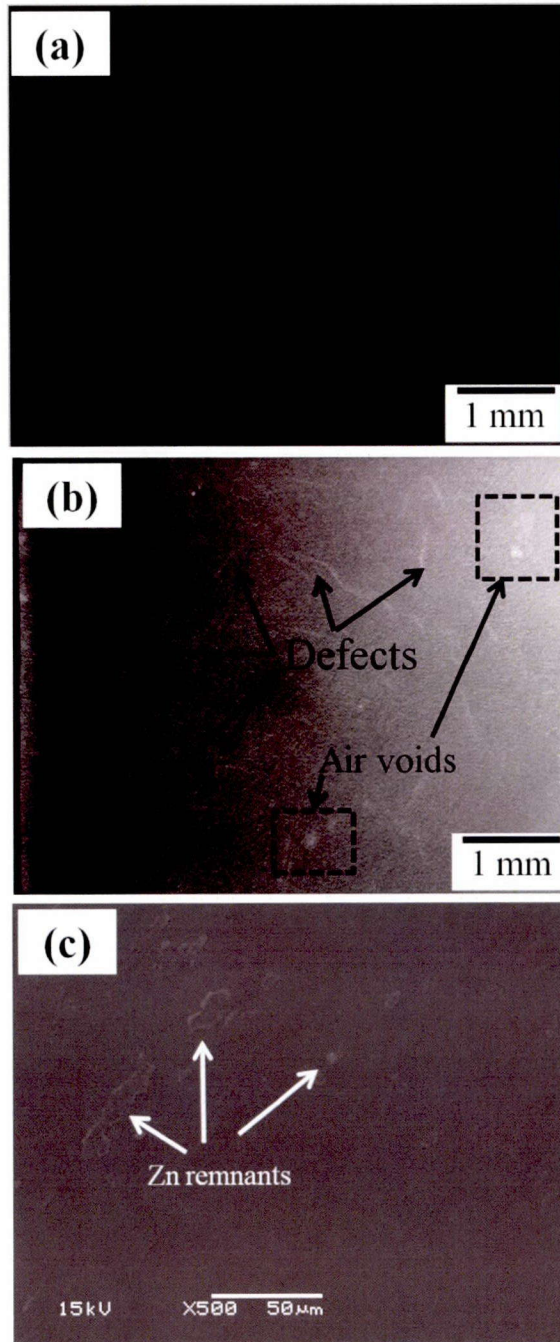


Fig. 5.6 (a) Transmission X-ray images with no air void in pure Zn bonding; (b) that with many defects in Au–20Sn soldering. (c) shows the no crater of Si wafer surface after etching.

Detailed investigation of the interface reaction layer has been made by electron-probe microanalyzer (EPMA) observation on the cross-section of the jointed specimens. The obtained EPMA mapping images in Fig. 5.6 (a) and (b) confirm that the reaction layer contains both Si and Zn, supporting that Si–Zn eutectic alloy is formed by the diffusion of Si into the molten Zn during the bonding process. The only trace amount of oxygen concentration detected in Zn side (see Fig. 5.6) indicates that the atomic diffusion occurs only from solid Si to liquid Zn during the bonding process. Due to the low-surface energy and poor adhesion [5], natural SiO₂ layer on Si surface appears to be dissolved and diffused into the molten Zn. Thus the natural oxide layer on Si wafer does not affect the pure Zn bonding process, but may cause a slight oxidization of intermediate Zn bonding layer.

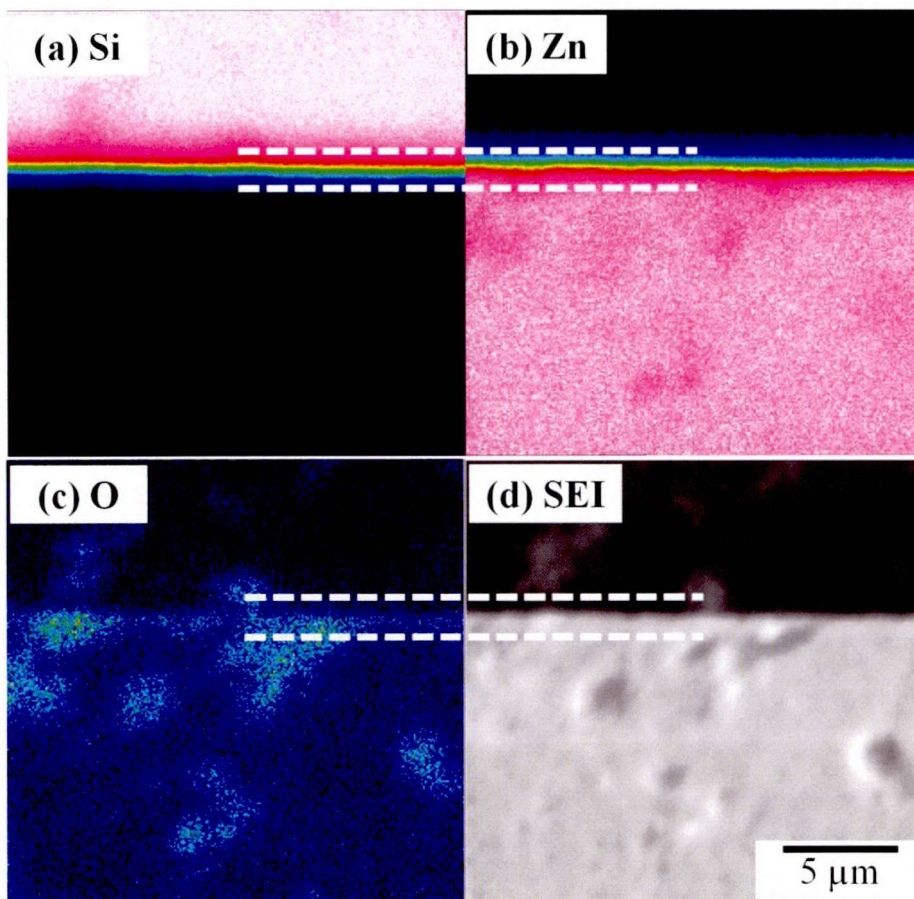


Fig. 5.7 EMPA mapping of a Si wafer/pure Zn interface: (a) Si, (b) Zn, (c) O, and (d) SEM image of the mapping region. Dotted lines indicate the range of reaction layer.

5.3.3 Self-regulated eutectic reaction

The formation process of the uniform reaction layer can be explained from the Si–Zn binary phase diagram near the eutectic point as presented in Fig. 5.7 [14]. In the diagram, one can find that Si–Zn eutectic transformation occurs at $T_e = 419.33\text{ }^\circ\text{C}$ for 99.981 wt.% of Zn concentration, which is very close to the melting point of pure Zn ($T_m = 419.58\text{ }^\circ\text{C}$) [13]. The bonding process temperature $T_p = 450\text{ }^\circ\text{C}$ higher than both T_m and T_e (see Fig. 5.7) ensures that the majority of atomic diffusion occurs from solid Si to molten Zn because of the large difference in the diffusion velocities of liquid and solid metal. This unique condition of Zn–Si eutectic phase leads to a scenario of the uniform reaction layer formation consisting of the following three steps; first, the molten pure Zn spreads well on wafer surface due to the good wettability of liquid Zn on naturally oxidized Si, and make a sound contact at Zn/Si interface. Second, Si starts diffusing into Zn to build up a Si–Zn eutectic liquid (see line A in Fig. 5.7). Third and finally, the increased amount of Si in liquid Zn shifts the liquidus line to high temperature side (line B in Fig. 5.7), and then the eutectic mixture solidifies to form the reaction layer of uniform thickness determined by the diffusion velocity of Si in Zn at T_p . The solid eutectic reaction layer once formed at the interface does not melt during the process, and the dissolution rate of Si into the bonding layer is regulated by the diffusion velocity of Si atoms in the solidified Si–Zn eutectic alloy. The reaction layer thus plays as a diffusion barrier to limit excess Si consumption in the bonding process. The high bond strength registered by the present study hence originates from the self-regulated eutectic reaction of Si and pure Zn.

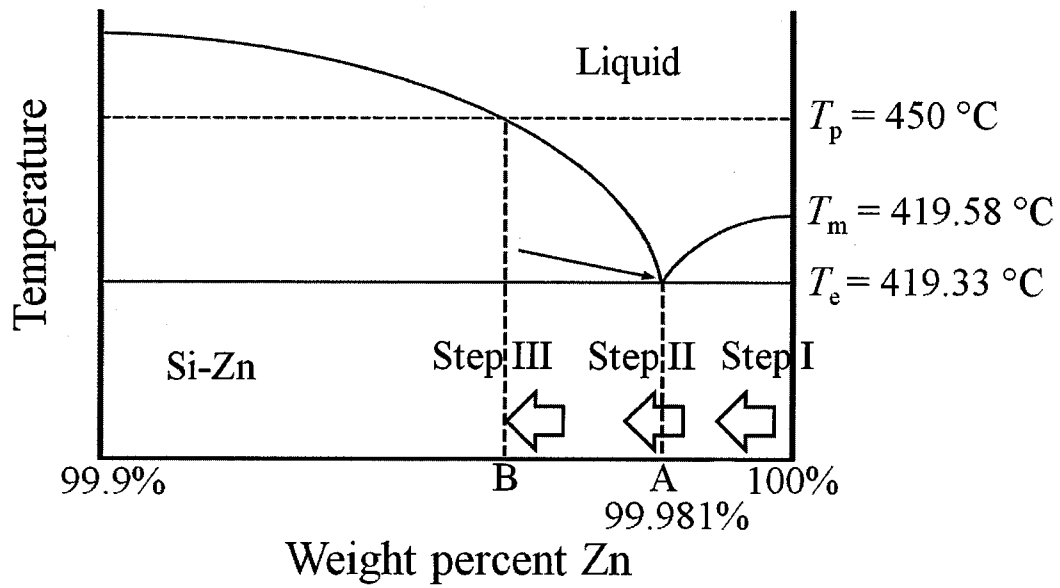


Fig. 5.8 Si-Zn phase diagram of near the eutectic point. The T_p , T_e , and T_m denote the processing temperature, Si-Zn eutectic point, and the melting point of pure Zn, respectively.

5.4 Conclusions

In summary, the present study reports a uniform and void-free Si wafer bonding process without metallization of wafers, realized by using pure Zn as solder. The achieved bonding strength is significantly higher than that by conventional Au–20Sn eutectic soldering. The formation of uniform Si–Zn eutectic reaction layer essentially prevents the air voids at the bonding interface. Moreover, the present bonding system needs not to concern crater formations on Si surface because the eutectic reaction regulates excessive Si dissolution into Zn. The proposed cost-efficient wafer bonding method thus provides a sound bonding interface, and is hence expected to have a wide range of applications for Si based devices with wafer bondings.

References

- [1] J.B. Lasky, "*Wafer bonding for silicononinsulator technologies*", Appl. Phys. Lett. 48 (1986) 78.
- [2] M. Shimbo, K. Furukawa, K. Fukuda, and K. Tanzawa, "*Silicontosilicon direct bonding method*", J. Appl. Phys. 60 (1986) 2987.
- [3] R.W. BOWER, M.S. ISMAIL, and S.N. FARRENS, "*Aligned Wafer Bonding: A Key to Three Dimensional Microstructures*", J. Electron. Mater. 20 (1991) 383.
- [4] Gertrud Kräuter, Andreas Schumacher, Ulrich Gösele, Thomas Jaworek, and Gerhard Wegner, "*Room Temperature Silicon Wafer Bonding with Ultra-Thin Polymer Films*", Adv. Mater. 9 (1997) 417.
- [5] R.F. Wolffenbuttel and K.D. Wise, "*Low-temperature silicon wafer-to-wafer bonding using gold at eutectic temperature*", Sens. Actuators A 43 (1994) 223.
- [6] R.F. Wolffenbuttel, "*Low-temperature intermediate Au-Si wafer bonding; eutectic or silicide bond*", Sens. Actuators A 62 (1994) 680.
- [7] Errong Jing, Bin Xiong, and Yuelin Wang, "*The Bond Strength of Au/Si Eutectic Bonding Studied by IR Microscope*", IEEE Trans. Electron. Packag. Manuf. 33 (2010) 31.
- [8] Wenming Tang, Anqiang He, Qi Liu, and Douglas G. Ivey, "*Fabrication and microstructures of sequentially electroplated Au-rich, eutectic Au/Sn alloy solder*", J. Mater. Sci.-Mater. Electron. 19 (2008) 1176.
- [9] P.H. Chen, C.L. Lin, and C.Y. Liu, "*Amorphous Si/Au wafer bonding*", Appl. Phys. Lett. 90 (2007) 132120.
- [10] K. Suganuma, "*Advances in lead-free electronics soldering*", Curr. Opin. Solid State Mater. Sci. 5 (2001) 55.
- [11] K. Suganuma and S. Kim, "*Ultra Heat-Shock Resistant Die Attachment for Silicon Carbide With Pure Zinc*", IEEE Electron Device Lett. 31(2010) 1467.

Chapter 5

Non-metallization Si wafer bonding by self-regulated eutectic reaction with pure Zn

- [12] Jin-Wook Jang, Scott Hayes, Jong-Kai Lin, and Darrel R. Frear, "*Interfacial reaction of eutectic AuSi solder with Si(100) and Si(111) surfaces*", J. Appl. Phys. 95 (2004) 6077.
- [13] R.W. Olesinski and G.J. Abbaschian, "*The Si-Zn (Silicon-Zinc) System*", Bull. Alloy Phase Diagrams. 6 (1985) 545.

Chapter 5
Non-metallization Si wafer bonding by self-regulated eutectic reaction with pure Zn

Chapter 6

Conclusions

6. 1 Conclusions

In this thesis, the ductility and oxidation resistance of Zn were enhanced through the addition of minor elements for use in SiC die-attachment and were investigated the interfacial reaction with Cu substrate. Additionally, pure Zn was proposed as a wafer bonding material with self-regulated eutectic reaction.

Chapter 1 introduced the necessity of SiC power device and the die-attach technologies. For the die-attachment, lead-free die-attach materials are required because lead has the serious problems to both human health and the environment. Chapter 1 also reviewed the present lead-free die-attach materials and pointed out its drawbacks and limitation. In the previous study, although pure Zn shows a great potential as die-attach material, it has a brittle nature and oxidation sensitivity. Supposing the improvement of pure Zn, the SiC die-attachment reliability can progress. Thus, the chapter 1 described the purposes.

In chapter 2, the ductility and oxidation resistance of pure Zn were enhanced by the addition of minor elements for use in die-attach materials. The results of tensile test we concluded that the addition of minor elements effectively improved ductility without degrading strength and suppressed twinning. The coarse grain could be refined preventing from the brittle fracture of pure Zn without coarse intermetallic compounds in the microstructure. The addition of all minor elements to pure Zn could obtain the advanced oxidation resistance. It is possible that minor elements preferentially leads to formation a compact and stable barrier layer at the surface or subsurface of Zn, and that these layers could stem the propagation of oxygen inside the metals. Among the alloys obtained by adding minor elements, the Zn–Cr alloy showed the slowest oxidation ratio. Therefore, the addition of minor elements to new Zn-based die-bonding materials is expected to be applicable to the interconnectivity

Chapter 6
Conclusions

of wide-gap semiconductor devices for use at high operating temperatures.

Chapter 3 discussed the interfacial reaction on Cu substrate with minor elements added Zn focusing on the intermetallic compounds (IMCs) growth and shear strength during thermal aging because the IMCs thickness is the important issue on the joint reliability.

Two reaction layers were observed at the solder/Cu interface, and they were identified as γ -Cu₅Zn₈ and ε -CuZn₅ phases. As soldered IMCs thicknesses of Zn-0.1X/Cu was about 15 μ m, which were much thinner than that of Zn/Cu reaction layer.

After thermal aging 100h at 150 °C, the IMC layer grew at the interface (about twice) in thickness. However, extended aging time until 500h indicated a considerable distinction between Zn/Cu and Zn-0.1X, especially Zn-0.1Cr/Cu interface. The IMC thickness of Zn/Cu and Zn-0.1Cr interface after aging for 500h were about 130 μ m, 63 μ m respectively. In case of the Ca and Ti additions, the delamination to be operated at high temperature, was occurred after aging 200h, it implies the addition of Ca or Ti is not a good choice for using high operation temperature devices. The growth rates were calculated as 3.77×10^{-15} m²/s, 2.82×10^{-15} m²/s, and 1.16×10^{-15} m²/s for Zn/Cu, Zn-0.1Mn/Cu, and Zn-0.1Cr/Cu, respectively, which indicates that the IMC growth rate of Zn-0.1Cr is significantly slower than pure Zn/Cu couple. Although shear strength of Cu/solder/Cu joints with Zn and minor elements added Zn solders showed almost the same value, about 60MPa, the shear strength of the joint with all solders decreases rapidly during the thermal aging, except with Zn-0.1Cr. The result of the IMC thickness and shear strength, it is supposed that the higher shear strength of the Zn-0.1Cr alloy can be attributed to its thinner IMC thickness.

Thermal aging at 250 °C was carried out in order to examine the SiC power device at realistic operating temperature. During aging treatment for 100h, the formation of a considerable crack was observed inside the γ -Cu₅Zn₈ IMC phase, except Zn-0.1Cr/Cu interface. Thermal aging for 500h the pure Zn lost even its own shape as solder while the Zn-0.1Cr remained the solder structure though crack was existed. The additive Cr had a beneficial effect for suppressing IMCs growth.

Chapter 6 Conclusions

In chapter 4, SiC die-attachment was carried out. A sound SiC die attachment (with the metallization layer of Au/TiN) onto a direct bonded copper (DBC) substrate was obtained with Zn-0.1Cr solder. The TiN diffusion barrier layer suppressed the IMC growth between DBC substrates and solder. The thermal cycle (between $-40 - 300$ °C) reliability of SiC die-attached joints with Zn-0.1Cr solder was evaluated. After 500 cycles, pure Zn and Zn-0.1Cr solders provide excellent heat-cycle resistance for the DBC die-attach structure without cracking. Thus, cost-efficient Zn-0.1Cr solder exhibits quite excellent thermal shock resistance as compared with the conventional Pb-5Sn solder. It is intriguing to investigate the mechanism behind the improvement, in a further study, though it is beyond the scope of this study.

Chapter 5 proposed the other application of pure Zn in packaging technologies, e.g. Si wafer bonding. A uniform and defect-free interface was obtained, realized by using pure Zn as solder. This bonding method gained significantly higher strength than that by conventional Au-20Sn eutectic soldering. Moreover, the formation of uniform interface was obtained using pure Zn due to Si-Zn self-regulated eutectic reaction layer excessive Si dissolution into Zn. The proposed cost-efficient wafer bonding method thus provides a sound bonding interface, and is hence expected to have a wide range of applications for Si based devices with wafer bonding.

In conclusion, it is found from a series of systematic investigations that addition of minor elements significantly improved Zn-based materials for die-attachment of SiC. The improved performance and reliability obtained are following: Improved ductility and oxidation resistance were expected to relieve thermo-mechanical stress and high temperature oxidation. In particular minor Cr showed depressing effect of IMC growth and excellent thermal cycle reliability. The SiC die-attached joints with Zn-0.1Cr solder were found to be more suitable than those with the currently used solders, e.g Au-20Sn and Pb-5Sn.

List of Publication

A. Papers

- (1) S.W. Park, T. Sugahara, S. Nagao, K. Sugauma, "High strength Si wafer bonding by self-regulated eutectic reaction with pure Zn", Scripta Mater., In press.
- (2) S.W. Park, T. Sugahara, K. S. Kim, K. Sugauma, "Enhanced ductility and oxidation resistance of Zn through the addition of minor elements for use in wide-gap semiconductor die-bonding materials", J. Alloys Compd., **542** (2012) 236–240.

B. Proceedings and Presentations (International Conference)

- (1) S.W. Park, S. Nagao, T. Sugahara, K. Sugauma, "Application of pure Zn for void-free Si wafer bonding without metallization layer", The 16th SANKEN International Symposium 2013/ The 11th SANKEN Nanotechnology Symposium, Osaka, Japan, 2013. 1.22 – 23.
- (2) S.W. Park, J. L. Jo, T. Sugahara, M. Ueshima, H. Iwamoto, K. Sugauma, "SiC die-attachment with minor elements addition pure Zn under formic acid reflow", Electronics System Integration Technology Conferences (ESTC) 2012, Amsterdam, Netherlands, 2012. 9.17 – 20.
- (3) K. Sugauma, S. Sakamoto, S.W. Park, "Heat-resistant die-attach technology for SiC," 8th Annual TMS Lead Free Solder and Interconnect Technology Workshop, Florida, USA, 2012. 3.11.
- (4) S.W. Park, K. Sugauma, "Characteristics of Die Attach Joints with Zn High Temperature Lead-Free Solders," Eco-mates 2011, Osaka, Japan, 2011.11.28 – 30.
- (5) S.W. Park, K.S. Kim, K. Sugauma, "Effect of Cr addition on mechanical property and oxidation resistance of pure Zn as SiC die bonding material," MS&T2011, Ohio, USA, 2011. 10.16 – 20.
- (6) S.W. Park, K.S. Kim, K. Sugauma, "Improvement of Brittleness of Pure Zn by Addition of Minor Elements as High Temperature Lead-free Solder," ICEP2011, Nara, Japan, 2011.4.13 – 15.

C. Proceedings and Presentations (Domestic Conference)

- (1) 菅沼 克昭、菅原 徹、朴 聖源、坂元 創一、” Heat-resistance die-attach materials for SiC” 溶接学会第 101 回マイクロ接合委員会、大阪、2012 年 9 月 4 日
- (2) 朴 聖源、菅原 徹、菅沼 克昭、“純 Zn はんだによる SiC 超高温ダイアタッチ技術の開発”、日本実装学会関西ワークショップ 2012、滋賀、2012 年 7 月 12 日 - 7 月 13 日
- (3) 宮崎 年彦、成田一人、宮原広郁、菅沼 克昭、菅原 徹、朴 聖源、” SiC ダイアタッチ用 Zn はんだの組織および特性に及ぼす微量添加元素の影響”、日本金属学会・日本鉄鋼協会・軽金属学会九州支部合同学術講演会、北九州市、2012 年 6 月 9 日
- (4) 朴 聖源、菅沼 克昭、SiC ダイアタッチ用 Zn 超耐熱はんだへの微量 Cr 添加の影響、2011 年秋期第 149 回日本金属学会学術講演会、沖縄、2011 年 11 月 7 日 - 11 月 9 日

ACKNOWLEDGEMENTS

I would like to express my sincere thanks to my supervisor, Prof. Katsuaki Sukanuma at Institute of Scientific and Industrial Research (ISIR) in Osaka University. With his guidance and support, I was able to engage in a broad range of research activities. His wide and deep knowledge of conducting research and ways of tackling problems spurred me to think out of the box in order to solve various technical issues. I feel it a great honor to have been studied with Prof. Sukanuma. I am indebted to my other committee members, Prof. Hideyuki Yasuda and Masato Yoshiya who are professor of the department of adaptive machine systems in Osaka University for agreeing to serve on my committee and offering me thoughtful advice and guidance.

I am deeply grateful to Prof. Keun-Soo Kim, the Fusion technology Lab., Hoseo University for his comprehensive guidance and constructive comments throughout this thesis. I am also grateful to Prof. Masahiro Inoue in Gunma University for his technical advice.

I wish to express my warm and sincere thanks to Prof. Chi-Hwan Lee in Inha University who give me a chance and courage to study abroad in Japan. And I am deeply grateful to Prof. Soong-Keun Hyun in Inha University who introduce me to the field of packaging technology and Sukanuma lab. in Osaka University.

I warmly thank Prof. Masaya Nogi, the Institute of Scientific and Industrial Research (ISIR), Osaka University, for their support and friendly help. I'd like to express thank to Assistant Professor Tohru Sugahara, Dr. Shijo Nagao, and Dr. Hirotaka Koga. And I also wish to thank Dr. Seongjun Kim and Dr. Kiju Lee, for their technical assist and kind support at the beginning of my doctoral course in Osaka University. I owe my sincere appreciation to Dr. Changjae Kim who have supported and encouraged me during Japan life.

I would like to mention and thank to colleagues Junglae Jo, Soichi Sakamoto, Natsuki Komoda, Youngseok Kim, Chulmin Oh, Teppei Araki, and Semin Park. I always cheer for master course student; Tetsuji Inui and Ryoji Uwataki. I would also like to thank other members of Sukanuma Lab. who helped me with official work, research and study, including Ms. Keiko Suzuki, Dr. Jinting Jiu, Dr. ThiThi Nge, Ms. Hatamura, Ms. Kagami, Ms. Hamasaki, and Ms. Sya. I would also like to acknowledge the old boys and girl; Dr. Daisuke Wakuda, and Dr. Alongheng Baated.

I thank for kind technical support; Prof. Miyahara(Kyushu University), Assistant Prof. Ichihito Narita (Kyushu University), Mr. Minoru Ueshima (Senju Metal Industry Co. Ltd.) and Mr. Yoshitaka Katoh (SiC device Lab. at Denso)

Finally and the most importantly, I wish to thank my parents and friends in Korea for their everlasting helps and supports. You are my precious treasure and the biggest driving forces.

This work was partly supported by a Grant-in-Aid for Scientific Research(S) Grant Number (24226017). The author would like to thank Comprehensive Analysis Center, ISIR, Osaka University, providing the analysis equipment TGA and EPMA.

